NASA Technical Memorandum 101043

A Conceptual Design Study of the Reusable Reentry Satellite

Byron L. Swenson, Alfred C. Mascy, Bruce Carter,
Alan Cartledge, Robert E. Corridan,
Larry E. Edsinger, Robert W. Jackson, Robert Keller,
Marcus S. Murbach, Paul F. Wercinski, and
Thomas Wong

October 1988

National Aeronautics and
Space Administration

NASA Technical Memorandum 101043

A Conceptual Design Study of the Reusable Reentry Satellite

Byron L. Swenson, Alfred C. Mascy, Bruce Carter, Alan Cartledge, Robert E. Corridan, Larry E. Edsinger, Robert W. Jackson, Robert Keller, Marcus S. Murbach, Paul F. Wercinski, and Thomas Wong, Ames Research Center, Moffett Field, California

October 1988

NASA

National Aeronautics and Space Administration

Ames Research Center
Moffett Field, California 94035

A CONCEPTUAL DESIGN STUDY OF THE REUSABLE REENTRY SATELLITE

Byron L. Swenson, Alfred C. Mascy, Bruce Carter,
Alan Cartledge, Robert E. Corridan, Larry E. Edsinger,
Robert W. Jackson , Robert Keller, Marcus S. Murbach,
Paul F. Wercinski, and Thomas Wong

NASA Ames Research Center
Moffett Field, California 94035

SUMMARY

Experimentation leading to an understanding of life processes under reduced and extremely low gravitational forces will profoundly contribute to the success of future space missions involving humans. In addition to research on gravitational biology, research on the effects of cosmic radiation and the interruption and change of circadian rhythms on life systems is also of prime importance. Research in space, however, is currently viewed by biological scientists as an arena that is essential, yet largely inacessible to them for their experimentation. To fulfill this need, a project and spacecraft system described as the Reusable Reentry Satellite or "LifeSat" has been proposed by NASA.

The Reusable Reentry Spacecraft (RRS) provides researchers in several diverse fields of interest with a relatively inexpensive method of access to space for extended periods of time and eventual intact recovery of the experiments on the surface of the Earth. The RRS is capable of (1) being launched by a variety of expendable launch vehicles, (2) operating in low Earth orbit as a free-flying unmanned laboratory, and (3) an independent atmospheric reentry and soft landing at a continental U.S. site providing the experimenter with a rapid access to the payload. The RRS exterior configuration is a blunt non-lifting reentry vehicle similar in concept to the USAF Discoverer reentry vehicle, the NASA Biosatellite vehicle, or other recoverable military vehicles. The principal differences between the RRS and the above vehicles are in the physical size of the vehicle and the subsystem changes necessary to permit a total intact, relatively soft recovery of the system on land and subsequent refurbishment and reflight with new and varied payloads. The total launch mass of the RRS system (including experiments) is about 1270 kg. The system is currently envisioned to be capable of three reflights per year over a 10-year program lifetime. The expected principal area of use for such a system is research on the effects of micro-gravity, artificial gravity, and radiation on small animals, plants, lower life forms, and tissue samples.

This research program is also of considerable interest to a number of foreign agencies and a cooperative international scientific and hardware development program is envisioned. Possible future uses might include the development of commercial materials and processes and the demonstration of new technologies in space.

The RRS vehicle is configured with a large and readily accessible volume for the Payload Module (PM) which contains the experimental hardware. The RRS can support a PM of mass of about 240 kg in a cylindrical envelope with a diameter of 111.8 cm and a length of 91.4 cm. The PM is supported by the RRS vehicle which provides utility sources of electrical energy and dissipative thermal control, command signals, and limited downlink telemetry capability. Approximately 45 kW-hr of power are available to support the PM during the mission.

It is expected that a Rodent Module (RM) will be developed to house and support up to 12 rodents for as long as 60 days. A General Biology Module (GBM) will also be developed to contain and support groups of experiments in their own containers for also as long as 60 days. In addition, it is currently planned that a module will be developed to support an appropriate modification of hardware derived from the ESA Botany Facility for plant experimentation. It is conceivable that, rather than multiple life science PMs, a single life science support module might be developed to provide a controlled environment (i.e., atmospheric composition, humidity, and temperature) and the experiment peculiar equipment, such as cages, cuvettes, or general biology experiment containers, could be integrated within this single container. The vehicle is also configured to permit the experimenter late access to the PM prior to launch and rapid access following landing.

The RRS operates as a free-flyer in orbit for up to 60 days. The vehicle is capable of either three-axis or spin stabilization to permit both the required orbital trim maneuvers and a precision deorbit maneuver. On orbit the spacecraft is capable of providing micro-gravity or artificial gravity environments. For the micro-gravity level experiments, the spacecraft is allowed to float in attitude, subject to angular rate-limit control, to provide the experimenter with an orbital acceleration environment of less than 10^{-5} g for 95% of the orbital mission. The acceleration environment during attitude or orbital trim maneuvers is less than 10^{-3} g. To provide artificial gravity acceleration levels from 0 to 1.5 g, the spacecraft can be spun about its longitudinal axis.

At completion of the orbital mission, the vehicle is commanded to deorbit with precision to a site in the White Sands Missile Range (WSMR) in New Mexico. The WSMR was selected as the recovery site because it provides a large controlled airspace required for a safe recovery. The particular site of interest within the WSMR is the so-called "Northrup Strip" area, a very large dry lake bed centered at 106° 25'

west longitude and 32° 57' north latitude. This area is also used as an alternate landing area for the Shuttle and has NASA facilities nearby at the Johnson Space Center White Sands Test Facility. After the vehicle reenters the atmosphere and decelerates to below sonic speeds, at about 6,000 m altitude, a parachute (possibly a lifting, steerable parafoil) is deployed permitting the vehicle to land relatively softly. For a conventional parachute landing, the RRS lands in a flat area which is sufficiently large to encompass the nominal 3-sigma dispersions. If a parafoil is used, the vehicle is able to glide to a preselected point. At that location the parafoil is remotely commanded by a ground "pilot" to approach into the local wind and aerodynamically flare at landing permitting a relatively soft and precision landing. After landing, the payload is removed, the vehicle is refurbished, requalified and readied for integration with another payload module for a subsequent mission. The minimum time between recovery and reflight is about 60 days.

CONTENTS

	Page
SUMMARY	III
INTRODUCTION	1
SCIENCE SUPPORT REQUIREMENTS	1
FLIGHT OPERATIONS REQUIREMENTS	7
MISSION DESCRIPTION	8
Pre-Launch and Launch Phase	9
Pre-Launch Phase	9
Launch	9
On-Orbit Phase	9
Orbit Selection Considerations	9
Integer Orbits	9
Day/Night Cycles	12
Orbital Lifetime	14
Micro-Gravity Environment	14
Artificial Gravity	16
Operations	16
Recovery Phase	17
Deorbit Maneuver	17
Reentry	18
Parachute Deployment	19
Landing	22
Payload Access and Removal	23
Refurbishment	23
Low Cost and Interchangeability	23
Turn-Around Time	24
SYSTEM DESCRIPTION	24
RRS Vehicle System	24
Payload Modules	24

	Page
Attitude and Spin Control Subsystem	25
Components	25
Capabilities	29
Outgassing Stabilization	30
Launch Errors Correction and Landing Site Synchronization	30
Micro-Gravity Control	31
Atmospheric Drag Makeup	32
Spin/Despin Stabilization Maneuvers	32
Artificial Gravity	32
Deorbit Thrust Vector Control	32
Deorbit Maneuver Trim	32
ASCS Weight	32
Deorbit Propulsion Subsystem	33
Structures	33
Loads	33
Structural Components	36
Power Subsystem	38
System Power Interface Units and Harness	42
Command Subsystem and Harness	42
Communications Subsystem	43
Data Handling Subsystem and Harness	44
Tracking Transponder	45
RRS Parachute Subsystem	45
Reentry Thermal Protection System	48
Thermal Control Subsystem	52
RRS Mass Properties and Configurational Layout	59
Requirements	59
Mass Statement	60

Page

Configurational Layout, Center of Gravity, and Moments of Inertia 61

CONCLUSIONS 68

APPENDIX A - INTEGER ORBITS, DUAL OVERFLIGHTS, AND DAY/NIGHT CYCLES 71

Integer Orbits 71
Dual Overflights 73
Day/Night Cycles 77

APPENDIX B - ORBIT SYNCHRONIZATION WITH THE LANDING SITE FOR DEORBIT 79

REFERENCES 81

INTRODUCTION

Experimentation leading to an understanding of life processes under reduced and extremely low gravitational forces will profoundly contribute to the success of future space missions involving humans. In addition to research on gravitational biology, research on the effects of cosmic radiation and the interruption and change of circadian rhythms on life systems is also of prime importance. To reach this fundamental understanding of effects of environment of space and other planetary bodies on life processes, the life science research program must encompass a wide range of experimentation involving animal and plant biology as well as interorganismal and ecosystem studies. The research program to achieve this goal is many faceted and involves experimentation in laboratories on Earth and in space. Research in space, however, is currently viewed by biological scientists as an arena that is essential, yet largely inacessible to them for their experimentation.

In the 1960s, the NASA Biosatellite program (ref. 1) provided some opportunity for experimentation in orbit. Prior to the Challenger disaster, some experimentation had been accomplished for relatively short periods on-board Shuttle and Spacelab. In addition, there have been limited opportunities on-board the Soviet Cosmos spacecraft. Eventually, of course, the Space Station holds the promise of providing an opportunity for long-term experimentation in space under controlled laboratory conditions.

In the interim and for some time to come, there exists a significant need for a stem which will provide the life science experimenter with relatively frequent and expensive access to the space environment for significant periods of time. In some ses, there is a need for a system which can provide environments (e.g., high cosmic- liation in conjunction with micro-gravity) for experimentation which the manned tems can not provide. This system could also be used to develop, in a cost effective nner, the necessary experimental protocols and techniques before relatively more ensive manned operations can be implemented. For these reasons, a project and ecraft system described as the Reusable Reentry Satellite (RRS) or "LifeSat" is g proposed by NASA to fulfill these needs (a preliminary study is contained in ?). A perspective view of the exterior configuration of the RRS is shown in figure he project and research program are designed to be complementary to other life ce research thrusts and to provide essential continuity to the research program ing the verification and the quick capitalization of significant results.

SCIENCE SUPPORT REQUIREMENTS

The mission and system designs of the RRS are driven by the requirements to ', in a cost effective manner with low programmatic risk and a high concern for

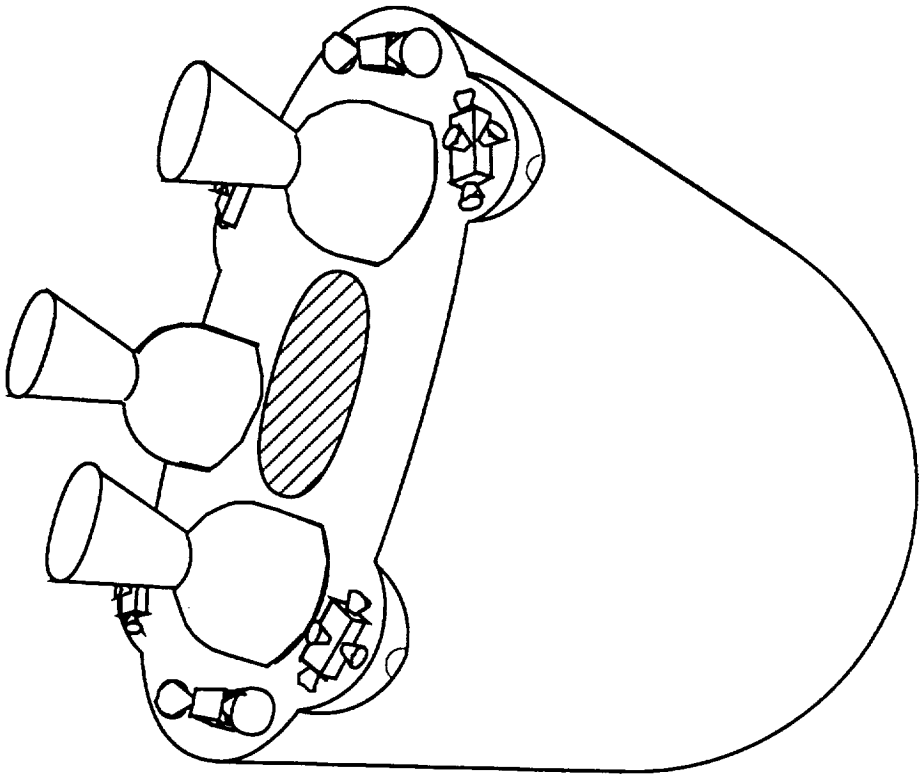

Figure 1. Exterior View of Reusable Reentry Satellite

public safety during operations, the Earth orbital life science research program articulated in reference 3. The conceptual design effort reported in this document focuses primarily on the design of the mission, operations, and the spacecraft which follows the above guiding principle. This design flexiblity is achieved through the use of the concept of a Payload Module (PM) which directly supports the experiments while on orbit. The PM, in turn, is carried and supported by the RRS vehicle which provides utility services of power, thermal control, data transmission, and uplinked commands through rather simple interfaces. A cross-sectional view of the RRS which locates the major subsystem components is shown in figure 2(a) and the related block diagram which illustrates the inter-relationalships of these subsystems is shown in figure 2(b).

The design for the PM has not, as yet, progressed to a level of description similar to the following material for the RRS vehicle system. However, it is expected that a Rodent Module (RM) will be developed to house and support up to 12 rodents for as long as 60 days. A General Biology Module (GBM) will also be developed to

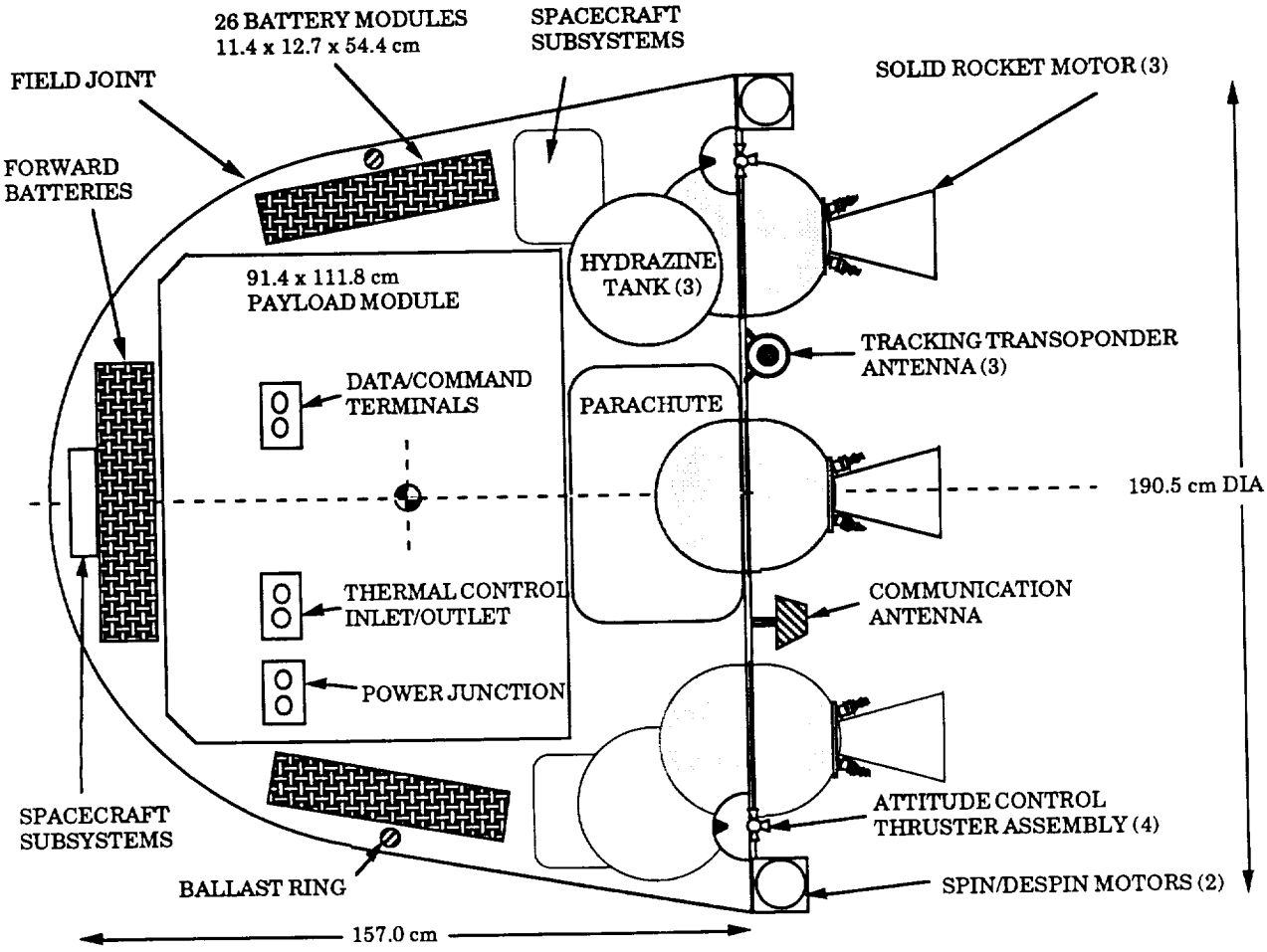

Figure 2(a). Major RRS Subsystems

contain and support groups of experiments in their own containers for also as long as 60 days. In addition, it is currently planned that a module will be developed to support hardware derived from the European Space Agency (ESA) Botany Facility for plant experimentation. It is conceivable that, rather than multiple life science PM's, a single life science support module might be developed to provide a controlled environment (i.e., atmospheric composition, humidity, and temperature) and the experiment peculiar equipment, such as cages, cuvettes, or general biology experiment containers, could be integrated within this single container. That decision must await further science analysis and possible decisions of program participation by various foreign agencies.

For the conceptual design effort reported herein, basic interface requirements for the PM had to be assumed. NASA Ames Research Center convened a number of

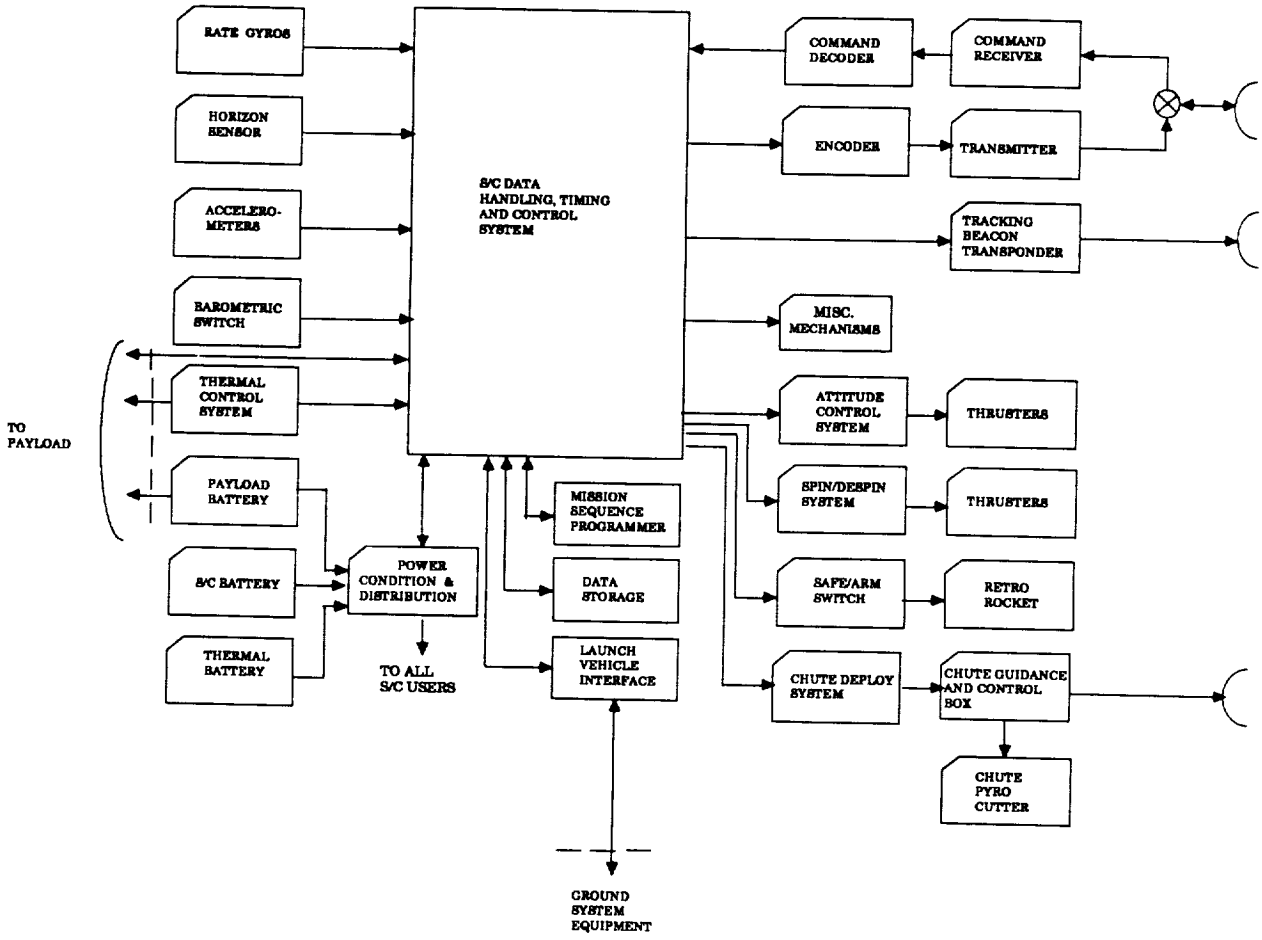

Figure 2(b). Block Diagram of Major Subsystems

life scientists, with interest and experience in orbital life science experimentation in several fields, into a LifeSat Science Working Group (LSSWG) to provide guidance in the definition of the science support requirements. In addition, the LSSWG provided advice on aspects of the RRS vehicle design and operation which affected the viability of the life science research to be accomplished. The LSSWG has produced three Science Requirements Documents (SRD's) for the fields of small animal (rodent) research, plant research, and general biology research (refs. 4, 5, and 6, respectively). The most important and driving science support requirements, extracted from those documents, are listed in Table 1. The most important mission operational requirements are listed in Table 2. A very preliminary examination of the translation of the total requirements contained in the SRD's indicates the necessity for the RRS vehicle to support a PM design of about 240 kg within a cylindrical envelope with a 111.8 cm diameter and a 91.4 cm length .

TABLE 1. SCIENCE REQUIREMENTS FOR A LIFE SCIENCES PM

1. Experiment Accomodation
1.1 Provide mounting provisions for a variety of experimental containers including : up to 12 rats, up to 18 small plant cuvettes, up to three Shuttle mid-deck lockers, or a large number of small individual packages.
1.2 Provide up to 50 W of contiuous electrical power.
1.3 Provide up to 500 W of heat rejection.
1.4 Provide venting provisions
1.5 Provide for specimen insertion as late as 12 hr before launch and specimen removal as soon as 2 hr after touchdown.
1.6 Support flight durations up to 60 days.

2. Mission Environment
2.1 Provide a steady acceleration level up to 1.5 g or a micro-gravity level less than 10^{-5} g for 95% of the orbital flight and less than 10^{-3} g during maneuvers.
2.2 Support flights within the Van Allen Belts.
2.3 Limit, to the extent possible, the reentry acceleration and landing shock to be less than 20 g.

3. Temperature within the Payload Module
3.1 Control experiment temperature to a set point in the range 4° C to 40° C (range and set point accuracy is experiment specific).

4. Atmosphere within the Payload Module
4.1 Maintain selected percentages of oxygen and carbon dioxide.
4.2 Maintain "sea level" pressure within reasonable limits.
4.3 Control relative humidity.
4.4 Control trace contaminate levels.
4.5 Circulate the atmosphere within the PM.

5. Experiment Vibration
5.1 Limit acoustical and mechanical vibration.

6. Cleanliness within the Payload Module
6.1 Control visible and microbiological contamination.

7. Data Collection
7.1 Record and telemeter houskeeping and status measurements.
7.2 Record radiation and acceleration measurements.

8. Control
8.1 Provide programmed and reactive commands and timing signals.

TABLE 2. - MISSION REQUIREMENTS FOR LIFESAT

1. Reuse Hardware Where Feasible
1.1 Recover at a land site, preferably in the continental U.S.
1.2 Design the RRS to be refurbished and reused up to three times per year.

2. Design for Frequent Flights with Different Payloads
2.1 Provide standard and modular interfaces for experiments.
2.2 Design for 60 day turn-around between flights.
2.3 Design to use several launch vehicles and alternative launch sites.
2.4 Design the ground system for easy modification.

3. Design for Modest Ground Support
3.1 Design to avoid the need for commands or data at specific times.

4. Design for Highly Reliable and Safe Recovery
4.1 Satisfy recovery area WSMR safety requirements.

FLIGHT OPERATIONS REQUIREMENTS

The flight operations requirements of the RRS are to manage the experimental payload, manage the RRS vehicle in support of the payload, and to recover the experiments for analysis. Each experiment flown by the RRS will include a flight operating protocol as well as the hardware and experimental specimens. The protocol describes the environment and operating timeline which are needed to satisfy the scientific objectives. Various experiments which are compatible in environment desires, research theme, resource utilization, and mission duration will be combined for a given flight. The separate and compatible experiment protocols will be combined before launch into a flight plan and mission timeline which will then be used to manage the flight.

An important feature of most experiment protocols will be the use of ground control experiments to expose control specimens to a simulation of the flight environment with the exception of the micro-gravity condition. The ground-control experiments will be run with a few days delay from the flight timeline to provide sufficient time to measure, transmit, and analyze the flight environment in order to duplicate it on the ground.

The Operations Concept for the RRS incorporates a mixture of autonomous and ground-controlled functions. The RRS needs to operate autonomously in order to control the experiments within the constraints of infrequent and irregularly scheduled communication opportunities with the ground. The RRS also needs to autonomously collect and store experiment monitoring data for post flight study. The ground system will be used for the non-routine functions of a RRS flight. The ground system performs recovery planning and controls the actual recovery and experiment retrieval. The ground system collects RRS status measurements during downlink periods and manages the ground control experiments. The ground system also performs anomaly diagnosis and will reconfigure operation of the RRS if needed via uplink commands.

A possible response to flight anomalies will be to terminate the mission and return the RRS vehicle and experimental specimens to the ground. Therefore, the RRS and the supporting ground system maintains readiness to recover the vehicle throughout the flight as well as on the planned recovery day. A single recovery site is contemplated for these missions and it is possible that weather at the recovery site may be unfavorable for the landing. If this occurs, a hold in orbit for a few days may be required. When the recovery day has been selected, the RRS and the ground system is managed to recover the vehicle from orbit and provide ground support functions of power and thermal control and quick access to the experiments and specimens after ground touchdown. The ground system is also responsible to rapidly deliver the stored data from the RRS to the experimenters.

MISSION DESCRIPTION

The RRS is designed to accommodate a variety of payloads and missions as indicated above. It is compatible with several expendable launch vehicles and has the capability of atmospheric reentry and recovery of the vehicle and rapid access to the PM. The RRS is designed for ease of maintenance and refurbishment between missions so that it may be reused up to three times a year for a program lifetime of 10 years. A typical mission profile for the RRS is shown in figure 3. The following is a detailed description of the various phases of a RRS mission.

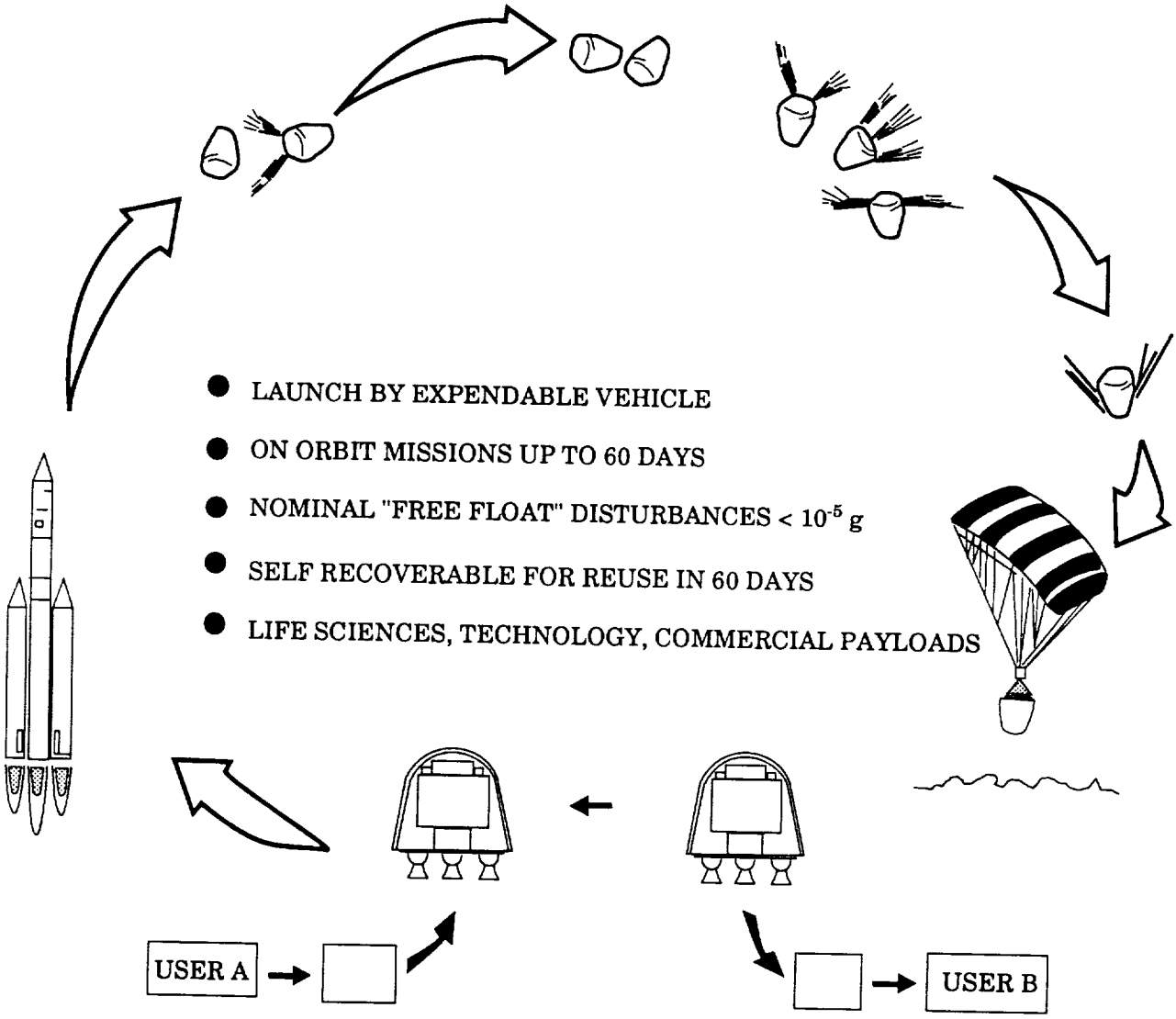

Figure 3. RRS Mission Profile

Pre-Launch and Launch Phase

Pre-Launch Phase - Prior to the launch, the PM, which contains the user experiments, is integrated into the spacecraft. Some of the experimental specimens and support equipment may also be installed into the PM before the RRS is mated with the launch vehicle. Final installation of the experimental specimens and support equipment into the PM is performed on the launch pad and is completed by no more than 12 hr. before launch. It is anticipated that final PM and RRS close out will be complete by 4 hr. before launch.

Launch Phase - After testing and preparing for launch, the RRS is launched by an expendable launch vehicle (ELV). The RRS may be part of a shared launch of multiple payloads which may place certain constraints on the orbital characteristics such as the altitude, inclination, or orbital insertion point and time. Expendible launch vehicles that may be suitable for the RRS mission include the Delta II (ref. 7), Titan II, the Japanese NASDA H-II and appropriate commercial vehicles which are likely to be available by the mid to late 1990s. The RRS is designed such that it is capable of being launched by any of the ELVs with minimum or no modification. The RRS is capable of being launched from the Eastern Test Range (ETR), the Western Test Range (WRT), other sites used for commercial launches in the U. S., and foreign launch sites provided that orbital constraints can be met.

On-Orbit Phase

Orbit Selection Considerations - The RRS is designed to have the capability of operating in a variety of user-specified orbits or orbits specified by the requirements of a shared launch. In general, circular orbits will be used, but elliptical orbits may be desired for some experimental purposes such as increased radiation exposure. Circular orbits within the altitude range of 350 to 900 km will satisfy the needs of most users. It is planned that the RRS will be recovered intact at a continental U.S. landing site. The proposed landing site is the White Sands Missile Range (WSMR) in New Mexico because of its extensive controlled recovery area and facilities. A map of the recovery area is shown in figure 4. The particular site of interest within the WSMR is the so-called "Northrup Strip" area, a very large dry lake bed centered at 106° 25' west longitude and 32° 57' north latitude. This area is also used as an alternate landing area for the Shuttle and has NASA facilities nearby at the Johnson Space Center (JSC) White Sands Test Facility. Because the RRS has no lateral maneuver capability during atmospheric reentry, it is necessary that the orbit inclination of the RRS be equal to or greater than the latitude of the landing site.

Integer Orbits - Although the nominal mission lifetime may be up to 60 days in duration, certain payloads may require shorter durations and, indeed, may require emergency deorbit due to an unexpected experimental condition. Another considera-

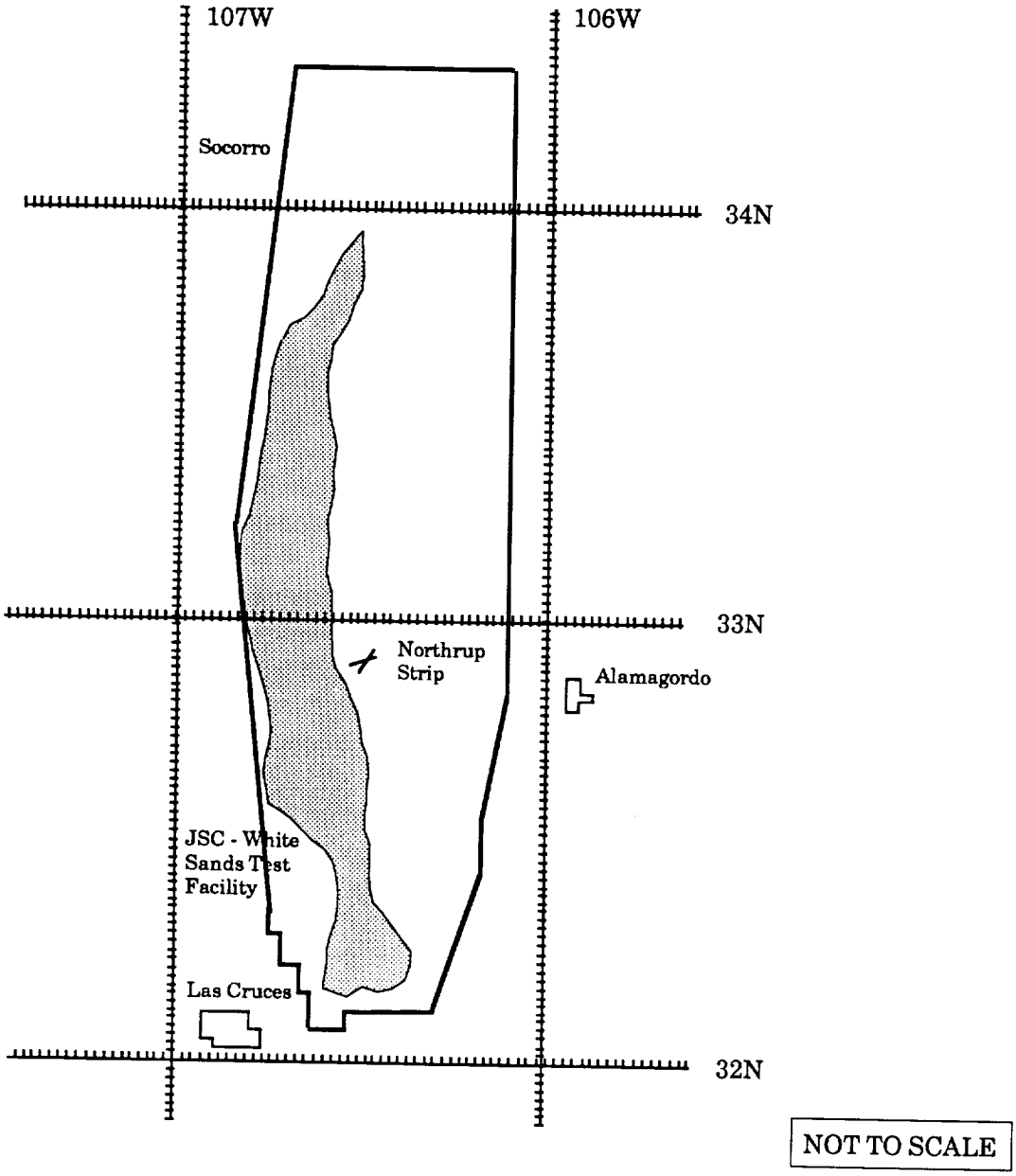

Figure 4. White Sands Missile Range, New Mexico

tion is that recovery at a single site could be delayed one or more days because of local weather conditions. Finally, it is desirable to recover during daylight and, in particular, during the cool morning hours when the surface winds are expected to be low.

One approach to accomplishing these requirements is to choose a proper altitude, inclination and nodal placement so as to insure that the ground track of the satellite permits deorbit and landing with precision at the designated recovery site twice a day throughout the mission (ref. 8). These orbits are termed "integer orbits"

in that the orbits have exactly repeating ground tracks each day. As indicated in Appendix A, a number of particular orbit inclinations and altitudes provide repeating ground tracks and precise dual overflights of the landing site each day; the first an ascending southwest to northeast pass followed by a descending northwest to southeast pass. From the analysis contained in Appendix A, a particular orbit has been derived which is consistent with a direct ascent launch from ETR and overflights of the site in WSMR as shown schematically in figure 5. This orbit is characterized by 15 revolutions per day relative to the landing site and a second overflight of the landing site on the second orbit following the first overflight. The orbit is circular with an inclination of 35.65° and an altitude of 479 km. With the above orbital charcterististics and with a proper node position, the orbit overflys the site twice each day (the overflights separated by 3 hr 23 min) for the duration of the mission.

Under such an orbit scenario, after launch, modification of the orbital parame-

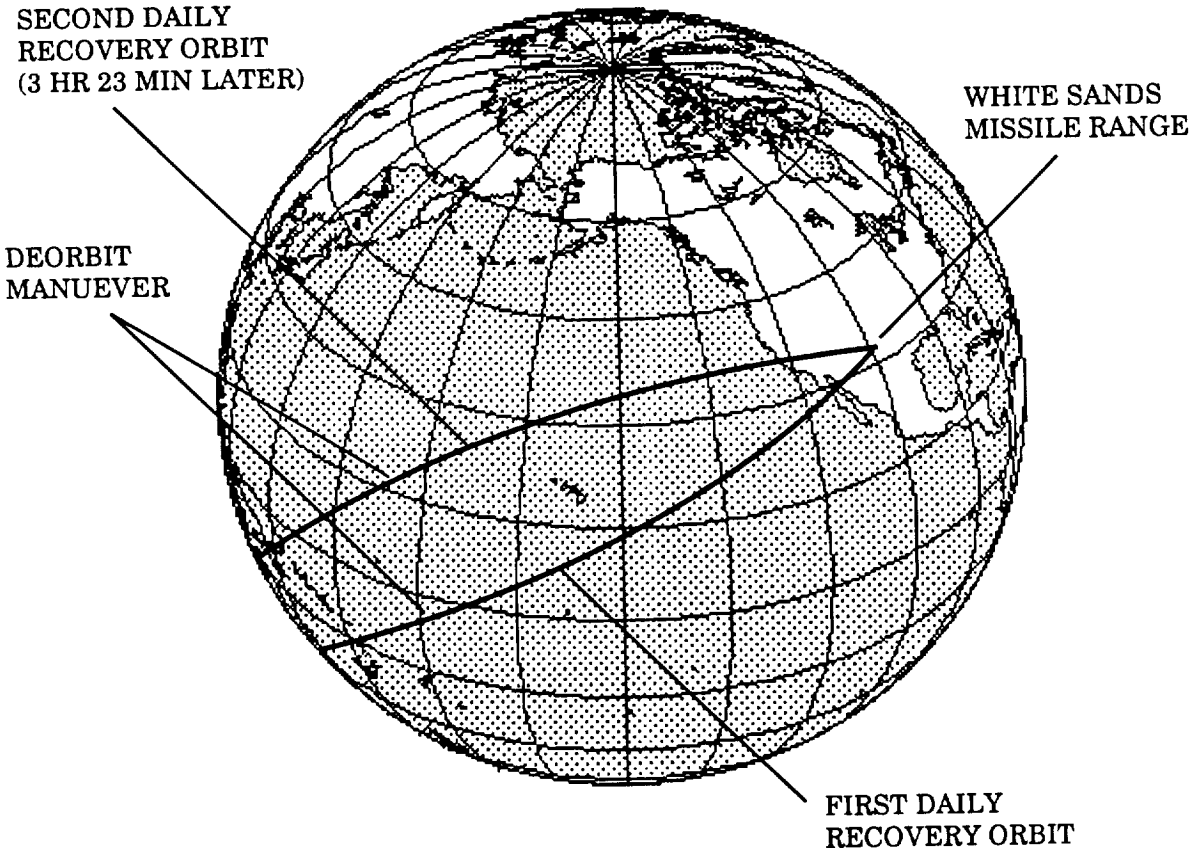

Figure 5. LifeSat Recovery Orbits

ters is necessary to correct insertion errors and to synchronize the orbit ground tracks with the landing site. As discussed later in the description of the attitude and spin control system (ASCS), enough propellant for maneuvers which total about 22 m/sec must be allocated for the correction of the orbit. Thereafter, the orbit need not be perturbed during the course of the mission except to correct for drag effects which for most cases are negligible.

For shared launches, the RRS may be either the first payload deposited in orbit or the last. If it is the first payload, all orbital maneuvers are limited by the capabilities of the RRS attitude and spin control system. If the RRS is the last payload deposited in orbit, it is possible that the ELV upper stage may have sufficient remaining performance (and if it is restartable) to alter the RRS orbit characteristics. In either case, it will probably not be possible to synchronize the orbit passes with the landing site except for the final deorbit.

As shown in Appendix B, the required propulsive maneuvers to phase to the landing site for deorbit are dependent upon two factors. The first is the required longitude change in the projected orbital track, at some future close pass to the landing site, to make it coincident with the landing site (never greater than one-half the orbital track shift distance between two adjacent orbit tracks). The second is the number of orbits over which the time phasing with landing site is to be permitted. The maximum phasing velocity increment, ΔV, (i.e., for a required phasing of one-half the orbital shift distance) is shown as a function the number of orbits allowed for phasing in figure 6. It can be seen that an ASCS propellant allowance equal to that required for the correction of insertion errors and synchronization for the integer orbit scenario (i.e., about 22 m/sec) requires phasing over a period of 120 orbits (about 8 days) before the deorbit maneuver.

Day/Night Landing Cycles - An additional consideration for the orbit selection is the occurrence of day/night cycles at the landing site relative to deorbit and landing opportunities (ref. 8). The combination of orbit nodal regression and the motion of the Earth about the sun causes the time of day of the orbital pass over the landing site to be about 30 min earlier each day; the time shift varies slightly with Earth season. Therefore, for example, the daylight cycle for the ascending (southwest to northeast) pass lasts for about 24 days followed by a like period of night passes. Similarly, the daylight cycle for the descending (northwest to southeast) pass is also 24 days. Depending on the orbit inclination and the latitude of the site, the two cycles overlap, increasing the length of time for daylight landings from one of the opportunities and decreasing the length of time for nighttime only landing opportunities. For example, the day/night landing opportunity cycles for the selected integer orbit relative to the landing site in WSMR are shown in figure 7. It can be seen that landing could be made in daylight for a period of about 33 days from one, and sometimes both, of the orbital passes over the landing site followed by a period of night passes for the next

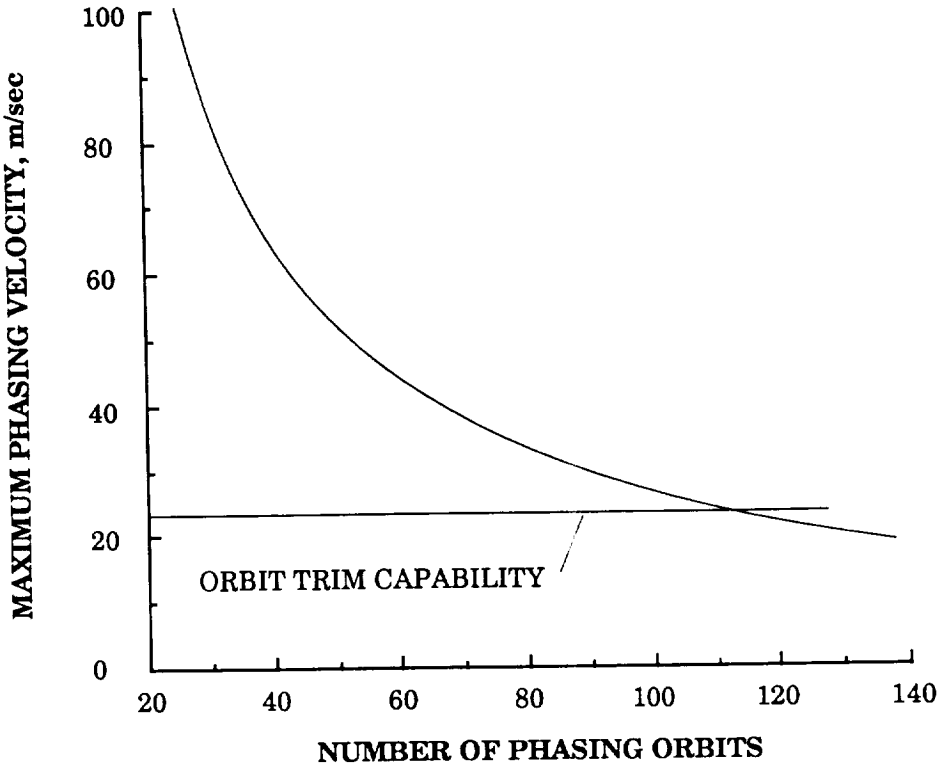

Figure 6. Deorbit Phasing Requirements

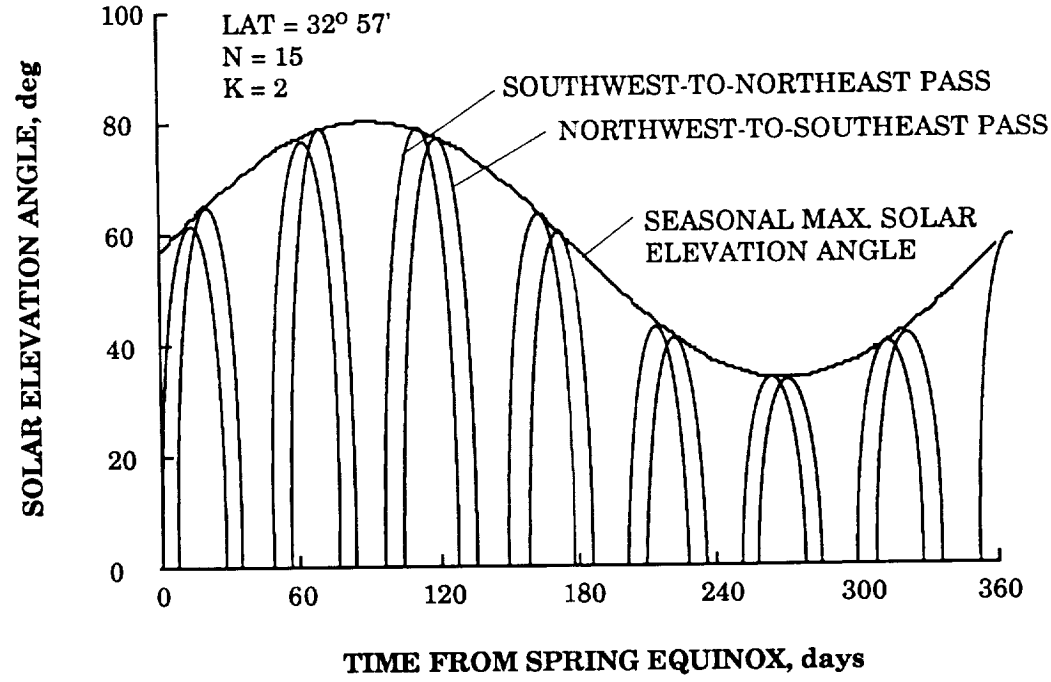

Figure 7. RRS Day/Night Cycle over WSMR

19 days. This day/night cycle then repeats with slight variation due to Earth seasonal effects. The last 19 days of the 33-day daylight landing period provides landing opportunities during the morning hours.

The day/night landing cycles for other non-integer orbits are very similar. For more highly inclined orbits, the motion of the orbit plane relative to the sun is considerably smaller and the lengths of the cycles are inversely longer. In addition, for high inclination orbits and low to moderate site latitudes, the time between the first and second pass approaches one-half day and the two cycles for ascending and descending passes overlap to such an extent that the combined night cycle is reduced to just a few days. A more complete discussion of day/night cycles can be found in reference 9.

Orbital Lifetime - An important advantage of the RRS is its ability to maintain experiments in orbit for reasonably long periods of time as compared to 1 to 2 week Shuttle flight times. Depending on the experiments and the satellite support systems, a typical mission may require lifetimes up to 60 days. Several factors affect the lifetime of a satellite including the orbital altitude, inclination, mass, coefficient of drag, exterior geometry of the satellite, and date of launch. One of the largest effects is the variation of solar heating to the atmosphere over the solar cycle (ref. 10). Because it is envisioned that the RRS will be flown many times over a period of many years, an analysis was conducted of the expected orbital lifetime at various altitudes of operation of the satellite. Upper atmospheric conditions which might occur over an entire solar cycle of 11 years were considered. Additionally, seasonal variations exist during any one year. These annual variations in density are thought to be due to the seasonal migration of helium within the atmosphere. For the anticipated spacecraft mass, coefficient of drag and frontal area, the orbital lifetime of the RRS is shown in figure 8(a) for a nominal and 2-sigma variations of the atmospheric models over a solar cycle from 1988 to 1999 for the single orbit altitude of 315 km. This figure shows the great variation in the lifetime during the solar cycle. Figure 8(b) then shows the lifetime of the RRS for a hypothetical launch date of January 1, 1993 as a function of altitude. It can be seen from results contained in the two figures that a minimum altitude of 315 km insures a mission lifetime of 60 days.

The decrease in altitude over the mission duration during the solar maximum year of 1991 and for a +2 sigma atmosphere model (the most difficult combination of conditions) is shown in figure 9. For the baseline orbit of 479 km, the loss in altitude is only 1.6 km over a 60-day mission. As discussed below, the attitude control system is used to maintain the orbital altitude over the mission duration thereby assuring integer-orbit-synchronization with the landing site.

Micro-Gravity Environment - During the orbital phase of the mission, the RRS is not continuously 3-axis stabilized, but is allowed to tumble very slowly according to the very small atmospheric pressure exerted on the exterior of the spacecraft. The

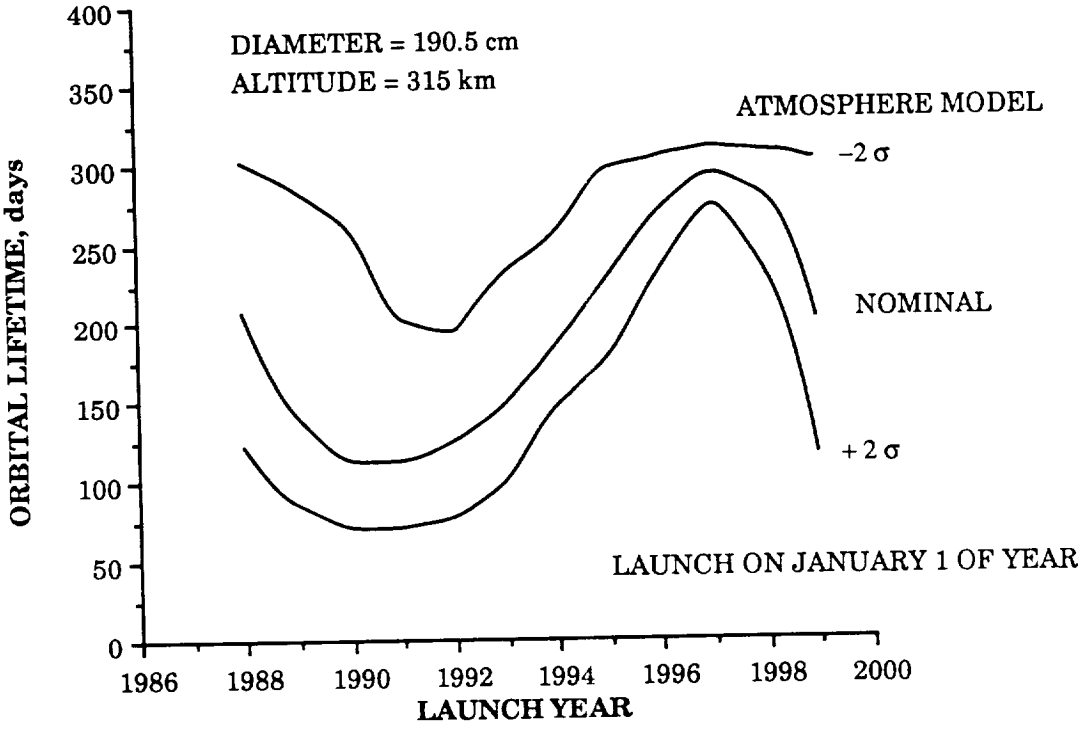

a) RRS Lifetime Over 11-Year Solar Cycle

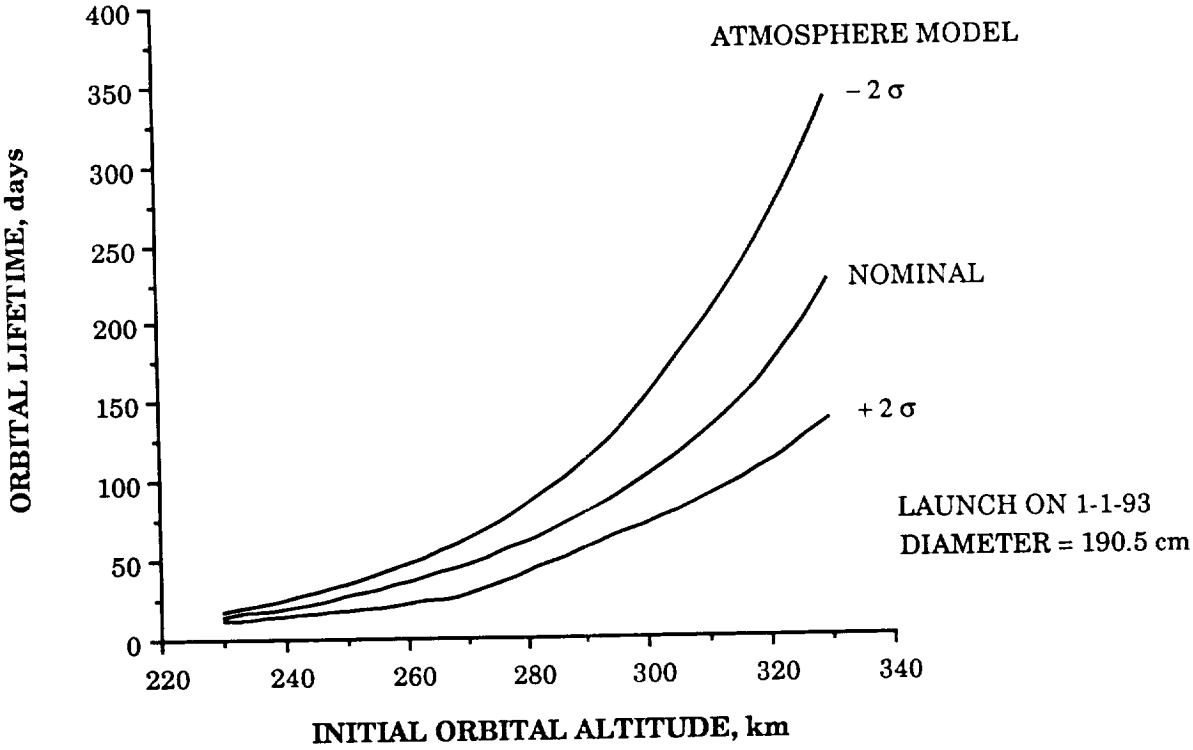

b) RRS Lifetime Versus Orbital Altitude

Figure 8. RRS Orbit Lifetime Analysis

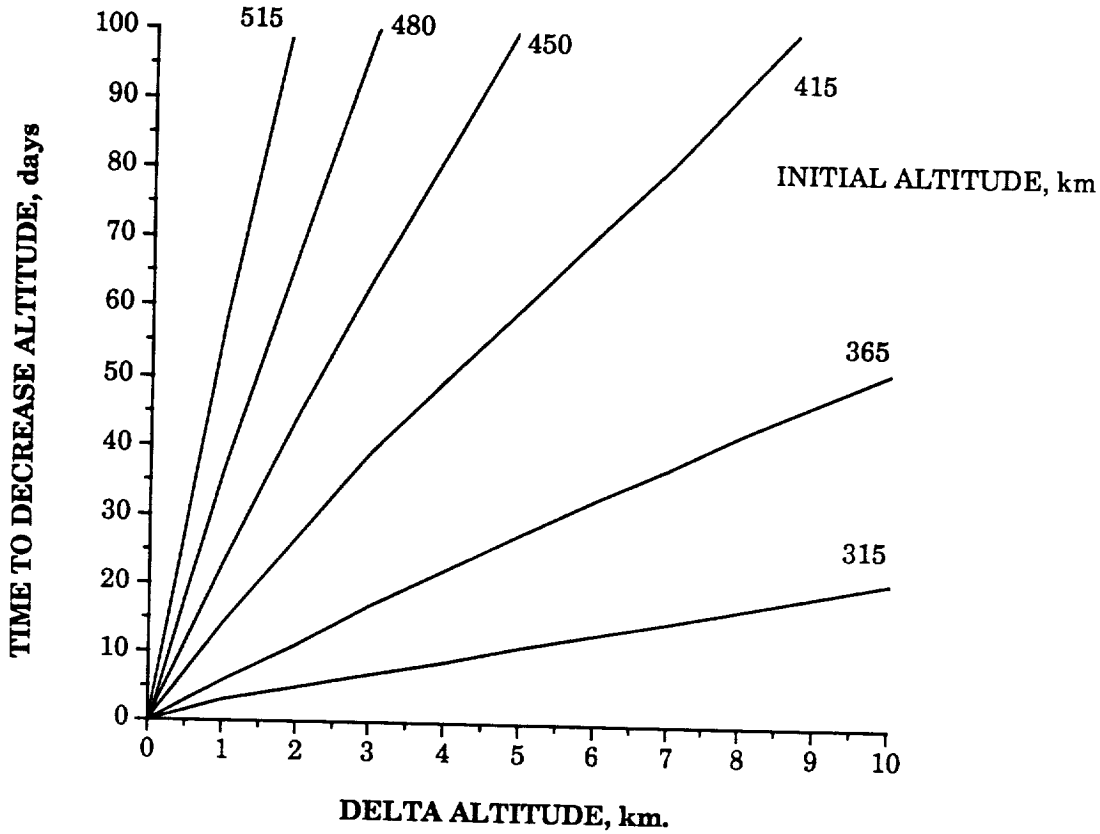

Figure 9. RRS Altitude Decay with Time

angular rates are uncontrolled, within limits, to provide a micro-gravity environment of less than 10^{-5} g for 95% of the mission. This is accomplished by rate sensors which activates the 3-axis attitude control system 4.5 N thrusters if the tumbling rate causes a acceleration environment in the PM to exceed 10^{-5} g. The ASCS thrusters have been sized to maintain the acceleration level below 10^{-3} g during the maneuver and angular-rate control periods. Analysis indicates that the aerodynamics torques affecting the attitude dynamics of the RRS for the operational orbits considered will not exceed the micro-gravity requirements (ref. 11).

Artificial Gravity - Some experimenters may wish to have a fractional artificial gravity environment at the periphery of the PM and this can be accomplished by the activation of spin thrusters which is capable of spinning the entire spacecraft about the RRS longitudinal axis so as to induce the desired fractional gravity from 0 to 1.5 g at the experiment station.

Operations - During orbital flight, the RRS and PM operates to support the experiments according to the planned experiment protocols. The RRS provides the utility services of power, thermal control, telemetry, and acceleration control. The PM is commanded by uplinked commands and by pre-planned command sequences

activated either by a timer or by direct uplinked commands. The PM also records experimental data as well as regular houskeeping and status data. Twice every day, communication periods are scheduled with ground stations for the uplinking of commands and the downlinking of telemetry. The downlinked telemetry is displayed and analyzed at the Lifesat Control Center to monitor the progress of the flight and to adjust the environment of identical life science ground control experiments (identical in environment except for micro-gravity) to correspond with the actual observed flight environment. The staff of the Lifesat Control Center maintains readiness to recover the RRS at the nominal end of the flight as well as at earlier opportunities if an early conclusion of the flight is needed. When the actual recovery time has been decided, the Lifesat Control Center commands the RRS to initiate the required recovery maneuvers and coordinate the recovery area activities to rapidly secure the RRS and remove the experiments from the PM.

Recovery Phase

Deorbit Maneuver - At the completion of the scheduled orbital flight phase (or sooner in the case of emergency), the vehicle is commanded by ground control, or by on-board sequence programmer commands, to position itself for the deorbit retro-thrust maneuver. If required, several days prior to this, the orbit period is trimmed, as required, to place the projected orbit track coincident with the landing site. The attitude control system makes measurements of the local horizon in two orthogonal directions and uses laser-gyroscope measurements to determine the flight direction. The ASCS thrusters are activated so as to position and stabilize the longitudinal axis (and therefore the thrust vector) in the correct attitude with respect to the orbital velocity vector. Dedicated 450 N thrusters then spin the vehicle about the longitudinal axis to approximately 60 rpm in order to inertially stabilize the thrust vector to within +/- 1° (3-sigma) relative to required deorbit attitude. This requires only a few seconds of thrusting. Thereafter, at the appropriate time, the main retro-rockets fire for approximately 15 sec to decelerate the vehicle and provide a sufficient velocity decrement to deorbit the RRS.

The main engine thrust imparts approximately 2 g load along the thrust axis from the aft to the nose of the RRS. The retro-rockets provide a 3-sigma performance within +/- 0.5 % of the advertised total impulse. The calculated 3-sigma landing dispersion ellipse for the above thrust application errors is shown in figure 10(a). In order to reduce these rather substantial landing dispersions, on-board accelerometers measure the acceleration level during the main engine burn and the actual velocity decrement achieved is computed by integrating the acceleration level with time; any off-nominal engine performance is trimmed to zero by the axial thrusters of the attitude control system. The resultant dispersion ellipse with this correction is about 6 km in radius as shown in figure 10(b). These values are for deorbit from the baseline 479 km orbit. If the RRS is placed in higher orbits, the dispersions are proportion-

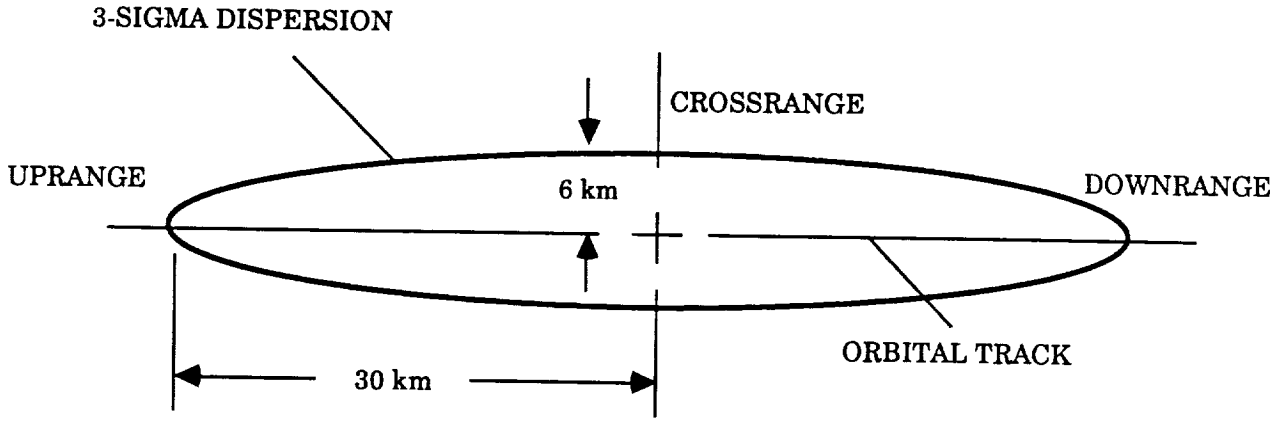

(a) Without Deorbit Thrust Tailoring

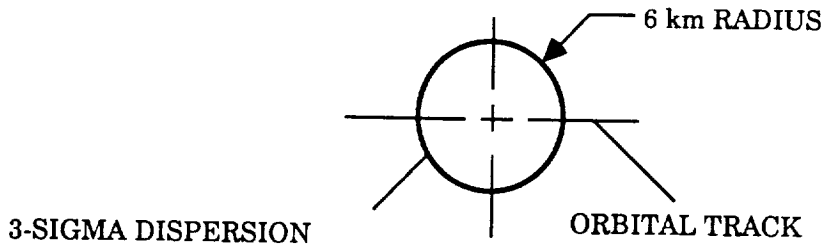

(b) With Deorbit Thrust Tailoring

Figure 10. RRS Landing Uncertainties

ately larger for the same amount of retro-propulsion. Figure 11 shows the effect on landing dispersions for various altitudes as a function of untrimmed deorbit velocity decrements. All precautions will be taken to insure public safety during this critical deorbit maneuver. If necessary, during this phase of the mission, an on-board destruct mechanism can be activated.

Reentry - Following the deorbit maneuver, a set of reverse spin thrusters despin the RRS to approximately 15 rpm prior to entering the upper atmosphere about 16 min after main engine cutoff. The RRS is spin stabilized during the deorbit trajectory from the deorbit maneuver to atmospheric reentry at an altitude of 120 km. The RRS retains the attitude of the deorbit burn maneuver and, as a result, encounters the atmosphere approximately 16 min after main engine burnout at an angle of attack of 80-90° depending primarily on orbit altitude. The RRS aerodynamic configuration is extremely stable and, at this low spin rate, the RRS quickly reorients itself into a nose-forward attitude. The anticipated axial reentry deceleration load is about 12 g, which occurs at approximately 35 km altitude about 19 min after main

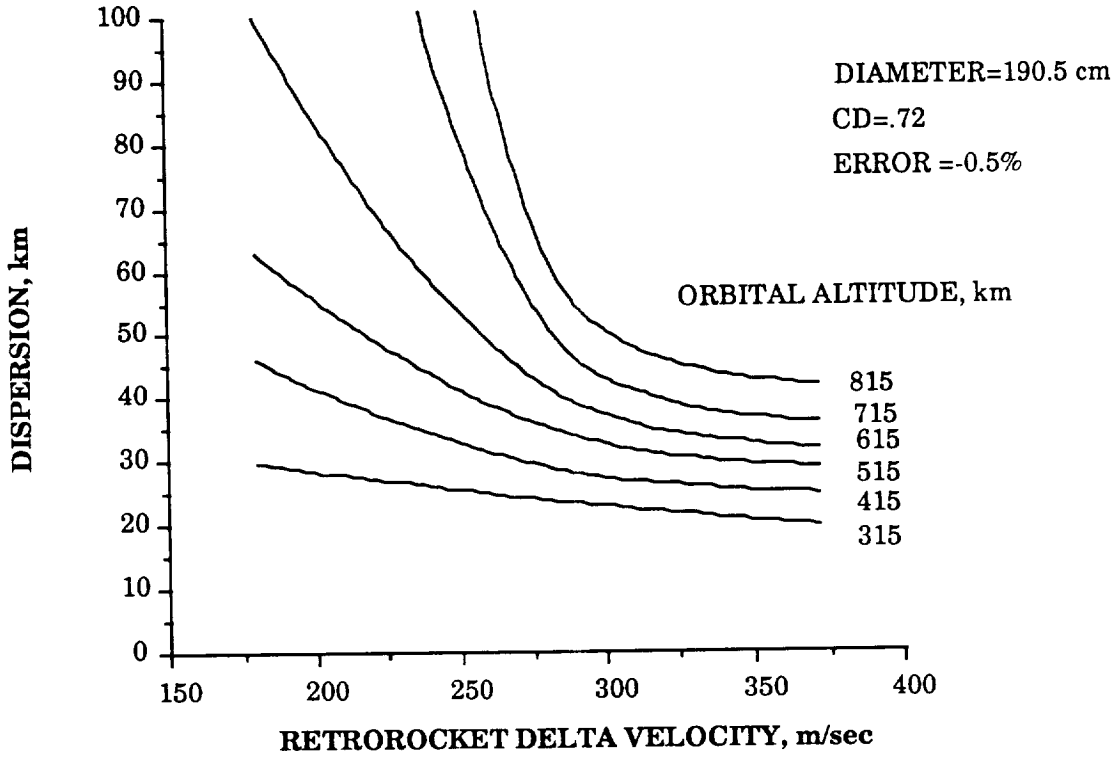

Figure 11. Dispersion Due to Error in Delta-v

engine burnout. A listing of the values of these and other characteristics of the reentry simulation is shown in Table 3. A summary of the time history of altitude, velocity, Mach number, acceleration, and stagnation-point heating rate for a typical atmospheric entry is shown in figure 12. The desired aim point is over the WSMR at 20 km altitude and in near-vertical descent. The RRS traverses approximately 69.7° of great circle arc along its deorbit trajectory from rocket burn to this position. A C-band radar transponder beacon is mounted on the RRS so that the landing site has knowledge of the vehicle track from reentry to landing.

Parachute Deployment - The RRS continues to descend over the WSMR through the altitude range of the generally prevalent high winds (i.e., the jet steam) to an altitude of, perhaps, 6000 m. At this point, a mortar deploys the pilot chute which pulls out the drogue chute, thereby slowing and stabilizing the vehicle. This deployment is commanded by timed sequence initiated by g-switches with a barometric switch as a backup. At the appropriate time, the drogue chute deploys the main parachute from the aft compartment of the RRS. This deployment may cause a 2 g deceleration load during the opening shock. The parachute may be of conventional form or may be a ram-air-filled lifting parafoil. The final choice is a matter for more detail engineering analysis.

If a conventional parachute is used, the RRS descends vertically to the ground

TABLE 3. REENTRY PROFILE DATA

MASS = 1130 kg
DELTAV = 290 m/s
H = 479 km
ß = 217 deg
VØ = 7.394822 km/s
GAMMAØ = -1.35237 deg

TIME (sec)	ALTITUDE (km)	VELOCITY (m/s)	LONGITUDE (deg)	QBAR (psf)	QCONV (Btu/f^2-s)	DECELERATION (G)	MACH NO.
0	123.3	7342	57.81	0	0.95	0	27.25
4	121.3	7344	58.07	0	1.09	0	27.26
8	119.3	7347	58.33	0	1.24	0	27.27
12	117.2	7349	58.58	0	1.41	0	27.28
16	115.2	7352	58.84	0	1.62	0	27.29
20	113.2	7354	59.1	0	1.86	0	27.3
24	111.2	7357	59.36	0	2.17	0	27.3
28	109.2	7360	59.62	0.1	2.54	0	27.31
32	107.2	7362	59.88	0.1	2.97	0	27.32
36	105.2	7365	60.14	0.1	3.48	0	27.33
40	103.1	7367	60.4	0.2	4.11	0	27.34
44	101.1	7370	60.66	0.2	4.90	0	27.35
48	99.1	7372	60.92	0.3	5.85	0	27.36
52	97.1	7375	61.18	0.5	7.00	0	27.37
56	95.1	7377	61.44	0.7	8.42	0.01	27.38
60	93.1	7379	61.7	1	10.19	0.01	27.39
64	91	7382	61.96	1.5	12.40	0.01	27.4
68	89	7384	62.22	2.2	15.06	0.02	27.4
72	87	7385	62.48	3.1	18.16	0.03	27.41
76	85	7387	62.75	4.6	21.88	0.04	27.41
80	82.9	7387	63.01	6.6	26.37	0.06	27.42
84	80.9	7387	63.27	9.6	31.77	0.09	27.42
88	78.9	7386	63.53	13.6	37.78	0.12	27.09
92	76.9	7383	63.79	18.6	44.18	0.17	26.52
96	74.9	7378	64.05	25.2	51.29	0.22	25.98
100	72.8	7370	64.31	33.6	59.14	0.3	25.45
104	70.8	7359	64.58	44.3	67.73	0.39	24.95
108	68.8	7344	64.84	57.8	77.04	0.51	24.46
112	66.8	7324	65.1	74.6	87.03	0.66	23.97
116	64.8	7297	65.36	95.3	97.61	0.84	23.49
120	62.8	7262	65.61	120.3	108.65	1.07	23
124	60.8	7218	65.87	151.3	120.37	1.34	22.58
128	58.8	7162	66.13	190.4	132.92	1.69	22.23
132	56.8	7090	66.38	237.5	145.50	2.11	21.85
136	54.8	7001	66.63	293.3	157.64	2.6	21.41
140	52.9	6890	66.88	358.2	168.76	3.18	20.93
144	50.9	6755	67.12	437.1	179.20	3.88	20.48

TIME (sec)	ALTITUDE (km)	VELOCITY (m/s)	LONGITUDE (deg)	QBAR (psf)	QCONV (Btu/f^2-s)	DECELERATION (G)	MACH NO.
148	49	6591	67.36	528.7	187.57	4.69	19.98
152	47.1	6392	67.59	632.1	192.92	5.6	19.41
156	45.2	6154	67.81	756.8	195.66	6.71	18.87
160	43.4	5870	68.03	890.2	193.11	7.89	18.17
164	41.5	5540	68.23	1024	184.49	9.08	17.32
168	39.8	5166	68.42	1147.5	169.76	10.18	16.3
172	38.1	4752	68.6	1247.4	149.76	11.06	15.14
176	36.5	4309	68.76	1311.6	126.29	11.63	13.86
180	34.9	3852	68.9	1331.6	101.67	11.81	12.5
184	33.4	3396	69.03	1305.9	78.25	11.58	11.12
188	32	2956	69.14	1237.6	57.75	10.97	9.76
192	30.7	2549	69.24	1129.1	41.00	10.01	8.44
196	29.4	2182	69.33	1006.6	28.38	8.93	7.24
200	28.2	1860	69.4	881.8	19.30	7.82	6.19
204	27	1581	69.46	762.7	12.96	6.76	5.27
208	25.9	1342	69.51	654.4	8.66	5.8	4.49
212	24.8	1140	69.55	559	5.77	4.96	3.82
216	23.8	970	69.59	477.2	3.86	4.23	3.26
220	22.8	827	69.62	408.1	2.60	3.62	2.79
224	21.8	708	69.64	350.8	1.76	3.11	2.39
228	20.8	609	69.67	303.7	1.22	2.69	2.06
232	19.8	527	69.69	265.2	0.85	2.35	1.79
236	18.9	459	69.7	233.8	0.60	2.07	1.56
240	17.9	404	69.71	209.1	0.44	1.85	1.37
244	17	358	69.72	190.2	0.33	1.69	1.21
248	16.1	321	69.73	175.9	0.25	1.56	1.09
252	15.2	290	69.74	165.4	0.20	1.47	0.98

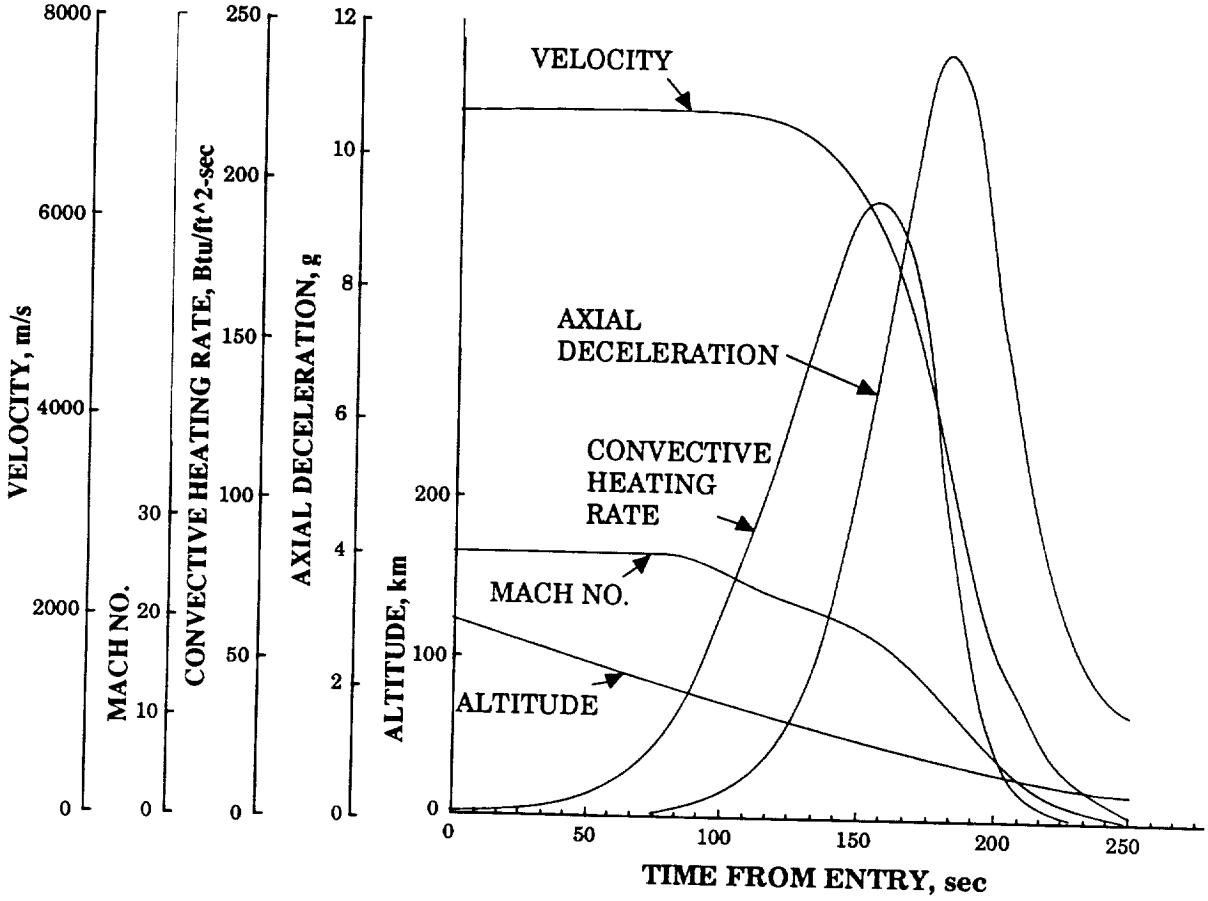

Figure 12. Reentry Profile of RRS

somewhere in the area defined by the nominal landing dispersions. If a parafoil is used, a lift-to-drag ratio of 3:1 (i.e., 3 m of horizontal motion to 1 m of vertical descent) appears feasible. Deployed at an altitude of about 6000 m the parafoil provides the RRS with a maneuvering circle of about 16 km in radius, which should encompass the extremes of dispersion due to the deorbit thrust maneuver. In the event that there is a malfunction of the parafoil control system or unpredicted winds should carry the descending vehicle in a direction away from the controlled space of WSMR, range safety considerations will require a pyrotechnic device be provided to sever the bridle lines of the parachute and permit a rapid descent of the vehicle.

Landing - Utilizing the descent capability of the conventional parachute, the RRS vehicle impacts the landing site at a vertical velocity as high as about 6 m/s. Various mechanisms such as crushable material may have to be included in the vehicle in order to absorb the impact loads and diminish their effects on the Payload Module. Landings using a conventional parachute should be possible under either

daylight or nighttime conditions.

If a parafoil is utilized, it should be possible to direct the descending vehicle to a prepared small area, perhaps 1-2 acres of soft material (possibly, sand), on which to land. Although it is considered feasible to provide autonomous homing, aerodynamic flare, and landing capability on-board the vehicle, a less technically challenging approach may be to position a ground-based "pilot" with hand-held radio controller to control the terminal approach into the local wind, the flare, and the landing maneuver. In this case, it is likely that daylight conditions may be required for the recovery operations. This may be a significant limitation on the use of shared launches.

Payload Access and Removal - Within a short time (perhaps only 10 min.) after touchdown of the RRS, Ground Support Equipment (GSE) is connected to the vehicle to provide the PM with necessary thermal control to dissipate the expected heating due to atmospheric reentry. External power may also be supplied at this time, however the spacecraft battery system should be functional. The RRS is designed to allow physical access to the PM within 2 hr of touchdown. This permits the experiments to be retrieved in the shortest possible time and transported to laboratories for analyses by the experiment investigators.

There are, at least, two ways to implement the removal of the PM from the RRS vehicle. The first is to remove the PM from the RRS and extract the experiments at the landing site. The desert conditions and the lack of proper facilities makes this very unattractive. The second and favored approach is to take appropriate actions to make the vehicle safe for transportation, immediately place the vehicle in a bag to prevent contamination, and transport the vehicle and GSE by helicopter sling to the NASA JSC White Sands Test Facility located just across a low range of mountains from the Northrup Strip recovery area (see fig. 4). At this location, there are high-bay and clean-room facilities to dismantle the RRS and PM in a controlled manner.

Refurbishment

Low cost and interchangeability - In order to provide access to many investigators, all operations and phases of the RRS mission must be accomplished at low cost while still maintaining a low risk to the program success and the highest possible public safety duing its operation. The RRS is designed such that all components, modules, and assemblies are physically and functionally interchangeable with spare units where feasible. Whenever possible, a component is designed to be reusable. Of course, some subsystems, such as the aeroshell ablative thermal protection material, the lithium thinoyl chloride batteries, and the main solid retro-rocket motors will have to be replaced.

Turn-Around Time - The goal of the RRS is to provide ready access to space on a frequent schedule. It is expected that a single RRS can be flown as often as three times a year. This requires that the space vehicle be refurbished, expendables replaced, and the vehicle be made ready for integration with another PM for a subsequent mission within 60 days after recovery of the prior mission. A RRS vehicle will undergo a set of appropriate tests before each launch. A 10-year program lifetime is contemplated.

SYSTEM DESCRIPTION

RRS Vehicle System

The RRS exterior configuration is a blunt non-lifting reentry vehicle similar in concept to the USAF Discoverer reentry vehicle, the NASA Biosatellite vehicle, or other recoverable military vehicles. A perspective drawing of the exterior configuration of the RRS is shown in figure 1. The principal differences between the RRS and the above vehicles are in the physical size of the vehicle and the subsystem changes necessary to permit a total intact, relatively soft recovery of the system on land and subsequent refurbishment and reflight with new and varied payloads. The system is currently envisioned to be capable of three flights per year over a 10-year program lifetime. The expected principal area of use for such a system is research on the effects of micro-gravity, artificial gravity, and radiation on small animals, plants, and lower life forms and tissue samples. Possible future uses might include the development of commercial materials and processes and the demonstration of new technologies in space.

The RRS vehicle is configured with a large and readily accessible volume for the PM which contains the experimental hardware as shown in the sectioned view in figure 2(a). A block diagram of essential functions and interrelationships is shown in figure 2(b). The PM is supported by the RRS vehicle which provides utility sources of electrical energy and dissipative thermal control, command signals, and limited downlink telemetry capability. The vehicle is also configured to permit the experimenter late access to the PM prior to launch and rapid access following landing. The various subsystems of RRS and their characteristics are described in detail in the material that follows.

Payload Modules

Most of the RRS experimental payloads are contained within one of several PMs, which, in turn, provide the interfaces with the RRS vehicle. In some very limited cases, where an experimental payload may not require any support during the mission, the payload could be mounted inside the payload envelope within the RRS,

but exterior to the PM. The PMs are designed to have simple interfaces with the RRS in order to allow easy accommodation of a variety of payloads. The PMs are also designed to have simple interfaces with the experiments.

The PMs receive utility services from the RRS vehicle which consist of: (a) unconditioned electrical power, (b) thermal control fluid, (c) command signals, and (d) timing signals. The PM provides experimental, internal environmental, and engineering data back to the RRS for transmission to the ground. The PM may also receive a few RRS measurements for inclusion in the PM data stream. The PM is mechanically supported by the RRS. A vent line to space is provided by the RRS for PM use.

The external envelope limitation for all PMs is a cylinder as shown in figure 13. The cylinder is 111.8 cm in diameter and 91.4 cm in length. The total mass limitation for a PM is 240 kg. The center of mass location must be forward of 40% of cylinder length. The inertia properties of the PM must be balanced about the longitudinal axis and must have a spin moment of inertia greater than 37.5 kg-m^2 and a pitch moment of inertia less than 22.8 kg-m^2 .

Several different PMs are currently envisioned for different types of payloads. An RM will be developed to house and support up to 12 rodents for as long as 60 days. A GBM will also be developed to contain and support groups of experiments in their own containers for also as long as 60 days. In addition, it is currently planned that a module will be developed to support hardware derived from the ESA Botany Facility for plant experimentation. It is conceivable that, rather than multiple life science PMs, a single life science support module might be developed to provide a controlled environment (i.e., atmospheric composition, humidity, and temperature). The experiment peculiar equipment, such as cages, cuvettes, or general biology experiment containers, could be integrated within this single container. That decision must await further science analysis and possible decisions of program participation by various foreign agencies.

Attitude and Spin Control Subsystem

Components - The ASCS of the RRS is comprised of a horizon sensors, laser rate gyroscopes, a spin/despin sensor, the control electronics, and several thruster assemblies. There are four sets of low thrust thruster assemblies which are mounted in protuberances on the base of the forward heatshield separated by 90° from each other as shown in figure 14. Each assembly has five thrusters (similar to the type used on the Agena Spacecraft as shown in figure 15) each capable of 2 to 6 N of thrust, depending on the tank pressure (ref. 12). The thrusters are oriented as follows: one facing forward (towards the nose of the RRS), one facing backward (in the same direction as the main retro-rocket engine), one facing radially outward, and two

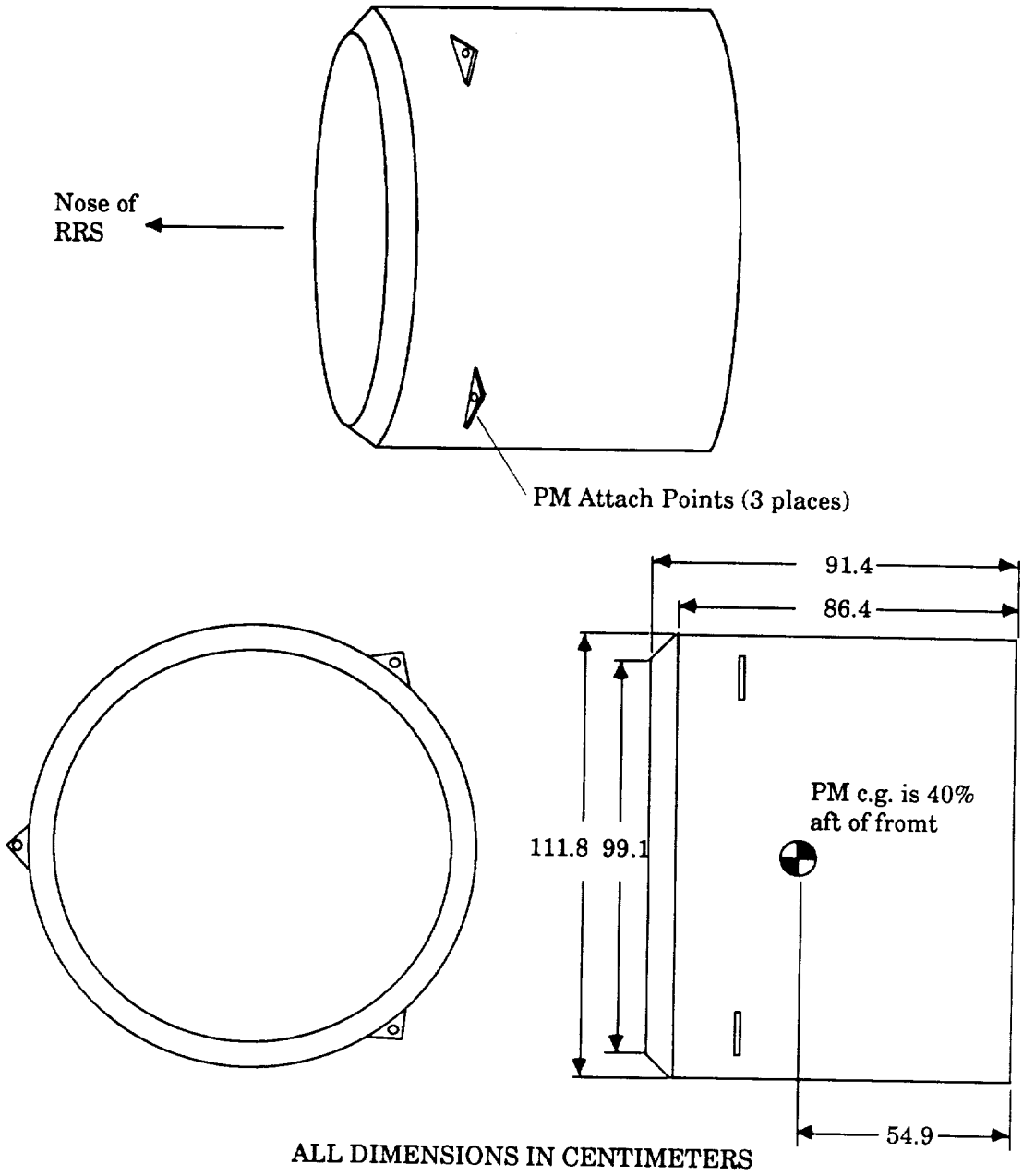

Figure 13. Payload Module External Envelope

facing tangentially outward and opposed to each other. The mounting of the thruster assemblies in protuberances is required to facilitate the forward firing of the attitude control thrusters. This mode is particularly important during the deorbit maneuver where forward directed thrust may be required to trim the magnitude of the deorbit maneuver and null any overburn error. The specific impulse of these thrusters is estimated to be approximately 230 sec in the continuous thrusting mode and approximately 140 sec in the pulsed mode.

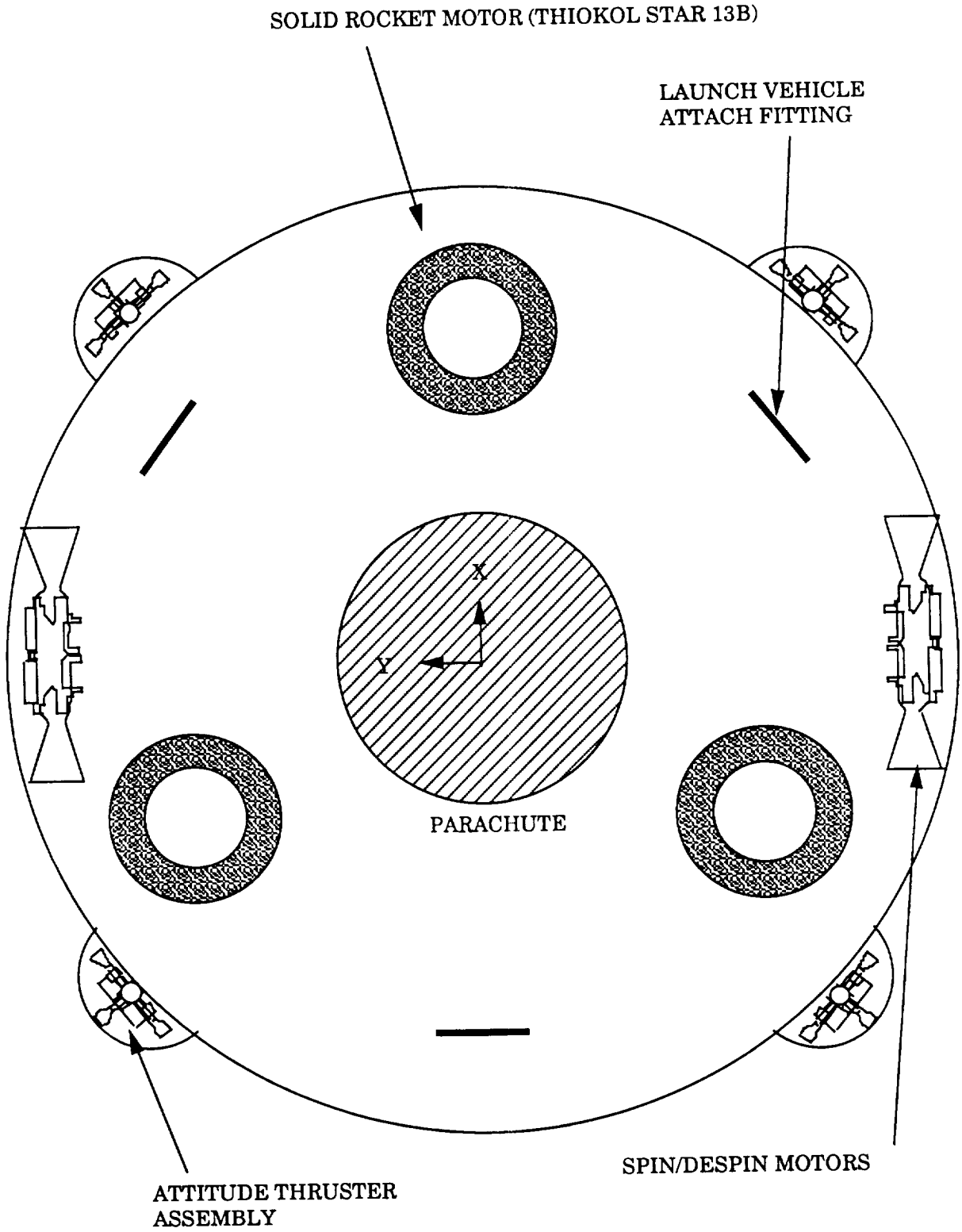

Figure 14. Aft View of RRS

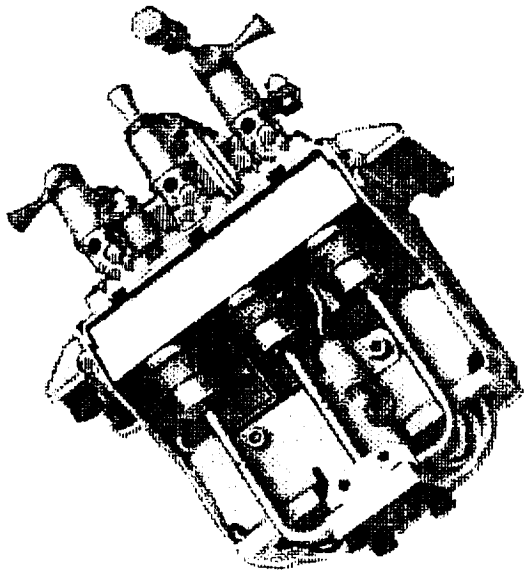

Figure 15. Typical Cluster of Hydrazine Thrusters

A separate set of spin/despin thrusters is provided on the RRS to: (a) spin the spacecraft in order to induce artificial gravity, and (b) spin the spacecraft to inertially fix the direction of the main retro-rocket thrust vector.

The common propellant for both the attitude control and spin control is hydrazine contained in titanium tanks (similar in construction to the Pioneer 10/11 tanks as shown in figure 16) pressurized by gaseous nitrogen (initially at approximately 2760 kPa) via a flexible bladder (ref. 13). The hydrazine is passed over a catalytic bed before expulsion from the nozzles. The thrust level is proportional to the nitrogen pressure in the tanks. The spin control system uses the same rate gyros and control electronics as the attitude control system, but has separate thrusters, valving, and plumbing. Four spin-control thrusters (two for spin-up, two for spin-down) are mounted on the aft cover as shown in figure 14. Each thruster is capable of approximately 450 N of thrust depending on remaining tank pressure (Private communication, Olin Rocket Research Company representatives).

The attitude of the RRS is determined by a 2-axis set of horizon sensors and a set of laser-gryoscopes. The horizon sensors determine the local nadir and the laser gyroscopes permit the determination of flight direction. This attitude information is processed by the control electronics which commands the appropriate set of thrusters to react.

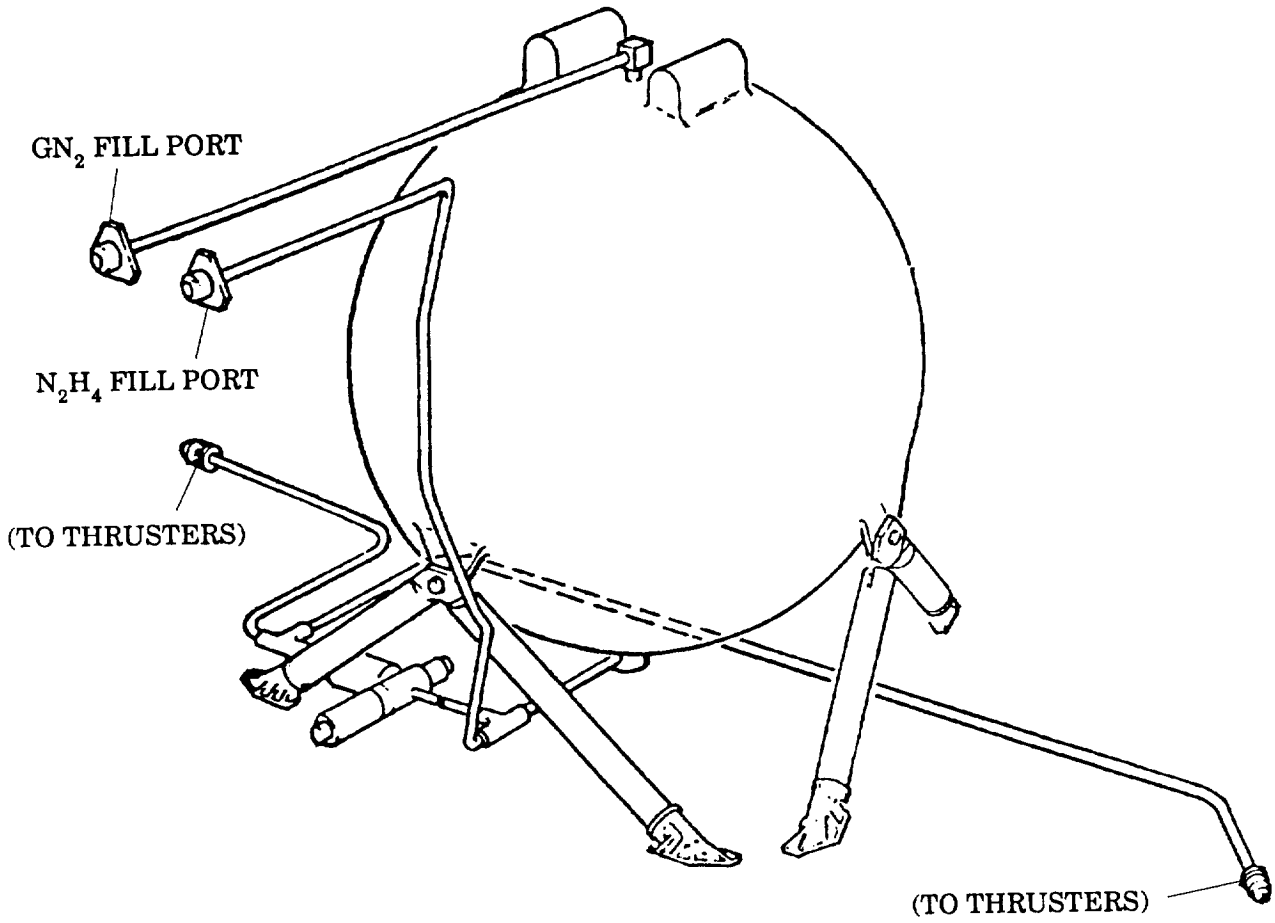

Figure 16. Typical Hydrazine/GN_2 Tank

Capabilities - The ASCS is used for a variety of functional tasks, as follows:

(a) to stabilize the RRS tumbling caused by outgassing;
(b) to correct errors in orbit placement caused by the launch vehicle and/or to trim the orbital period, as required, to adjust a projected orbital ground track to be coincident with the landing site in preparation for the deorbit maneuver;
(c) to stabilize, as required, the RRS from tumbling caused by atmospheric drag forces and solar radiation pressure and to maintain 10^{-5} g level for 95 % of the on-orbit mission;
(d) to maintain, as required, the spacecraft orbital altitude which is subject to

decay due to atmospheric drag;
(e) to stabilize the RRS before spin-up maneuvers;
(f) to spin the spacecraft about its longitudinal axis in order to induce artificial gravity;
(g) to spin the spacecraft about its longitudinal axis to inertially fix the direction of the main retro-rocket thrust vector; and
(h) to trim the deorbit maneuver, as required, to null the nominal 3-sigma errors in the performance of the solid rocket burn.

Each of the functional capabilities is discussed in detail below.

Outgassing Stabilization - After insertion into orbit, the spacecraft will outgas over a period of about 36 hr. The ASCS is used to stabilize the spacecraft and to counter the reaction of any further outgassing. Based upon the experience gained with the operation of Biosatellite (ref. 1), it is estimated that approximately 1.0 kg of propellant is required for this maneuver.

Launch Errors Correction and Landing Site Synchronization - Although it is anticipated that the launch vehicle will be capable of inserting the RRS into the desired orbit, there will be small errors in that orbit. If the launch is dedicated to the RRS and if an integer orbit scenario is selected, it is necessary to correct these small errors in the orbital parameters to obtain the desired orbital charateristics for an integer orbit. An estimate of the required maneuver capability to be provided by the RRS vehicle to correct these errors can be made based on the performance capabilities of the Delta II launch vehicle for a nominal due east launch into a low earth orbit. The following 3-sigma errors are possible (Private communication, McDonnell Douglas Astronautics Company representatives).

(a) semi-major axis = +/- 2.8 km
(b) eccentricity = +/- 0.0005
(c) inclination = +/- 0.010°
(d) longitude of ascending node = +/- 0.080°

After the correction of these orbital elements, the orbit ground track must still be phased with the landing site to achieve synchronization of the orbit ground tracks with the landing site. As discussed in the mission description section, a dedicated launch from the ETR or other launch site places the RRS in an orbit which, in general, must be adjusted to permit the necessary landing site synchronization. An ETR launch for the 35.65° inclination, 479 km altitude orbit results in an ascending node which is skewed by only 1° in longitude to the east from that which overflys the landing site in WSMR. This amount of nodal movement can readily be achieved with the on-board ASCS by increasing the semi-major axis of the orbit very slightly to allow a slightly longer period for a number of orbits until the orbital track takes the RRS over

the landing site. The orbit is then recircularized at the correct integer orbit altitude which synchronizes the orbit with the landing site. If an integer orbit is desired from another launch site, the maximum drift in the longitude of the ascending node is one-half the longitude shift between two adjacent orbit ground tracks; generally less than 8°. To limit the requirements on the RRS ACS, it may be attractive to deliberately launch into a slightly higher or lower orbit than that required for an integer orbit such that the orbit ground track will in the future drift over the landing site. The orbit can then be synchronized with the landing site using the ASCS. An analysis was conducted of the delta velocity requirements necessary to correct these possible errors using the on-board ASCS. The following velocity increment, ΔV, is needed to correct the orbital parameter. Based on a continuous thrusting mode, the ASCS requires approximately 11.8 kg of hydrazine to accomplish these corrections.

Element	ΔV, m/sec
(a) semi-major axis	1.7
(b) eccentricity	2.0
(c) inclination	1.3
(d) ascending node	5.4
(e) synchronization with landing site*	11.0
Total	21.4 m/sec

* Assumes the maximum longitude drift correction over 8 days.

If the RRS is on a shared launch and unable to achieve an integer orbit, there is no point in correcting the small orbital insertion errors or to synchronize the orbit ground tracks with the landing site at the start of the mission. Instead, all the fuel allotted to this function should be used to synchronize the ground track with the landing site at the end of the mission. As indicated in figure 6, about 22 m/sec are required to phase the orbital ground track to the landing site in 120 orbits or about 8 days. Thus the 11.8 kg of propellant allocated to launch insertion errors and synchronization of integer orbits to the landing site are sufficient to accomplish the phasing prior to deorbit for a shared launch scenario.

Microgravity Control - The RRS is capable of two modes of on-orbit attitude control to satisfy payload requirements. One mode, which provides artificial gravity, is discussed in the Spin/Despin Maneuvers and Artificial Gravity functional description sections below. For those experiments which require a micro-gravity environment, the attitude control system stabilizes the spacecraft about the three axes and then allows the RRS to float freely. The spacecraft is subject to the very low, but ever present, forces of atmospheric drag and solar radiation pressure which cause the RRS to slowly tumble. Rate gyros near the payload sense the rate of rotation in any of three axes and the centripetal acceleration on internal experiments caused by such

motion. When the acceleration level experienced at the payload due to the tumbling is nearly 10^{-5} g, the ASCS thrusters again stabilize the spacecraft by firing the necessary sequence of correctly oriented 4.5 N thrusters in a pulse mode. During these maneuvers, the g-level should not exceed 10^{-3} g. These maneuvers require 2.0 kg of propellant for a 60 day mission.

Atmospheric Drag Makeup - As discussed in the MISSION DESCRIPTION, the nominal orbital altitude of the RRS is about 479 km. Even during a year of maximum solar activity, at this altitude the atmospheric drag is small and the loss in altitude is minimal (1.6 km in 60 days). The fuel that must be provided to reboost the orbit to its desired altitude is 1.5 kg.

Spin/Despin Stabilization Maneuvers - The amount of ASCS propellant required to stabilize the RRS for spin-up maneuvers is estimated at 0.03 kg which is accomplished in a sequence of short pulses about all three axes. When the RRS is despun, an additional 0.03 kg of fuel is provided to stabilize any residual tumbling. To allow for two complete spin-up/spin-down maneuvers in orbit, a total of 0.12 kg of propellant is needed.

Artificial Gravity - In order to provide an artificial gravity environment at the periphery of the payload, the RRS can be spun about its longitudinal axis. Two of the 450 N spin thrusters (180° apart) fire and spin the spacecraft to the desired spin rate which simulates the required g-level at the payload module. For an artificial gravity level of 1.5 g at 53.3 cm from the longitudinal axis (approximately the floor of the rodent cages), 1.9 kg of fuel are required for the spin-up to 50 rpm. After the artificial gravity experiment is completed, the two despin thrusters are activated and a similar amount of fuel, 1.9 kg, is required for the spin-down maneuver.

Deorbit Thrust Vector Control - In preparation for the final retro-rocket thrust to deorbit the RRS, the ASCS will stabilize the spacecraft about all 3 axes and will align the thrust vector in the proper orientation. The spin-up thrusters then bring the spacecraft to approximately 60 rpm in order to inertially fix the thrust vector during the main engine burn. This maneuver consumes 1.7 kg of fuel. The spin-down maneuver to 15 rpm, in preparation for atmospheric reentry, consumes 1.2 kg of fuel.

Deorbit Maneuver Trim - The ASCS will also be used to provide a program of axial thrust to trim the main retro-rocket thrust and null out burn errors as discussed in the mission description. The amount of ASCS fuel needed for the deorbit trim maneuver, calculated for the worst case of main retro-rocket error of +/- 0.5%, is 7.1 N applied in the continuous thrusting mode.

ASCS Weight - Total propellant requirements for the ASCS for all velocity, attitude, and spin requirements is 29.5 kg which includes 23.8 kg for the maneuvers

described above and an additional 24%, or 5.7 kg, to allow for plume impingement (8%), leakage (4%), fuel trapped and therefore unusable (2%), and contingencies (10%).

Deorbit Propulsion Subsystem

A main rocket propulsion subsystem provides the required velocity decrement to deorbit the RRS and to place it nominally on a trajectory which is aimed at the landing site within WSMR. For the nominal 479 km altitude orbit, the velocity decrement required is 290 m/sec. For a RRS with an entry weight of approximately 1262 kg, three solid rocket motors similar to the Morton Thiokol Star 13B (ref. 14), as shown in figure 17, provide the required delta velocity. These engines provide about 347,000 N-sec with about 22,800 N of thrust over a burn time of about 15 sec. are fired simultaneously (within 2 msec. of each other, ref. 14). Each engine weighs about 47.2 kg. The propellant is aluminized ammonium perchlorate in a carboxyl terminated poly-butadiene binder. It has an effective specific impulse of 286 sec and delivers its total impulse to within +/- 0.5% (3-sigma). An actual delivered engine will be refined by the engine manufacturer to meet the stated specifications and is accompanied by an engineering report which will estimate its performance (probably well within the +/- 0.5%). As discussed in the section on ASCS, the impulse of the solid motors is measured and the axial ASCS thrusters are used to null out impulse dispersions in order to achieve an accurate landing footprint.

The engine is equipped with two pyrogen igniters which require approximately 4.5 amp firing current. Thermal batteries or the main battery supply the necessary current and a safe and arm device is included for the initiation. Following thrust initiation, the engine produces a thermal pulse which lasts approximately 10 min. The temperature on the outside of the casing, nearest the PM, approaches 370° C. Multilayer insulation and conduction isolation between the engine and the PM should be sufficient to prevent heating of the payload.

Structures

Loads - The Delta II is used for the preliminary launch vehicle interface studies, but others being considered for the RRS mission include possible commercial launch vehicles such as the Connestoga, Liberty, or Amroc vehicles. The RRS may also be a secondary payload on the Titan II or NASDA H-II. The launch loads selected for preliminary design encompass the greatest variation in environments expected for these vehicles. These load factors represent the superposition of maximum steady state, harmonic, and random accelerations from liftoff to orbit insertion.

Loads on the structure during normal orbital operation are limited to centri-

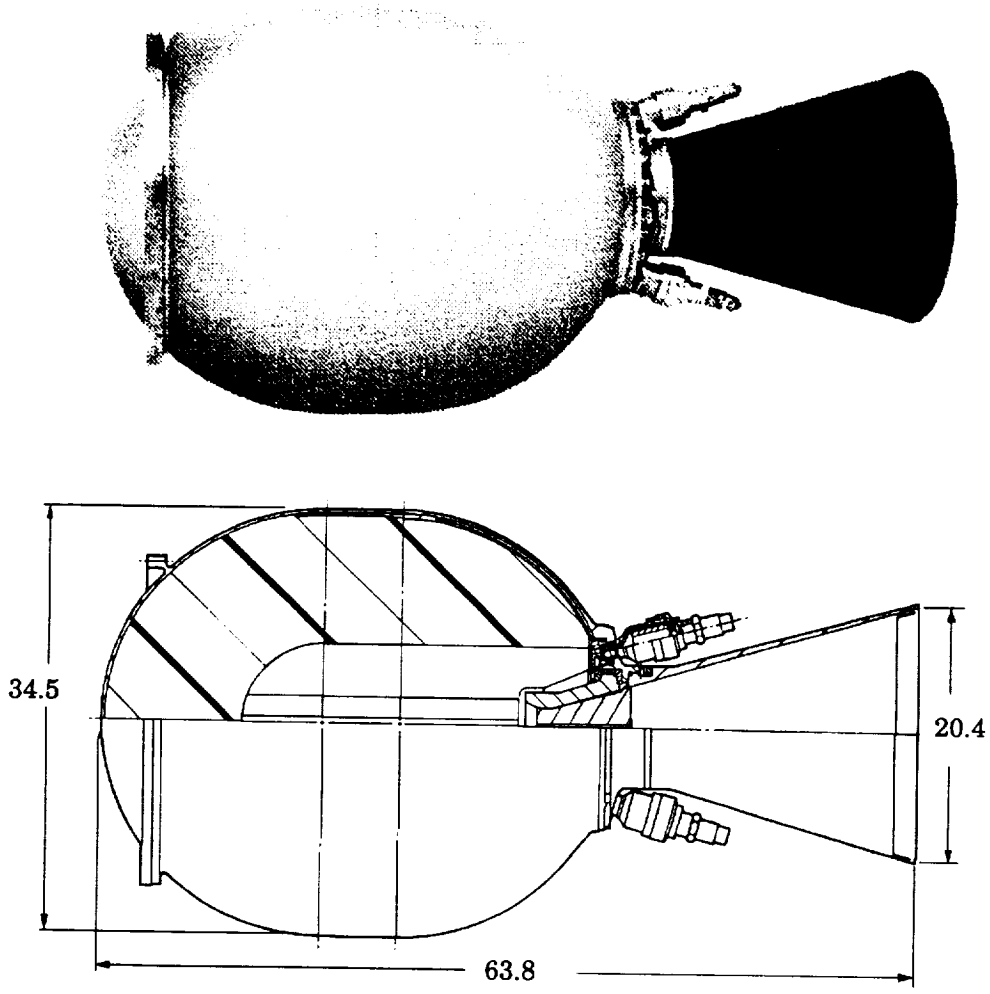

ALL DIMENSIONS IN CENTIMETERS

Figure 17. Star 13B Rocket Engine

fugual forces generated while the vehicle is spinning. Centrifugual loads are induced proportional to the radius from the vehicle centerline, up to ~3.8 g for the components mounted on the aft plate near the greatest diameter.

During the deorbit maneuver, the vehicle is spinning at up to 60 rpm and the retro-rockets fire providing approximately 22,700 N of thrust. For nominal thrust rise times (on the order of 50 msec), the dynamic response of the vehicle is not significant, assuming the natural frequency of the retro-rocket supporting structure is above 25 Hz. For preliminary design purposes, the load is considered as a static load, producing an average acceleration of 2 g.

The aerodynamic loads during reentry are somewhat dependent on the orbit characteristics and the vehicle attitude (angle of attack) at reentry. To encompass the greatest deceleration expected during the return from an eccentric orbit, a peak deceleration of 15 g is used for preliminary design. This deceleration, when reacted by the large frontal area of the spacecraft, produces quite low pressure loadings (~90 kPa) on the skin of the forward nose shell and midshell. By reefing the chute to deploy at a prescribed rate, the peak deceleration forces can be limited to 2 g in the axial direction. This load is applied at three equally spaced riser attach points on the aft cover. The peak load factor may be further reduced, if necessary, by using springs to attach the chute risers to the vehicle. Mortar firing to deploy the drogue chute induces a shock load into the aft panel and supporting structure. Because of the short duration of this impulse, it is considered to be an input of energy which must be absorbed by the surrounding structure.

Landing loads represent the greatest unknown in the loading environment, and are likely to greatly influence subsequent structural design and component placement efforts which are beyond this conceptual design effort. The severity of impact loads is influenced by operational procedures, design developments in the recovery system, and the recovery site ground characteristics. The duration of the landing impact determines the peak forces and the degree of dynamic shock loading on the vehicle. Expected maximum deceleration rates were used to derive equivalent static load factors for this preliminary design effort. The following table summarizes the loads assumed in the structural sizing effort.

Acceleration Load Factors for Preliminary Design:

Load Case	Axial, g	Lateral, g	Other Loads
Launch	8	2	
On Orbit	0	0	Spin 60 rpm
Deorbit Burn	2	0	Spin 60 rpm
Reentry	-15	0	Pressure ~ 90 kPa
Chute Deployment	-2	?	Additional shock from mortar firing
Landing Impact	-20	20	

All of the above load factors are multiplied by a factor of 1.5 to account for uncertainties in the expected environment and the analysis methods used. It is also assumed that all structure which is reused on subsequent flights must sustain these loads without detrimental permanent yield. More detailed structural design studies may indicate that some structural elements (e.g., the forward nosecap) should incorporate crushable materials to limit loads on the payload.

Structural Components - In order to reduce cost and development risk, the use of advanced materials or manufacturing methods has been avoided. Therefore, the baseline structural components are assumed to be composed of aluminum sheet or machined plate. The preferred alloy is 6061-T6, which combines high strength, corrosion resistance, and weldability. It is anticipated that other stuctural concerns beyond the scope of this conceptual design effort may direct the use of other alloys, metals, or composite materials. These concerns include the severity of landing impact loads, vehicle service life, refurbishment costs, the corrosion environment at the launch and recovery sites, weight restrictions, and material availability.

Figure 18 shows the primary structural components in cross section. The key elements selected for detailed design during this study were: the outer shell and aft plate, the inner conical cylinder, the PM mounts, the launch vehicle attachments, and the upper equipment shelf. Secondary structures, such as equipment brackets, are not shown in the figure. The total weight of secondary structure is estimated to be a maximum of 10% of the primary structure weight. The spherical and conical shells which form the outer shell of the vehicle support the heat shield and coolant loops and resist aerodynamic loads during reentry. No other major spacecraft components are mounted to the outer skin, so these shells are relatively light. Under the predicted pressures of reentry, membrane stresses are low, and the buckling margin of safety is high (refs. 15 and 16). Axial stringers strengthen the aft shell and improve buckling resistance. Rings at the field joint, at the juncture between the spherical and cylindrical segments, and at the aft plate provide resistance to local bending stresses. Impact loads are expected to be severe. Damage incurred during landing may preclude reusing the outer shell. A layer of expanded aluminum honeycomb or other crushable material will help absorb the energy of impact and protect the interior spacecraft components and PM.

The aft panel is a honeycomb sandwich panel which closes the vehicle and provides mounts for the retro-rockets, parachute, attitude control thrusters, spin/despin thrusters, and other spacecraft hardware. This provides bending strength for local point loads and attenuates shock and vibration. The expanded aluminum core is 10 mm thick and the aluminum face sheets are 0.4 mm thick.

The primary load path of the vehicle is through an inner conical cylinder. This structure extends parallel to the 10° half cone-angle of the outer shell from the aft plate to the PM mounting ring. The 2 mm thick shell is stiffened by axial stringers spaced every 12° around the circumference, and by rings spaced approximately every 11.4 cm along its length. Larger rings transfer lateral loads from the PM mounts, the retro-rocket thrust cone, and the aft plate. Six shear webs attach the inner frustrum to the outer shell. These webs are approximately 19.1 cm deep and 91.4 cm long. They are sized to 0.5 mm thick to withstand the largest axial shear loads during reentry deceleration. Batteries and other components are mounted between the axial

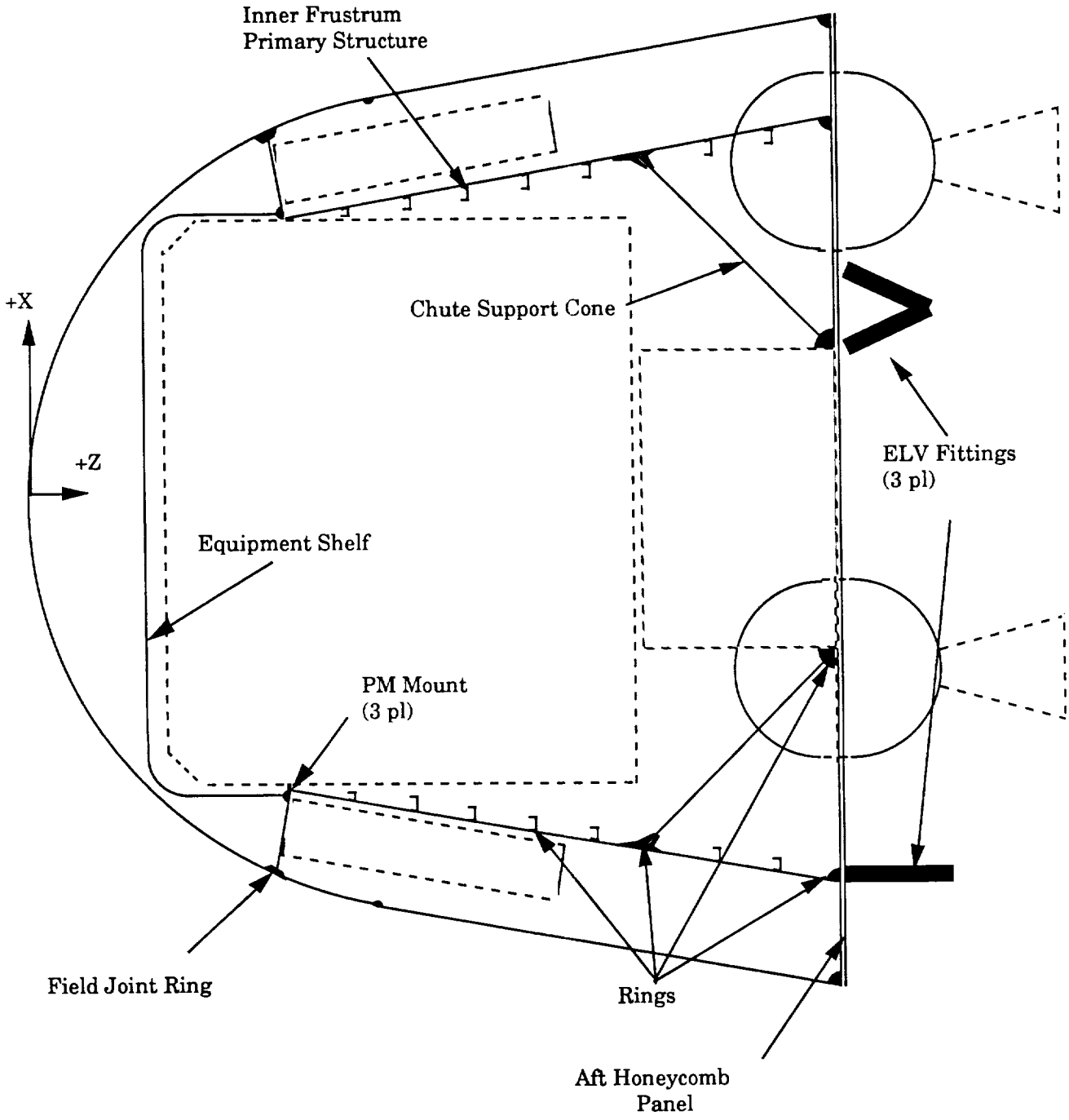

Figure 18. RRS Primary Structural Components

stiffeners and rings on the outer surface of the cylinder.

The PM is attached to the vehicle by a kinematic mount. A determinate interface between the vehicle and PM will ease integration, and structural loads due to deformations of the vehicle are not transmitted to the experimenter's hardware. The three PM mounts are at three points placed 120° apart around a ring 22.9 cm from the forward edge of the PM. The maximum tangential and axial loads from the PM depend slightly on the axial offset of the PM c.g. to the attach points. For the selected configuration under the loading cases considered, the maximum loads at a single attach point are 15,600 N axially and 31,600 N tangentially.

The equipment shelf provides a mount for batteries and other vehicle components forward of the payload module. The shelf is integrally attached to an upper cylinder which carries the load down to the main inner frustrum. The equipment shelf supports up to 113.3 kg of equipment at deceleration levels of 20 g's (during impact). The structure is sized to provide the required bending stiffness which ensures clearance between the equipment shelf and the PM below. The forward shelf is a honeycomb panel with a 10 mm thick expanded aluminum core and 0.5 mm aluminum face sheets (ref. 17). The 22.9 cm high support cylinder is 2 mm thick aluminum sheet. The equipment shelf and its support cylinder are bolted to the upper surface of the PM mounting ring after the last access to the PM on the launch pad. Electrical connections are made between the batteries and spacecraft systems on the equipment shelf and the rest of the RRS, and final checkout tests are performed before installing the forward nose shell.

An existing adapter fitting design developed for NASA's Multi-mission Modular Spacecraft is selected for mounting the RRS to the Delta II. Three attach points on a 152.4 cm diameter circle mount the spacecraft to the second stage. To provide clearance for the retro-rocket nozzle and access for the installation of explosive bolt catchers, three smaller fittings must extend 17.8 cm from the RRS aft panel to the separation plane. These fittings were sized to support a 1263 kg spacecraft with a mass center 99.0 cm above the separation plane.

Power Subsystem

The choice of type of power for the RRS mission is driven by a number of factors. First, the vehicle is randomly oriented during micro-gravity phases of the mission and is in a low Earth orbit where significant solar occultations occur every orbit making solar cell systems impractical. In addition, it is highly desirable that the development costs and the life-cycle costs for the RRS system and its operation be kept reasonably low. Fuel cells might be a possible choice for a power system which could have very low refurbishment cost, but the development cost of a light weight system might be prohibitively high. In addition, the complications associated with

cryogenic storage of reactants and a low volumetric packaging efficiency will undoubtedly cause further design problems for the RRS vehicle. For these reasons, a battery power system is chosen for this conceptual design effort. In particular, a lithium thionyl chloride ($Li/SOCl_2$) battery is assumed as the utility power source for the RRS vehicle and its PM. Lithium thionyl choride batteries have been developed and qualified for space applications (ref. 18) and are characterized by a high power density and volumetric efficiency and a high cell voltage.

The total electrical load for the RRS vehicle, sized for a 60 day mission, is 20 kW-hr. Table 4 shows the power allocation for the various subsystems. These values are based on experiences from Pioneer and Galileo Probe projects and current information from vendors. Note that there is a 7% contingency, which is listed as miscellaneous.

TABLE 4. SPACECRAFT POWER BUDGET

ITEM	POWER w	DUTY CYCLE %	AVERAGE POWER, w	TOTAL POWER, kwHr
SYSTEM POWER INTERFACE UNIT	1	10	0.1	0.1
COMMAND SUBSYSTEM UNIT	2	100	2.0	2.9
DATA HANDLING UNIT	2.5	100	2.5	3.6
INTERFACE ELECTRONICS (analog sensors, etc.)	2	100	2.0	2.9
CONTROL ELECTRONICS (air temp, pressure, humidity,etc.)	2	100	2.0	2.9
TRANSMITTER	10	1	0.1	0.1
RECEIVER	10	2	0.2	0.3
VOLTAGE CONVERTERS	2	100	2.0	2.9
THERMAL CONTROL PUMPS	4	50	2.0	2.9
MISC.	2	50	1.0	1.4
			TOTAL	20.0

A summary of the characteristics of the power subsystem is as follows:

(a) 28 V DC at 1.5 A steady state
(b) 65 kW-hr, with the following energy allocation:
    45 kW-hr for PM;
    20 kW-hr for RRS Vehicle
(c) Source impedance less than 0.1 ohm

This type of battery is selected because of the following characteristics:

(a) Very high density source
(b) Very long shelf life (10 years)
(c) Insensitive to temperature
(d) Insensitive to orientation
(e) Insensitive to rotation
(f) Insensitive to high accelerations
(g) Minimum voltage variation with peak load demands
(h) Minimum preparation
(i) Ease of module configuration
(j) Space flight history

The implementation and physical buildup of the battery system is very similar to a very recent system development by the Altus Corporation for John Hopkins University/Applied Physics Laboratory for use on a USAF spacecraft (ref. 18). The system is composed of 1170 F-size cells packaged in 130 battery submodules. The nominal open voltage of each cell is 3.2 V DC. Nine cells are connected in series to form the basic submodule with a nominal voltage of 28 V DC. Four of the these submodules are in turn are packaged together in a linear fashion to form a standard battery module as shown in figure 19. To take advantage of the high weight density, symmetry, and form factor, these battery modules are distributed and selectively located in the RRS to obtain the desired inertia properties for the vehicle. The majority of the modules are located about the PM in a conical band conforming to exterior half-cone angle and the remaining are located in the forward nosecap section of the vehicle as shown in figure 20. An increase in battery size could be accommodated with minimum perturbation of the spacecraft system layout. The submodule and module units are connected in a unique parallel combination. This is to allow for the switch-in and/or switch-out of selective blocks should an anomaly or an increased power demand occur during flight.

The battery package includes electrical and thermal protection. Diodes protect against reverse voltage charging or similar undesirable effects. Thermocouples protect against high temperature limits. The wiring harness has cross-strapping, test points, test connectors, as well as quick disconnects. The latter allows ease of module

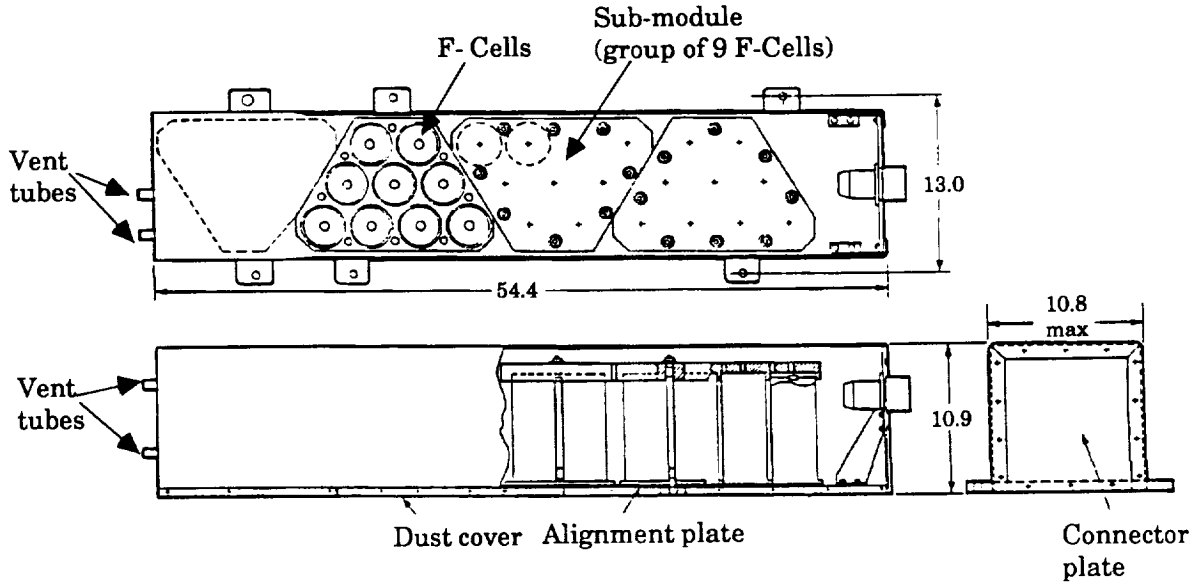

ALL DIMENSIONS IN CENTIMETERS

Figure 19. Typical Battery Module

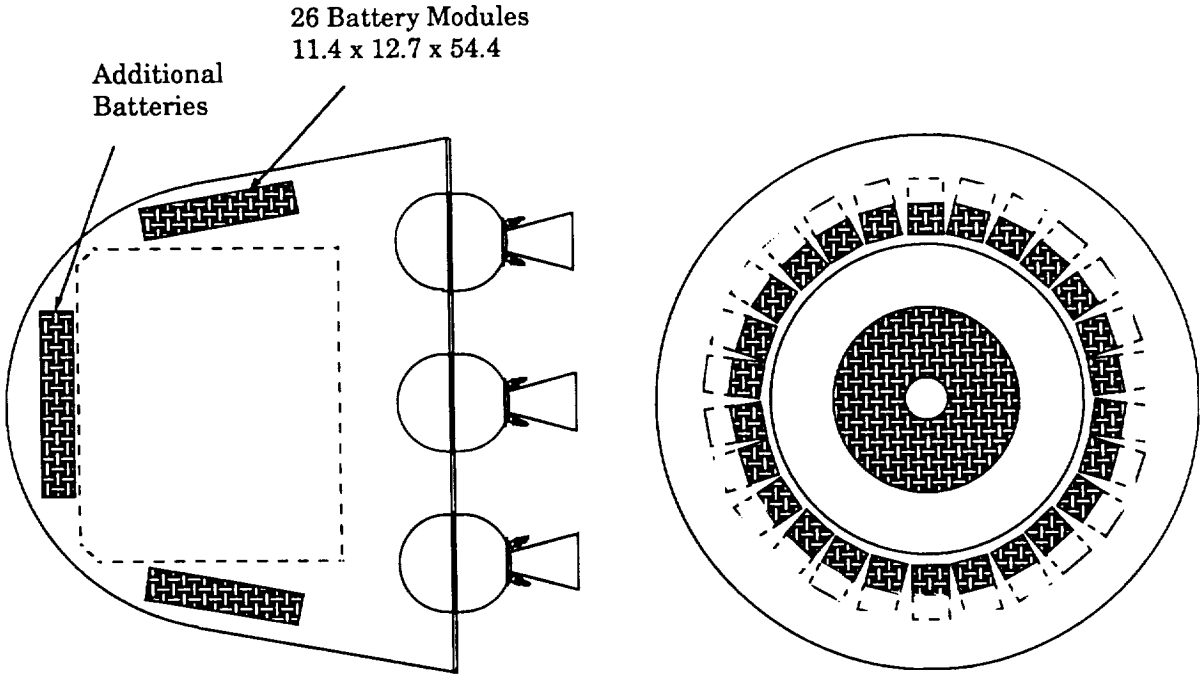

Figure 20. Location of Batteries Within the RRS

replacements without major rework. The total weight of the battery system is 239 kg and an additional 10.4 kg are required for wiring, connectors, and other electrical parts.

System Power Interface Units and Harness

The System Power Interface Unit (SPIU) controls and distributes primary power at 28 V DC to the PM and the RRS vehicle. The SPIU includes voltage regulation circuitry, switches, fuses, overvoltage protection, filters etc., to maintain normal power operation. Users in the PM can incorporate DC to DC converters for different voltages or electrical isolation requirements. Except for mission critical operations, all non-essential loads can be disconnected either automatically or by ground command. Switching circuits turn loads on or off as dictated by the RRS Sequencer Controller (SC) or by ground commands. In addition, redundant relays and logic switching circuits are included to provide alternate power paths if a failure is detected during a mission critical event. Based largely on a similar unit for the Galileo Probe (ref. 19), the weight and volume of the SPIU are as follows.

SPIU Weight:

(a) Housing	1.8 kg
(b) PC Cards	0.5
(c) Foam	0.3
(d) Relays	0.9
(e) Fuses	0.3
(f) Current Sensors	0.3
(g) Voltage Sensors	0.3
(h) Connectors	0.5
(i) Filters	0.5
(j) Misc	0.5
Total	5.9 kg
Cable Harness and Connectors: (Size 22 AWG Twisted Pairs, Copper Wire)	1.8 kg
SPIU Volume:	12.7 x 15.2 x 20.3 cm

Command Subsystem and Harness

The Command Subsystem Unit (CSU) provides commands to the RRS vehicle subsystems. Typical routine operations are controlled by stored commands issued by the RRS SC contained in the CSU. Commands can also originate in real time from

Earth or from a mission event. Real time commands may also be used to modify the stored commands in the SC. Appropriate electronics and logic circuitry protect against Single Event Upsets (SEU). A command hierarchy is used to protect against erroneous command operations affecting mission critical functions. The CSU issues commands to the PM via the PM Sequence Controller (PMSC). Most routine stored commands for the PM are issued in this manner. Real time commands may be used to alter this command structure. Based largely on a similar unit for the Galileo Probe (ref. 20), the estimated weight and volume of the CSU are as follows.

CSU Weight:

(a) Housing	0.9 kg
(b) Electronics	1.4
(c) Sequencer Controller	0.7
(d) Connectors	0.7
(e) Foam	0.2
(f) Misc	0.2
Total	4.1 kg
Cable Harness and Connectors: (Size 22 AWG Shielded Pairs, Copper Wire)	1.4 kg
CSU Volume:	7.6 x 17.8 x 20.3 cm

Communications Subsystem

The communications subsystem consist of a 10-W S-band transponder, oscillator, exciter, and omni-directional antennas. Because of the random orientation and limited power of the RRS vehicle, data are transmitted to and commands are received directly from ground stations rather than through the Tracking and Data Relay Satellite System (TDRSS). This decision should be examined in greater detail during future system design studies. During non-transmitting periods, data is stored for transmissions during a subsequent acquisition pass. A coding scheme is employed in the design to minimize bit errors. Based largely on a similar unit for the Galileo Probe (ref. 21), the weight, power, and volume of the communications system are as follows.

Communications Subsystem:

(a) Antennas	1.4 kg
(b) Transponders	4.5
(c) Wiring	0.5

(d) Oscillator	0.5
(e) Exciter	2.3
Total	9.1 kg
Input Power Required:	50 W
Volume:	10.2 x 20.3 x 50.8 cm

Data Handling Subsystem and Harness

The RRS accepts information from its subsystems and the PM in analog, serial digital, and bilevel digital form; converts the analog and bilevel information to serial digital form; incorporates bit error code; and arranges all information in an appropriate format for transmission to the ground station. Various combinations of bit rates and formats may be selected for a given mission. The data obtained during any non-transmitting period is stored for playback at a later time. The RRS supplies the PM with timing signals. Unique RRS events, such as parachute deployment, memory storage initiation, etc., are time tagged for mission profile reconstruction. It should be noted that the Data Handling Subsystem (DHS) is housed separately from the CSU. This is to allow maximum layout and configuration flexibility, as was done in the Pioneer spacecraft. Based on components of very similar units for the Galileo Probe (ref. 20) and the Pioneer spacecraft (ref. 13), the weight, power, and volume of the data handling subsystem are as follows.

Data Handling Subsystem Weight:

(a) Housing	1.4 kg
(b) Electronics & Microprocessor	4.5
(c) Memory Storage Unit	0.7
(d) "G" Switches	0.5
(e) Connectors	0.9
(f) Foam	0.2
Total	8.2 kg
Cable Harness and Connectors: (Size 22 AWG Shielded Pairs, Copper Wire)	1.8 kg
Volume:	7.6 x 22.9 x 40.6 cm

Note, if a television or frame camera is required in the PM, additional data capacity and timing signals are required.

Tracking Transponder

A C-band radar tracking transponder is installed in the RRS as an aid in recovery of the spacecraft. The type selected has been flight qualified and approved for use at WSMR (ref. 22). It is an ultraminiature moderate power transponder with low current drain and high sensitivity for small angle radar tracking applications. The general specification for a typical unit is given below.

General Characteristics:	
(a) Frequency Range:	5.4 to 5.9 GHz
(b) Trigger Sensitivity:	-65 dBm minimum
(c) Peak Power Output:	50 W minimum
(d) Nominal Operating Voltage:	+28 V DC
(e) Operating Stabilization Time:	3 min
Physical Specifications:	
(a) Dimensions (without protrusions):	10.8 x 8.9 x 5.1 cm
(b) Weight:	0.7 kg excluding mating power and antenna connectors

Antenna - The antenna system incompases three flush mounted circularly polarized cavity-backed helix units spaced 120° apart in order to achieve the desired pattern coverage. The total weight, including the power divider and cabling is 1.4 kg.

RRS Parachute Subsystem

The RRS parachute subsystem is designed to retard the RRS vehicle's vertical velocity and provide a relatively soft touchdown. Two types of parachute systems are conceptually possible for this application; a conventional type and a lifting parafoil. The lifting system has the advantage of being able to correct the 3-sigma dispersions associated with the deorbit and reentry trajectories by using its maneuverability to glide to a predetermined point. A further advantage is the ability to maneuver the parafoil into the local wind followed by an aerodynamic flare potentially making the ground touchdown very soft. The principal disadvantages are weight and operational complexity. For the purposes of this conceptual design study, a lifting parafoil system is described. The final choice of parachute system should be examined in detail in future system design studies.

The parafoil system consists of two ribbon type parachutes and a ram-air inflated parafoil type gliding parachute which are deployed sequentially. The first ribbon parachute, the pilot parachute, is deployed by mortar at a preselected time after the RRS encounters a preselected deceleration level during atmospheric entry. The inflated pilot parachute deploys a second, larger ribbon parachute, the decelera-

tion or drogue parachute, which, after inflation decelerates and stabilizes the RRS to a velocity and altitude suitable for the deployment of the reefed main parafoil parachute and below significant high altitude winds. The following table contains a breakout of the main components including their weight and volume. The total weight of the parachute system is approximately 60 kg which includes the pilot and drogue chutes, the main parafoil, and all pryotechnic devices, motors, and the control unit.

Summary of Parachute Subsystem:

Pilot Parachute: Similar to Galileo Probe (see ref. 23)

Design Type	20° Conical Ribbon
Constructed Diameter	1.14 m
Projected Diameter	0.74 m
Drag Area	0.51 m^2
Weight (including mortar)	2.13 kg
Volume of mortar	0.003 m^3

Drogue Parachute: Similar to Galileo Probe main parachute (see ref. 23)

Design Type	20° Conical Ribbon
Construction Diameter	3.80 m
Projected Diameter	2.47 m
Drag Area	5.46 m^2
Weight	5.95 kg
Packed Volume	0.013 m^3

Descent Parachute:

Design Type	Ram-Air Gliding Parafoil (ref. 24)
Lift-to-Drag Ratio	3:1 Approx.
Aspect Ratio	2:1
Span	15.85 m
Chord	7.92 m
Planform Area	125.6 m^2
Weight	29.5 kg
Packed Volume	0.046 m^3 at 640 kg/m^3 Density

Airborne Guidance Unit:

Weight	22.7 kg
Volume	0.06 m^3
Total System Weight:	60.3 kg

The deceleration parachute deploys the main descent parafoil parachute in a fully reefed condition. To reduce the opening loads, after a few seconds the parachute is partially disreefed and then, shortly thereafter, the parachute is fully disreefed and then becomes fully inflated. At that time the airborne guidance unit begins the process of homing in on the ground-based RF beacon. It is also conceivable that, instead of using a ground beacon, signals from the Global Positioning Satellite (GPS) system could be used to inertially guide the vehicle terminal descent. Late in the parafoil descent a manual operating mode may be substituted for the automatic homing mode. In the manual mode the parafoil responds to steering commands from a ground controller. At a short distance from the ground the parachute, either automatically or manually, is maneuvered into the local wind and initiates the flare maneuver to provide for a low impact ground touchdown. Figure 21 depicts the parachute deployment and landing sequence.

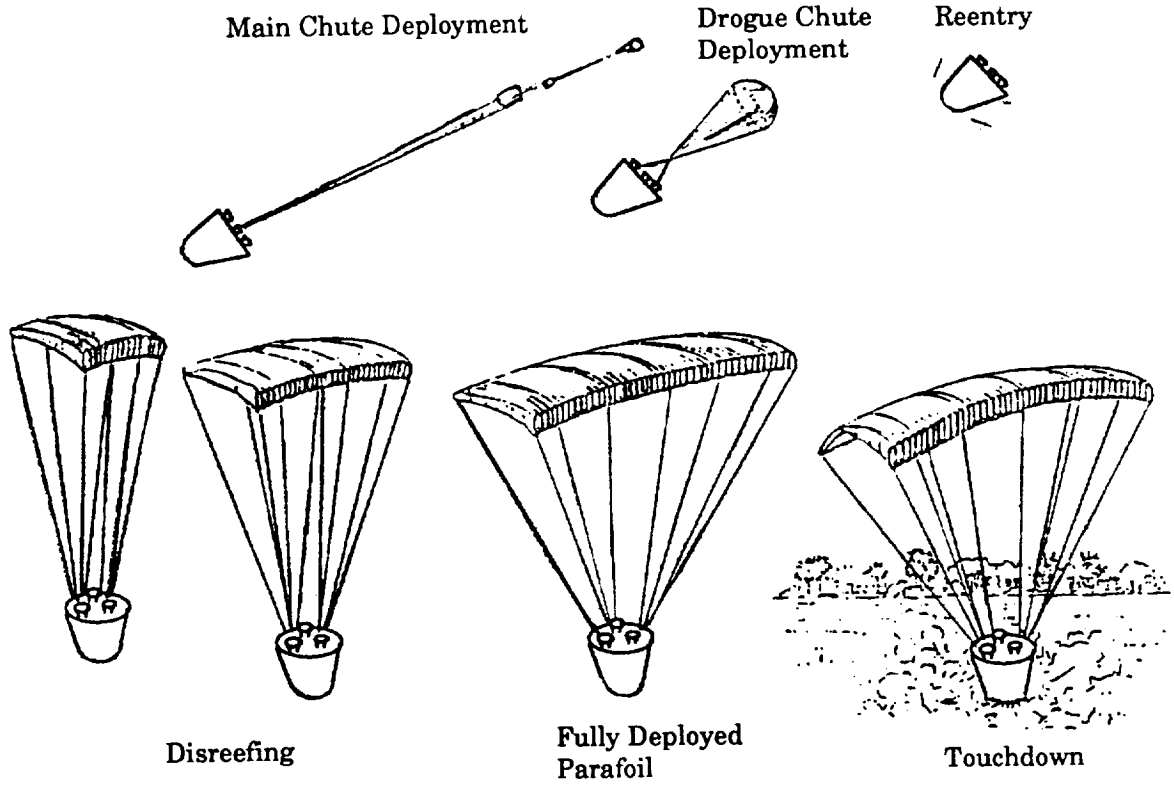

Figure 21. Parafoil Deployment and Landing Sequence

Reentry Thermal Protection System

The function of the reentry thermal protection system is to protect the vehicle from the aerothermodynamic heating which occurs during atmospheric entry. A typical stagnation point heating rate history during reentry is shown in figure 12. The variation of heating away from the stagnation point is shown in non-dimensional form in figure 22. For protection against the peak heating rates which occur near the stagnation point, an ablative system is the only feasible choice. For protection against the considerably lower heating rates which occur on the conical skirt of the vehicle, two types of thermal protection systems are feasible; the ablative type or a ceramic-based surface insulation type. The surface insulation type (similar to the blanket system used on the top surface of the Shuttle) does have a considerable advantage because of its reusability. However the rigors of handling and the landing impact could negate the system reusability. For the purposes of this conceptual design study, an all ablative system of a low-temperature ablative material, similar to Elastomeric Silicon Material (ESM), is used for the reentry thermal protection system. These materials can be formulated with a fairly wide range of densities and associated thermal conductivities.

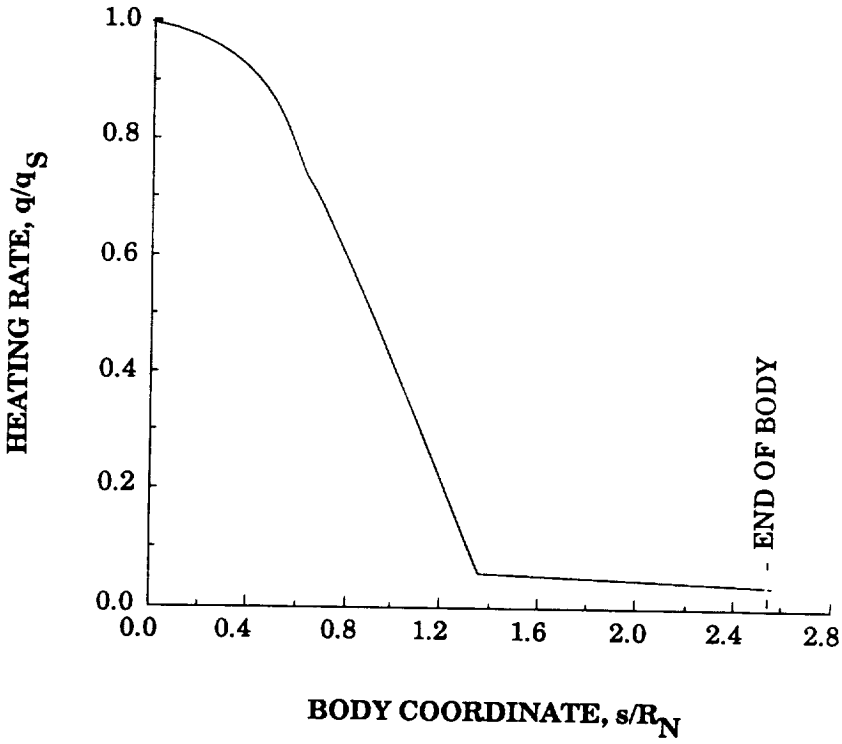

Figure 22. Reentry Heating Rate

The ablative thermal protection system is made up of two components. The first is the amount of material consumed or pyrolized by the absorption of the reentry heat pulse and the second is the amount of ablation material which must be left to insulate the aeroshell structure and heatshield bond line to keep it within safe temperature limits. This is particularly important during the longer-duration, low-speed descent to the ground because there is significant soakback of the heat, stored in the remaining heatshield material, to the aeroshell structure. The insulation of this heat must hold temperatures below the desired limits until appropriate cooling, supplied from GSE, can be provided after the landing.

The required thickness of the heatshield is determined using generic ablation and thermal properties, typical of several specific low-temperature ablation materials which could be used for this application. The final choice of ablation material properties is a subject of a detailed study beyond the scope of the current effort. However, experience indicates that the total weight of the thermal protection system, i.e., ablation plus insulation, is relatively insensitive to the specific properties assumed. If a material has superior ablative properties, the insulation requirements are generally larger and vise versa. The generic properties used in the analysis are indicated below.

Typical Abalative Material Properties:

Thermal Properties:

Density	1153 kg/m^3
Thermal Conductivity	0.294 J/m-K-sec
Specific Heat	517 J/kg-K

Ablative Properties:

Intrinsic Heat of Ablation	2326 kJ/kg
Ablator Blowing Efficiency	0.5
Pyrolysis Temperature	427 C

With the heat pulse shown in figure 12 and the above material properties, the ablation rates over the body and throughout the reentry trajectory can be calculated. The amount of material ablated, at a given body station, varies in the same non-dimensional way as the heating rate shown in figure 22. The amount of ablation varies from about 1.3 cm at the stagnation point to about 0.064 cm at the end of the skirt.

With the above thermal properties of the material and the calculated ablation rates as the surface boundary condition, the total amount of ablation plus insulation material requirements at several points around the body have been determined from

material requirements at several points around the body have been determined from one-dimensional transient moving-boundary heat conduction solutions at those points. Examples of these transient solutions are shown in figures 23(a), (b) and (c) for the stagnation point, a point 40° away from the stagnation point (i.e.,at $s/R_N = 0.7$ in fig. 22), and for a mid-point on the skirt, respectively.

At the stagnation point (fig. 23(a)), the surface temperature reaches the pyrolysis temperature of 427° C about 40 sec after atmospheric entry. The surface begins to ablate as shown until the heating rate at about 220 sec after entry drops to a value which no longer sustains the 427° C surface temperature. About 1.3 cm of material are ablated. The heating rate continues to decrease until about 260 sec when the aerdynamic heating stops. It can be seen from the figure that the backface temperature does not appreciably rise during the heat pulse. However, the stored heat in the outer material begins to soak back and an equilibrium temperature of about 145° C is eventually reached at the backface. The total amount of material required to achieve the equilibrium temperature of about 149° C is 2.0 cm. These calculations are conservative in that no account is taken for convective heat transfer from the forward surface of the heat shield material during the subsonic terminal descent.

Similar results are shown in figures 23(b) and (c) for other points on the body. Notice where the heating rate is high, the ablation requirements are also high and the insulation requirements are lower. At low heating rates (as on the conical skirt), the opposite situation occurs. The total ablation material requirement to keep the backface temperature below about 149° C is about 1.8 cm at a point about 40° away

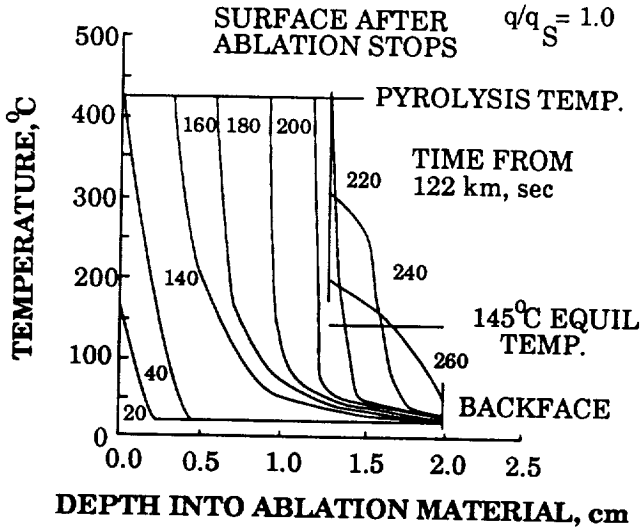

Figure 23(a). Transient Ablation Solution

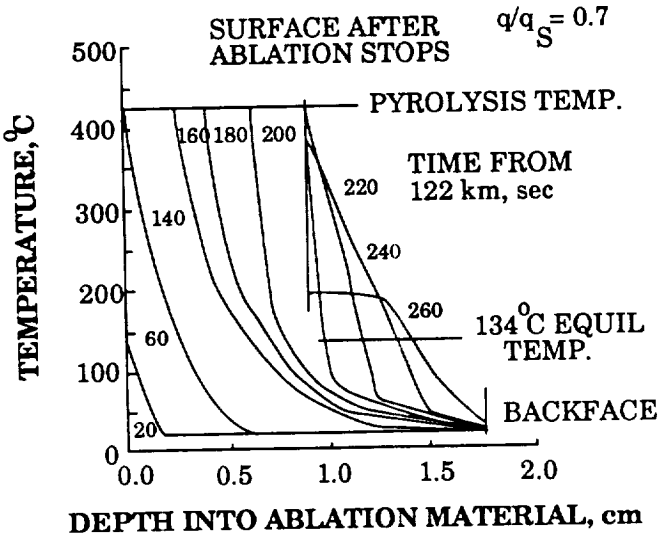

Figure 23(b). Transient Ablation Solution

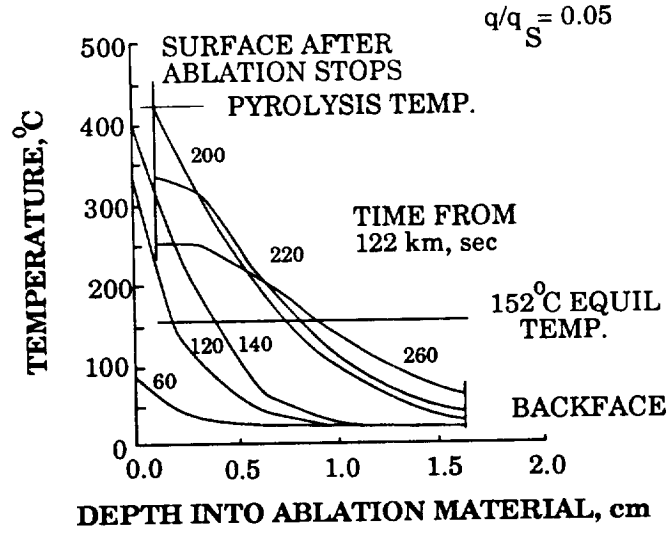

Figure 23(c). Transient Ablation Solution

The total amount of thermal protection material has been integrated over the body. About 64.0 kg of material is required on the nosecap (to the point of tangency with the skirt) and about is 73.1 kg is required for the conical skirt.

Thermal Control Subsystem

The RRS mission poses some unique design problems concerning the thermal control and management aspects of the spacecraft. Through the modular payload concept, the vehicle is intended to support and accommodate a wide range of payloads through a generic interface. This wide range of payload types with different associated thermal requirements also implies that the RRS vehicle and payload thermal control system must be capable of accommodating a wide range of thermal loads. The total heat generation capacity of the RRS support subsystems, due to electrical power dissipation, averages about 15 W over the duration of the mission. The total electrical power supplied to the PM is 45 kW-hr so that, for missions of 30 to 60 days, an average heat generation of 30 to 60 W must be considered. In addition, the biological specimens also generate some heat. For example, the 12 rodents generate an average of about 30 W. Therefore, the thermal control system for the RRS must be capabable of rejecting about 105 W.

A further constraint on the design of the thermal control system is the requirement that the vehicle is to be recovered intact at the end of the mission for further reuse. The Biosatellite vehicle flown in the 1960s had an adapter module which contained all of the housekeeping functions. At the termination of the orbital phase of the mission, the adapter module, along with other system components, were separated and left in orbit. An active cooling system is used in which a coolant is pumped through the PM section and to radiator panels located on the exterior of the adapter module. The RRS mission concept of high reusability does not permit the use of an expendable adapter which houses the environmental control system. Rather, all of the components of the thermal control system are housed within the entry vehicle itself.

Because of the limited power capability of the RRS, a passive thermal control system was first examined. Such a system consists of heat pipes which transport heat from the insulated payload cavity to a radiator on the aft or skirt section of the vehicle. The passive system was rejected for various reasons. First, the use of heat pipes does not allow for the tight temperature range specified for the PM. Second, if a different temperature or humidity set point is desired, it is difficult to adjust the heat pipes. Lastly, the transient behavior of heat pipes is very non-linear.

Thus, it is evident that an active, power consuming system is necessary to meet the science and mission requirements. For simplicity, it is desirable that the cooling

the science and mission requirements. For simplicity, it is desirable that the cooling system operate by providing a moderately cold operating fluid (about 0° C) to the PM and spacecraft systems. Because the PM and other spacecraft subsystems tend to operate at about 20° C, the warm side of the fluid loop and radiator should operate at about the 20° C temperature level. The design issue then arises concerning the appropriate location of the required radiator, given the design constraints.

The aft cover, at first, seems an immediate choice for the location of the radiator. However, there are several problems. First, the aft cover is already cluttered with a variety of rocket motors and the parachute cover severely limiting the available area and that area has an unfavorable view factor with the retro-rocket nozzles. Second, the addition of cooling lines greatly impacts the design and increases the complexity of the aft cover. Finally, with a randomly oriented vehicle there are times when the aft cover is pointing at the sun and the capability of radiator to dissipate heat is greatly decreased.

The other possibility is to use the vehicle conical midsection as the location of the radiator. The difficulty with this is that, even though there is over 4.65 m^2 for a radiating area, heat must first be conducted across an insulator (i.e., the reentry heat shield) before being radiated to space by the exterior surface. Such a radiator configuration is shown in figure 24. Note that there are five circumferential radiator tubes which are attached to the aeroshell inner structure. The tubes are spaced 17.8 cm apart. The radiator tubes are fed through a longitudinal inlet manifold and the cooled fluid is removed through an outlet manifold located 180° from the inlet manifold. The diagram of the operation of the thermal control system is shown in figure 25. A control unit senses the temperature in the accumulator and controls the position of the bypass valve control the fluid temperature. The estimated subsystem mass for the thermal control system is 37.2 kg for tubing and cooling fluid and two pumps.

In order to analyze the effectiveness of the conical skirt radiator, a number of factors must be considered. The first is the orbital operations of the spacecraft. The spacecraft is either very slowly drifting in attitude to maintain a micro-gravity environment of 10^{-5} g or is spinning rather rapidly (up to 50 rpm) to provide artificial gravity. The second most important consideration is that the vehicle is in a moderately inclined, low orbit and is therefore subject to alternate sunlight and occultation and to reflected and emitted light from the Earth. A schematic of the thermal behavior of the radiator is illustrated by the section view of an element of radiator area in figure 26. The fluid is introduced into the fluid loop at a temperature of T_f (20° C at the inlet) and exits at the desired cool temperature of 0° C, therefore circumferentially the fluid temperature varies from 20° C to 0° C. The heat from the fluid, q_f, is dissipated by conduction through the ablator to the surface at temperature T_s. At the surface, the heat is then radiated away. The surface is, however, exposed to variable

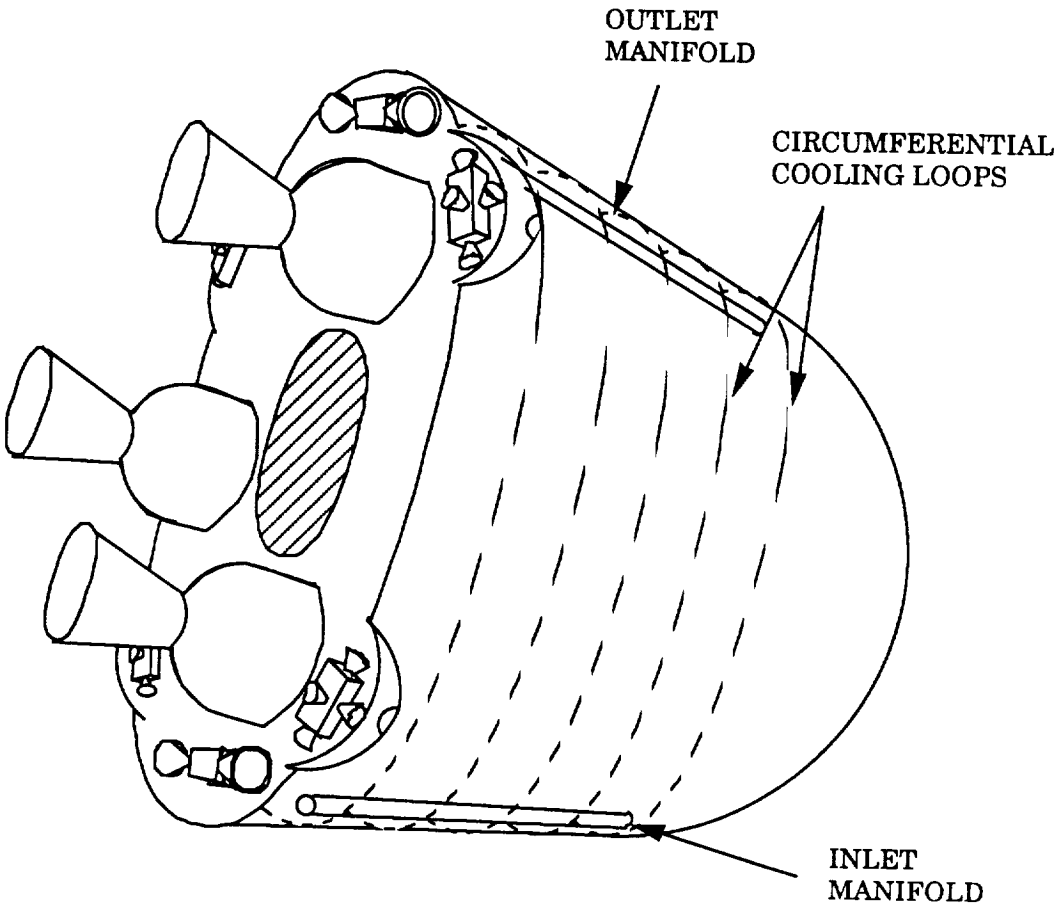

Figure 24. Orientation of Thermal Control Loops

amounts of solar radiation and thermal emission from the Earth. To enhance the effectiveness of the radiator, the surface is coated with a low-absorptivity surface material. A surface absorptivity of 0.16 and a surface emissivity of 0.8 is used. In addition, the radiator backface is covered with a low-density insulation to prevent the heat in the fluid loop from being conducted or radiated to the interior of the vehicle.

To determine the effectiveness of the radiator, consider first the non-spinning case with the longitudinal axis of the vehicle perpendicular to the direction to the sun and perpendicular to the orbit plane. This orientation is a very conservative case which maximizes the solar and Earth emission inputs to the radiator. Consider also the case where the vehicle is inserted into orbit at the morning terminator such that it immediately proceeds into sunlight along its orbital path. This condition presents the worst transient starting condition for the radiator operation.

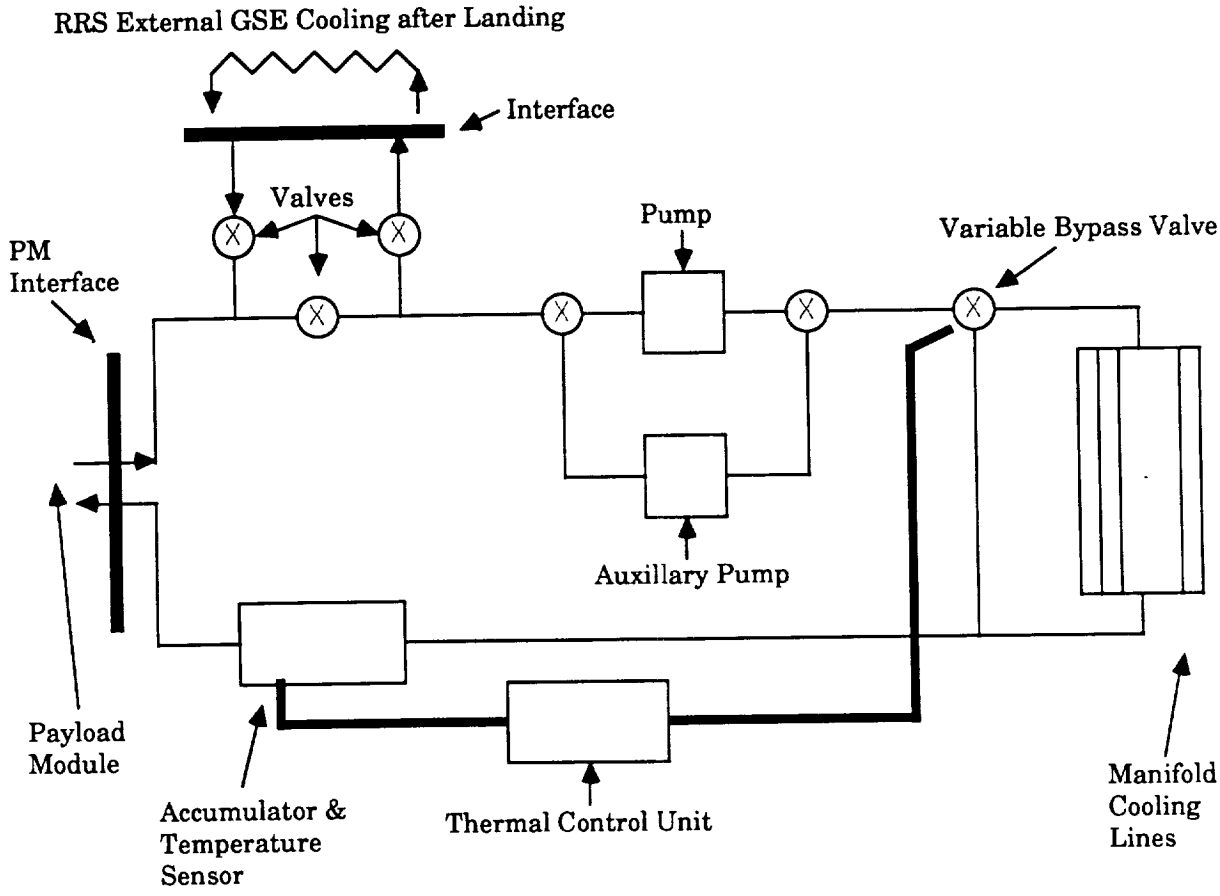

Figure 25. Thermal Control Subsystem

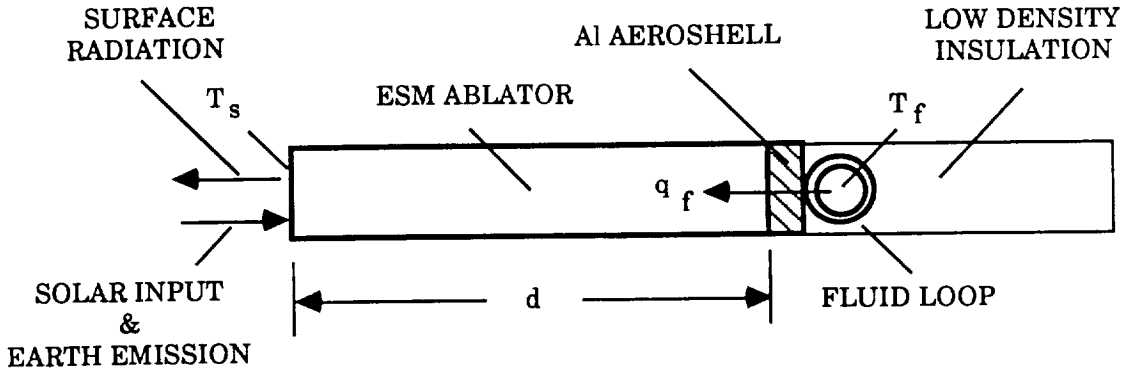

Figure 26. Thermal Control System Schematic

Because the vehicle is nearly stable in inertial orientation, each element of the radiator is exposed to different and time variable external thermal environments. The circumferential element of area which is perpendicular to the direction to the sun ($\theta = 0°$) is exposed directly to the sun for the first half orbit followed by exposure to the emission from Earth during the occultation period for the second half orbit. The peak thermal emission of the Earth is similar to that of a 293 K black body. Because the spacecraft is in a low Earth orbit, the Earth is viewed as an extended source radiating on the side of the vehicle towards it in a uniform manner. The transient response of that radiator element for the first one and one-half orbits is shown in figure 27(a). The curve with open square symbols is the transient response of the surface temperature, T_s. The curve with the solid diamond symbols is the transient dissipative heat flux, q_f, from the fluid loop. The temperature of the fluid is 293 K (20° C) so that this case is representative of an element very near the inlet manifold. The ablation material on the conical skirt of the vehicle (1.3 cm thick) has a time constant for thermal diffusion of about 8 min. Therefore, the ablative material achieves steady state conditions in a period of time of two to three time constants or about 20 min. This period is short compared with the time period spent by the vehicle in either sunlight or occultation so the radiator responds in a nearly square-wave fashion to the imposed exterior thermal environment as indicated in the figure. As can be seen from the figure, the surface temperature initially cools from the assumed launch temperature of 293 K (20° C) to slightly less than 288 K (15° C) and the dissipated heat flux from the fluid loop at this location is about 397 kJ/m^2-hr. As the spacecraft moves into solar occultation, the surface temperature drops to about 283 K (10° C) and the dissipative heat flux increases to about 852 kJ/m^2-hr.

The circumferential element of area which is oriented parallel to the direction to the sun ($\theta = 90°$) is not exposed to sunlight and views only free space, but after one-quarter orbit, it begins to be exposed to the Earth emission. This exposure lasts for one-half orbit until the surface again views only free space. The transient behavior of this surface element is shown in figure 27(b). It can be seen for this radiator area element, that the suface temperature varies between 281 to 283 K (8° to 10° C). The dissipative heat flux vaies from 852 to 1022 kJ/m^2-hr.

The circumferential element of area which is oriented exactly opposed to the direction to the sun ($\theta = 180°$) is never exposed to sunlight, but is exposed to Earth emission during the first half of the orbit. The second half of the orbit it views only free space. The transient behavior is shown in figure 27(c). Here the surface temperature also varies from 281 to 283 K (8° to 10° C) and the dissipative heat flux varies from 852 to 1022 kJ/m^2-hr.

Very similar results are obtained for a location on the inner skin near the outlet manifold where the fluid temperature is 0° C. However, the levels of dissipative heat

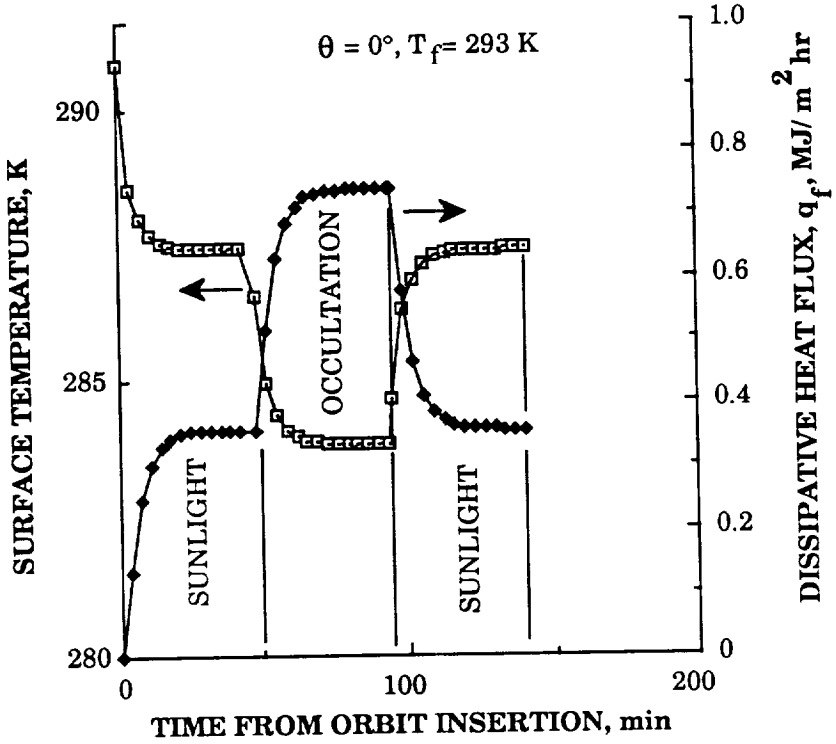

Figure 27(a) Transient Response of Radiator

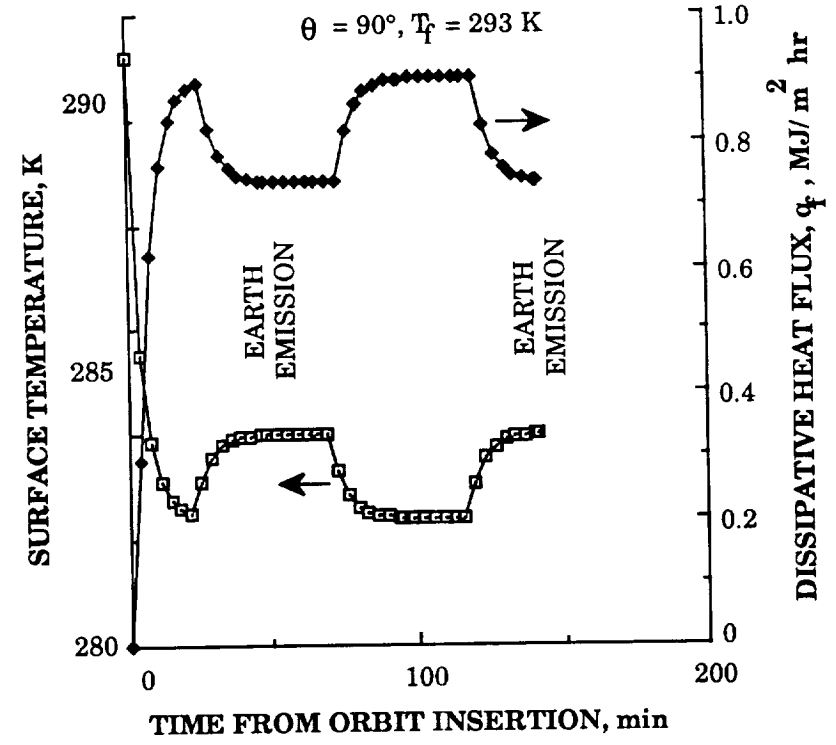

Figure 27(b) Transient Response of Radiator

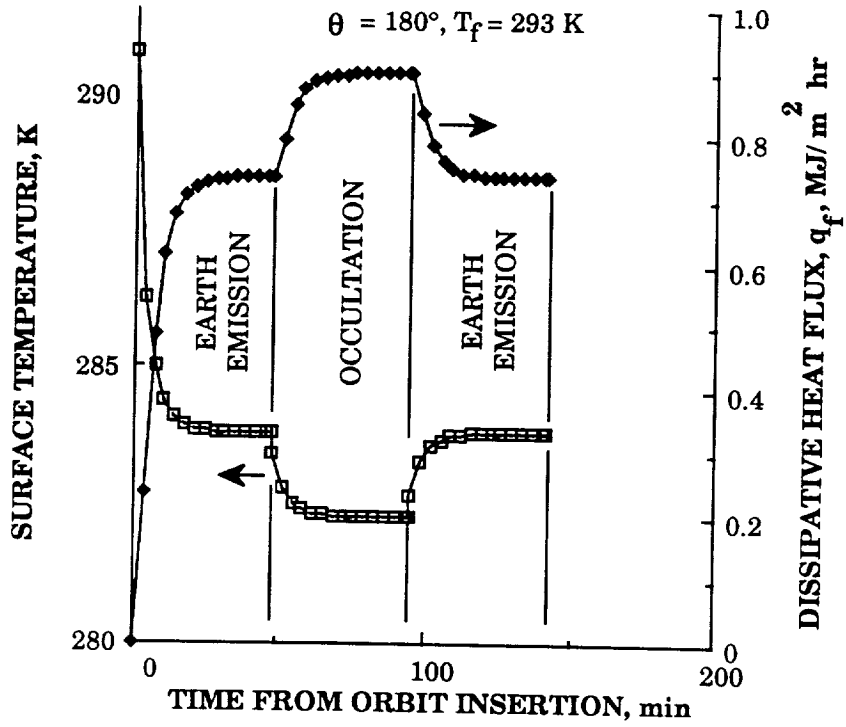

Figure 27(c) Transient Response of Radiator

flux are somewhat smaller because of the decreased temperature difference between the inner surface and the outer surface. At a position of $\theta = 0°$, the dissipative heat flux varies from 159 kJ/m^2-hr in sunlight to about 602 kJ/m^2-hr during occultation. The variation of dissipative heat flux at $\theta = 90°$ and 180° is between 602 to 795 kJ/m^2-hr.

Integrating the above dissipative heat fluxes over the body and over the orbit and considering the variation of fluid temperature from 0° to 20° C around the radiator indicates that the radiator has an average thermal dissipation capability of about 33,000 kJ/m^2-hr (850 W). Note that this is about a factor of eight larger than the required heat dissipation of about 100 W. The size of this factor indicates that the radiator is considerably over designed, but this overcapacity may be required to account for analysis uncertainties and for the requirements of other future payloads with high power consumption such as materials processing experiments.

RRS Mass Properties and Configurational Layout

Requirements - The packaging and interior arrangement of the above subsystems is very important to the proper design of the RRS vehicle. The location of the c.g. and the moments of inertia about the principal axes affect the dynamic characteristics of the RRS vehicle during all flight phases. During the orbital flight phase the vehicle is spun about the longitudinal axis for the simulation of gravity, for stability in the setup for the important deorbit maneuver, and for stability during the deorbit trajectory from orbit to the edge of the atmosphere. During these spinning flight phases, in order to maintain the alignment and stability of the longitudinal axis relative to the momentum vector, it is necessary that the longitudinal axis be the principal axis (with the largest moment of inertia). It should be noted that this may not be a requirement for the spin maneuver before the retro-maneuver. In this case only short-term spin stability is required if the retro-maneuver occurs shortly after the spin-up maneuver. It is also important that the moments of inertia about the other orthogonal axes be equal to prevent the onset of nutation. During the atmospheric reentry phase, it is very important, for aerodynamic stability, that the c.g. be very near the longitudinal axis and forward of the center of pressure (c.p.) by a sufficient amount to provide an adequate amount of static margin. The exterior configuration of the RRS has a base diameter of 1.9 m with a body length of 1.57 m from the nose to the aft cover. The specific requirements for the c.g. location and moments of inertia, relative to an orthogonal set of axes as shown in figure 28, are based on the

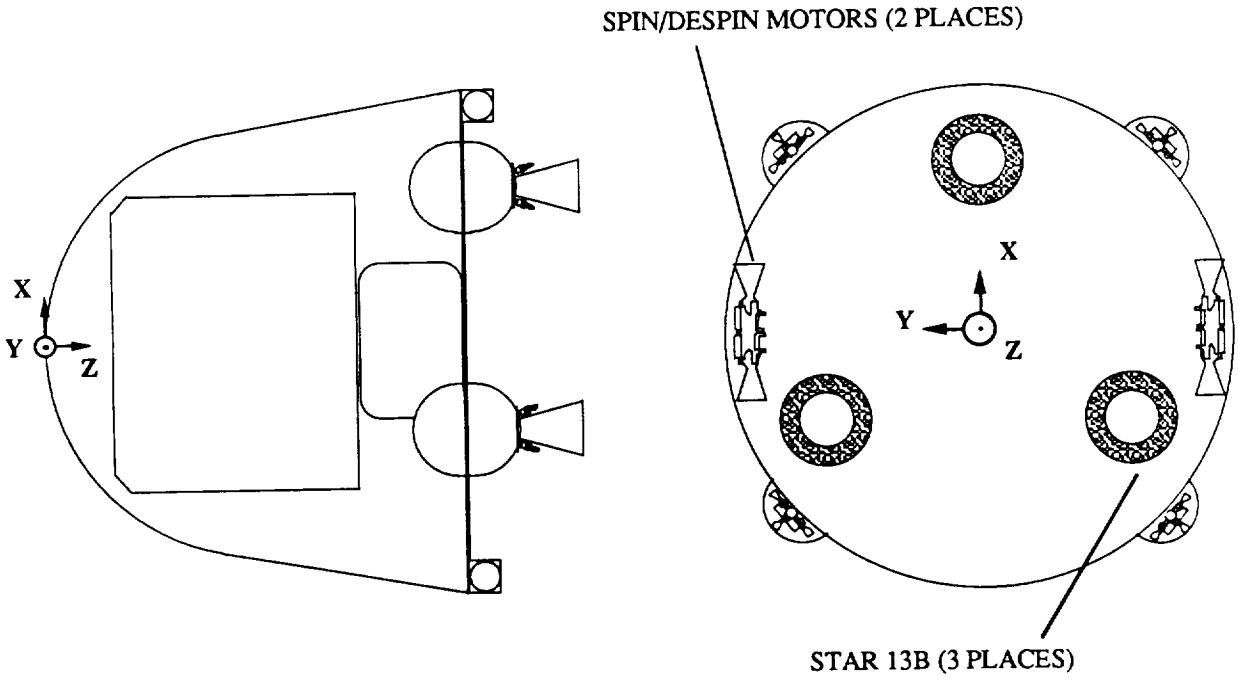

Figure 28. Orthogonal Axes

criteria given below.

(a) Minimum forward c.g. position aft of the nose during reentry is 42.45 % of the RRS base diameter; i.e., $z_{cg} < 80.9$ cm.
(b) Off-axis c.g. location no greater than 0.25 cm.
(c) Ratio of the roll moment of inertia over the pitch moment of inertia greater than 1.0; perferably 1.05.
(d) Principal axis colinear with longitudinal body axis.
(e) Transverse moments of inertia (i.e., pitch and yaw) must be equal within 0.5%.

Mass Statement - A summary of the masses of the various systems and subsystems previously described is provided in Table 5. For each tabular entry, a rationale is provided for the selected numerical value of the component. The total launch mass of the system is 1263 kg. The pie chart in figure 29 provides a visual understanding of each major system's contribution to the total RRS launch mass. Figure 30 shows the mass breakout of each major component.

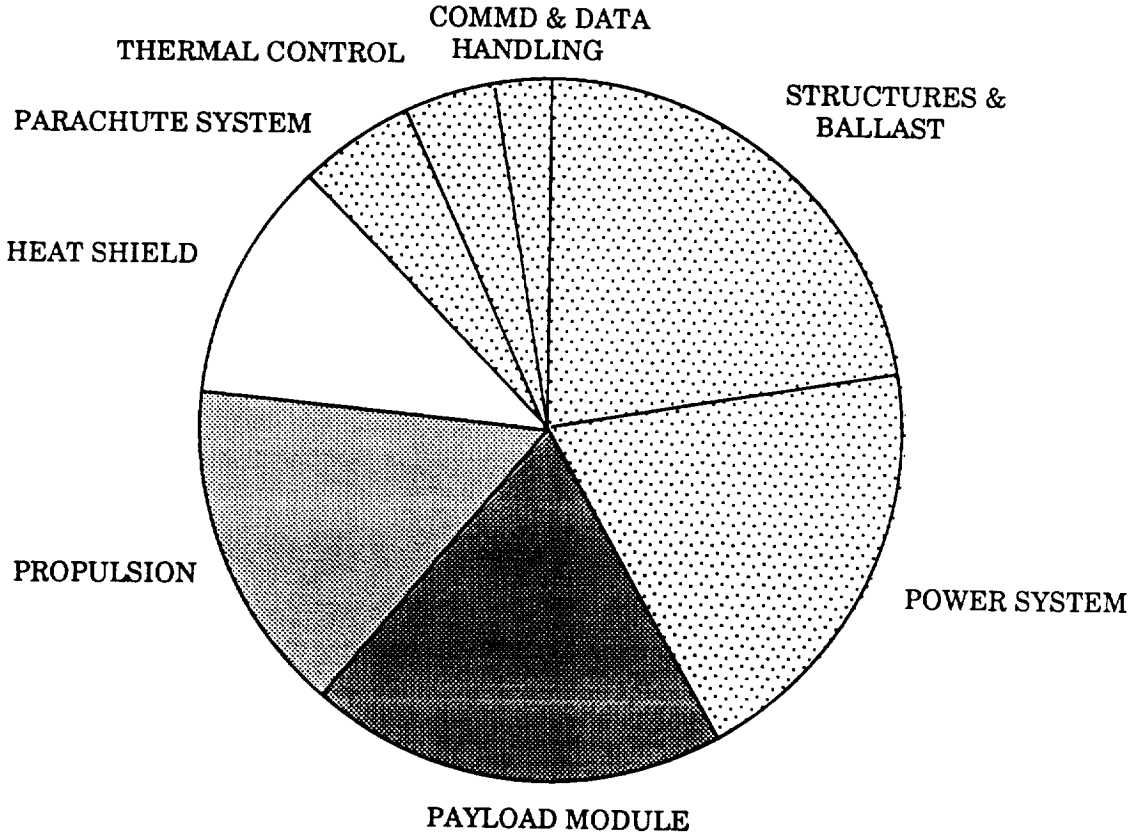

Figure 29. Weight Proportions of Major Components

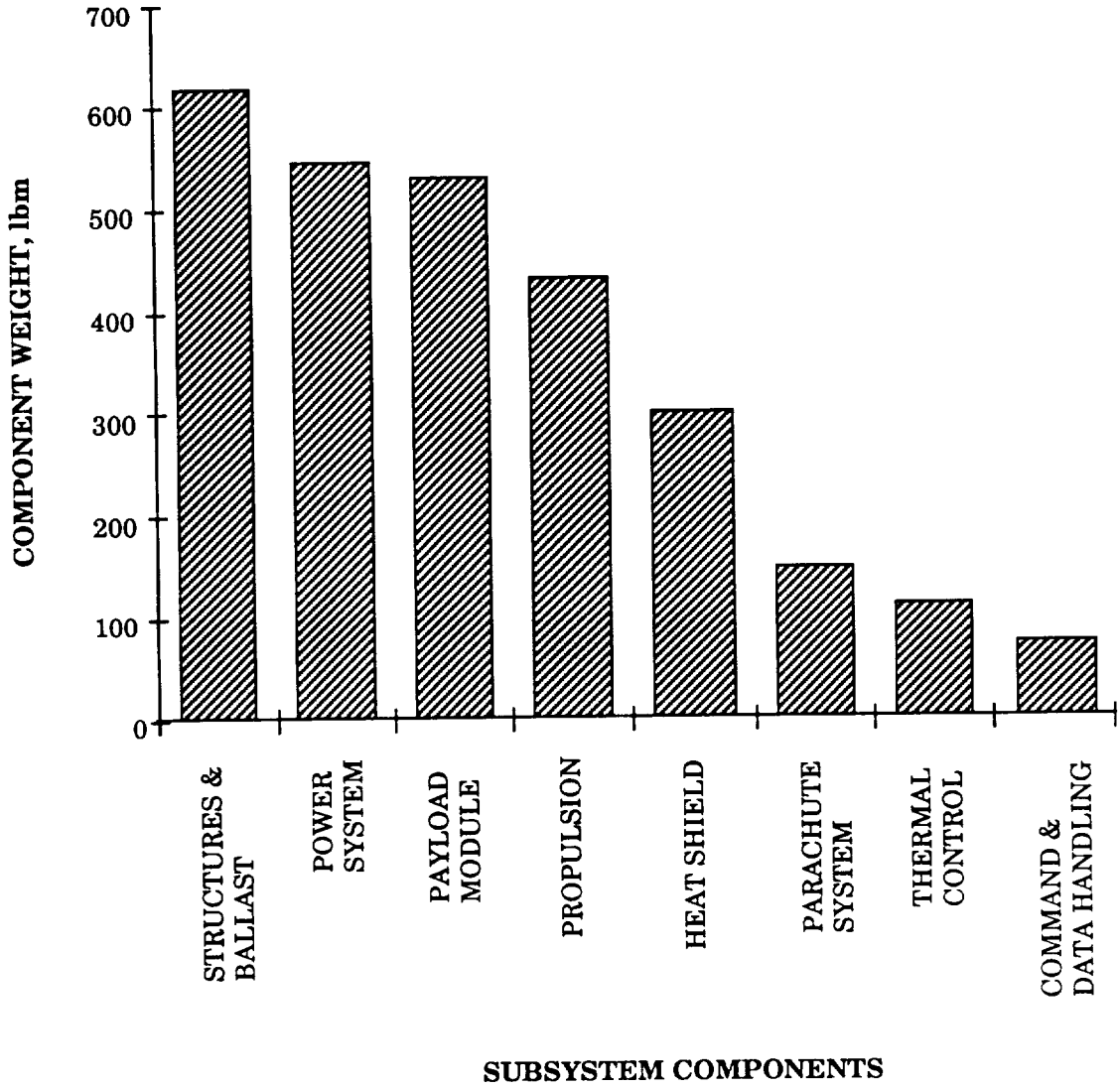

Figure 30. Weight Breakout of Major Components

Configurational Layout, Center of Gravity, and Moments of Inertia - Several alternative layouts of the major subsystem components were examined to meet the above mentioned criteria and to accommodate the individual component geometries, considerations of subsystem interactions, preferred location constraints, and overall mission operations. In the analysis, the mass, geometry and placement of over 70 spacecraft elements were considered.

The task of positioning the c.g. and simultaneously meeting the moment of inertia criteria often conflicted with the other requirements of the system layout. The final layout of the RRS vehicle was the result of an evolution of several configura-

TABLE 5. RRS COMPONENT WEIGHT SUMMARY

COMPONENT	WEIGHT, kg sub-total	total	RATIONALE FOR SELECTION
EXTERIOR SHELL		59.3	
Forward nose skin (.20 cm)	19		Aerodynamic Loads
Mid ship skirt (.13 cm)	18		Aerodynamic Loads
Stringers (2.5 cm T section)	4		Increased buckling resistance
Aft honeycomb cover & ring	16		Preliminary computation
Launch Vehicle Mounts	2.3		For Delta 6019 adapter fitting
MAIN SUPPORT STRUCTURE		129.0	
Mid ship Cone (.20 cm)	24		Launch & worst-case reentry loads
PM mounting ring	14		Landing loads
PM axial load fittings	3		Landing loads
Thrust cone & Ring	22		De-orbit burn and launch loads
S/C systems shelf & cyl.	33		Supports up to 250 lbs at landing
Field joint ring	9		Provides mating surface for nose
Contingency (15%)	24		estimate
PAYLOAD MODULE		240.0	
ESA Botany module	240		Based on in-house study
Rodent module (same weight)			Based on in-house study
Plant module (same weight)			Based on in-house study
POWER SYSTEM		246.8	
Batteries for P/L 45 kw	167		Based on APL/USAF project
Batteries for S/C 20 kw	74		Based on APL/USAF project
Power Conditioning Unit	3		Based on Galileo probe
Cabling	1.4		Based on Galileo probe
Test & monitor harness	0.9		Based on Galileo probe
Miscellaneous	0.5		estimate
RETRO ROCKET MOTOR SYSTEM		144.7	
Propellant, 70AP/16AL	124		Size selected based on computed DV
Case, dry	17		Catalogue -Thiokol Star 13B
Support structure	0.9		other than thrust structure
Wiring	0.5		estimated from Biosatelite
Safe & Arm Device	1.4		catalogue lookup
Thermal batteries & wiring	0.9		catalogue lookup

TABLE 5. CONTINUED

COMPONENT	WEIGHT, kg sub-total	total	RATIONALE FOR SELECTION
INSULATION		11.2	
Between batteries & PM	1.5		calculated
Between thermal loops & PM	4		calculated
Between PM and aft motor	2		calculated
Between nose & batteries	3		calculated
Around tankage	0.2		calculated
miscellaneous	0.5		estimated
ATTITUDE CONTROL SYSTEM		40.2	
Hydrazine & nitrogen	21		computed based on delta velocity
tankage	5		sized and catalogue lookup
plumbing	0.9		estimated from Pioneer 10
valving & fittings	0.9		Based on PV
support structures	1.4		computed
controls, wiring & sensors	0.9		sized from Pioneer 10
thrustor assembly (4)	5		sized & catalogue lookup (4.5 N)
heaters,filters,transducers	0.5		based on PV
Rate gyros	1.8		catalogue lookup
Horizon sensor/magnetometer	2.3		catalogue lookup
Accelerometer	0.5		Bell Textron .00000001 to 450 g
SPIN/DESPIN SYSTEM		17.4	
Hydrazine rocket motors (4)	8		sized & catalogue lookup (450 N)
Support structures	0.9		computed
tankage			included in attitude control system
Hydrazine & nitrogen	8		computed based on inertia & RPM
Controls, wiring & sensors	0.5		estimated from Biosatellite
PARACHUTE SYSTEM		73.1	
Mortar & Pilot chute	2.3		Based on Galileo technology
drogue chute	6		Based on Galileo technology
Airbourne guidance unit	23		Communications with vendor
gliding chute	30		Communications with vendor
Risers/bridles/bags	4		estimate
Swivel	0.5		estimate
thermal batteries	0.9		catalogue (part of electrical S/S)
Electo Explosive Devices	1.8		estimate
controls and sensors	2.3		estimate
wiring & switches, etc.	0.5		estimate (part of structures S/S)
covers	1.8		estimate (part of electrical S/S)

TABLE 5. CONTINUED

COMPONENT	WEIGHT, kg sub-total	total	RATIONALE FOR SELECTION
THERMAL CONTROL SYSTEM		40.5	
Pumps (2)	2.3		catalogue lookup
cooling loops (spaced 19.1 cm)	21		calculation
fluids	13		calculation
valving (7)	1.6		Based on Biosatellite
sensors	0.5		Based on Biosatellite
controls	0.5		Based on Biosatellite
wiring	0.2		estimate
support structures	0.9		estimate
miscellaneous	0.5		estimate
REENTRY THERMAL PROTECTION		137	
Heat shield,nose (2.0-1.5 cm)	64		Computed based on reentry heating
Heat shield,skirt (1.5-1.3 cm)	73		Computed based on reentry heating
COMMUNICATIONS		12.5	
antennae	1.4		Based on Galileo probe
transponders	5		Based on Galileo probe
wiring	0.5		Based on Galileo probe
oscillator	0.5		Based on Galileo probe
exciter	2.3		Based on Galileo probe
Radar tracking transponder	1.4		Communications with White Sands
Radar Tracking antenna	1.4		Communications with White Sands
DATA HANDLING/CONTROLS		9.8	
Microprocessor	7		Based on Galileo & Pioneer probes
Sequencer	0.5		Based on Galileo & Pioneer probes
"G" switches (2)	0.5		Based on Galileo & Pioneer probes
Cable harness & connectors	1.8		Based on Galileo & Pioneer probes
COMMAND		5.4	
electronics	2.5		Based on Galileo & Pioneer probes
sequence controller	0.7		Based on Galileo & Pioneer probes
cable harness & connectors	2.0		Based on Galileo & Pioneer probes
miscellaneous	0.2		Based on Galileo & Pioneer probes
DESTRUCT DEVICE		4.9	
Squibs and wiring	0.9		Catalog lookup
Explosive and disarm device	4		Catalog lookup
BALLAST		91	for proper moment of inertia ratio
TOTAL WEIGHT, kg		1262.8	

tions. This evolution of configurations started at an Initial Configuration following that proposed in reference 2 and described below and proceeded through a series of configurational modifications as shown in figures 31(a) - (e). Each of these modifications is described below with the resultant c.g. location and moments of inertia. In general, the overall design goal is to maximize radial symmetry about the longitudinal axis and wherever possible, to place more massive items forward. Furthermore, placement of items at a large radial distance away from the longitudinal axis is necessary to maximize the spin or longitudinal moment of inertia. It should be noted that the forward placement of massive components ahead of the c.g. has a simultaneous detrimental effect of increasing the pitch moment of inertia. The mass properties analysis studied both the configuration of the spacecraft just after launch ("Wet RRS") and at its reentry condition, with ASCS and the retro-rocket fuel expended ("Dry RRS").

The internal arrangement of the Initial Configuration is illustrated in figure 31(a). Note the placement of several key components. The initial configuration uses a single Thiokol STAR 17A retro-rocket located on the longitudinal axis. The parachute system is necessarily offset from the longitudinal axis as indicated in the figure. The 26 battery modules are located in a cylindrical ring about the PM envelope. The PM envelope is a cylinder with a diameter of 111.8 cm and a length of 91.4 cm. As indicated in figure 31(a), the Initial Configuration in the "wet" condition has a c.g. location of 96.4 cm and a moment of inertia ratio of 0.966. In the "dry" condition the vehicle has a c.g. of 89.23 cm and a moment of inertia ratio of 1.081. Unfortunately the configuration is dynamically unstable in spin while on-orbit after launch. In addition, while the vehicle is dynamically stable in spin after the retro-rocket firing, the c.g. location is about 8.38 cm aft of the location required for aerodynamic stability during reentry. It should also be noted that the offset location for the parachute system made it difficult to align the longitudinal axis and the principal axis. In addition, it created some concern relative to the deployment of the parachute risers around the retro-rocket motor.

For the Modification 1 Configuration, as shown in figure 31(b), the single retro-rocket motor is replaced with three smaller motors symmetrically placed around the longitudinal axis. The Thiokol STAR 13A motor is used. This allowed the parachute system to be placed on the longitudinal axis eliminating the problem of deployment and providing longitudinal symmetry. In the wet condition, the vehicle has a c.g. location of 96.01 cm and a moment of inertia ratio of 1.017. In the dry condition, the c.g. location is at 87.96 cm and the moment of inertia ratio is 1.091. The vehicle is just barely dynamically stable in spin while on-orbit and the c.g. location has been improved by 1.3 cm at atmospheric reentry, but it still remains about 7.1 cm aft of the required location.

In order to improve the c.g. location at reentry, the Modification 2 Configuration

(a) Initial Configuration

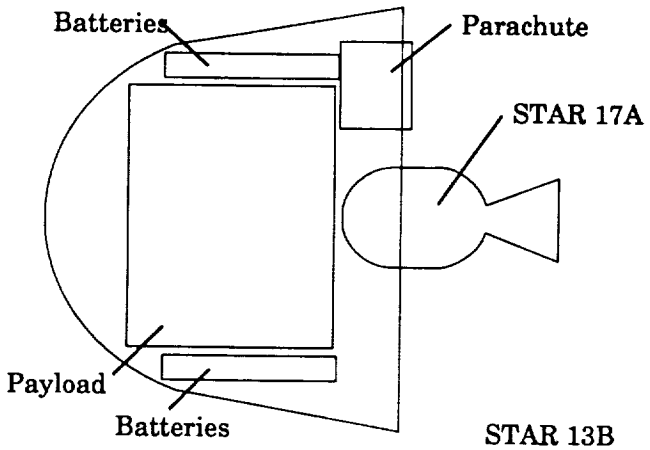

(b) Modification 1

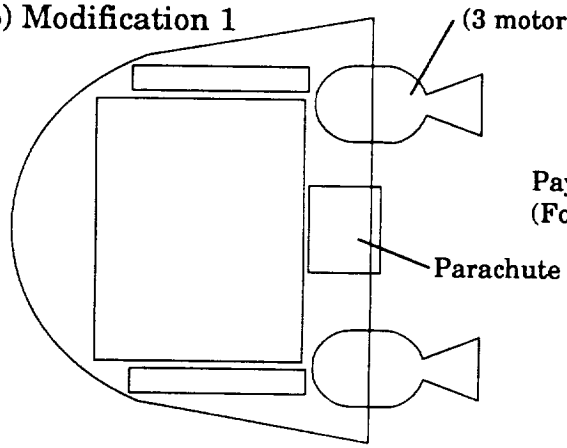

(c) Modification 2

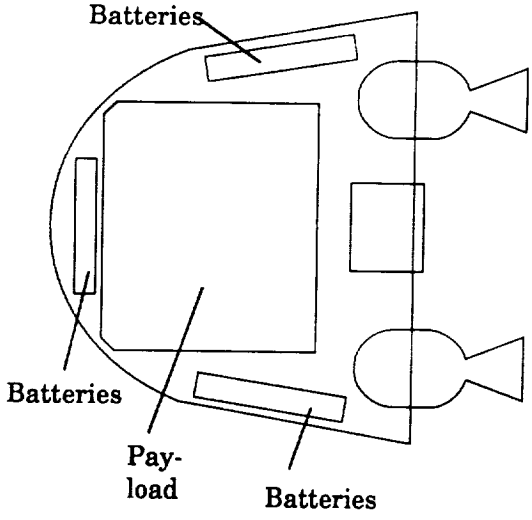

(d) Modification 3

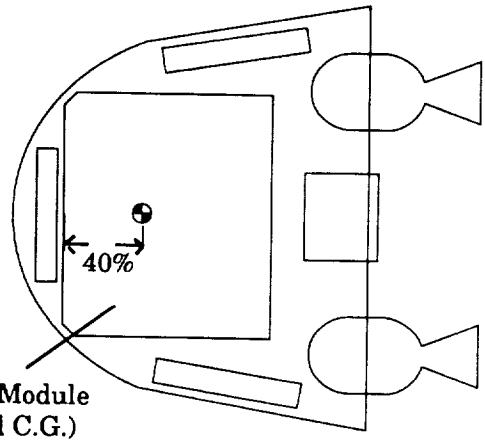

(e) Modification 4

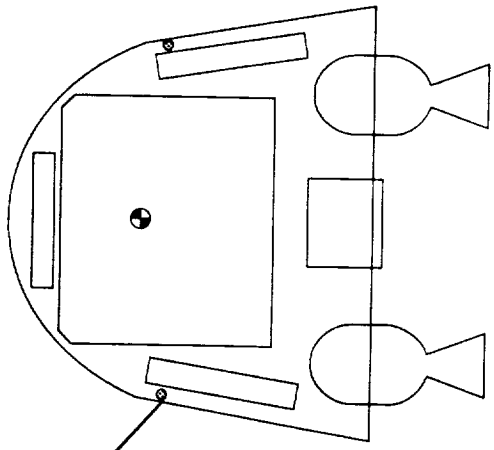

	WET		DRY	
	C.G.	Izz/Iyy	C.G.	Izz/Iyy
Initial Configuration	96.39	0.966	89.23	1.081
Modification 1	96.01	1.017	87.96	1.091
Modification 2	91.31	0.949	82.45	1.028
Modification 3	89.41	0.932	80.29	1.015
Modification 4	88.72	0.989	80.29	1.081

Figure 31. RRS Configuration Evolution

was produced as shown in figure 31(c). First, the PM envelope was moved forward 3 in toward the nose of the vehicle. To accommodate this movement, however, the PM envelope had to be decreased in radius to 55.9 cm and the forward corner of the envelope has a 5 cm chamfer at a 45° angle. Second, the battery modules are shortened by 11.4 cm and the eliminated batteries are moved to a forward shelf in the nose of the vehicle ahead of the PM envelope. Third, the shortened battery modules are flared out to conform with the 10° skirt to increase their contribution to the spin moment of inertia. As can be seen from figure 31(c), the c.g. location for reentry is improved over the Modification 1 Configuration by 5.51 cm. However, this is still 1.52 cm aft of the required location. In addition, the movement of elements forward has increased the pitch moment of inertia and has had a detrimental effect on the moment of inertia ratio of the vehicle. The vehicle is now dynamically unstable in spin in the wet condition and only just barely stable in spin for the dry, deorbit condition.

Because the c.g. location for the Modification 2 Configuration is aft of the required position, a third configurational layout was produced; the Modification 3 Configuration shown in figure 31(d). All elements have been moved as far forward as possible in the Modification 2 Configuration, therefore the only latitude left is to redefine that the c.g. of the PM to be located forward of the geometric center of the cylindrical envelope. For the Modification 3 Configuration the c.g. is defined to be at or forward of a point 40% of the length of the cylinder aft of the forward face. The effect of this modification (or really redefinition) is to move the vehicle c.g. forward 2.16 cm or about 0.5 cm forward of the required location for aerodynamic stability during reentry. However, the forward movement of the PM c.g. has also resulted in an increase in the pitch moment of inertia such that the moment of inertia ratio is now 0.932 in the wet, on-orbit condition and 1.015 for the dry, reentry condition. Therefore the vehicle is unstable in spin on-orbit and just barely stable for the deorbit trajectory.

It appears that it is not possible to materially increase the spin moment of inertia of the Modification 3 Configuration by simply moving internal components. Therefore, a final configuration, Modification 4, was produced which simply increases the spin moment of inertia through the inclusion of a rather massive inertia ring with the plane of the ring located at the c.g. and perpendicular to the longitudinal axis (see fig. 31 (e)). The ring has a radius of 76.2 cm. If the ring is sized at 90.7 kg, the moment of inertia ratio for the vehicle increases to 0.989 in the wet condition and 1.081 in the dry condition. The resulting vehicle is thus completely stable in spin about the longitudinal axis for the deorbit trajectory and the c.g. location is slightly forward of the required location for aerodynamic stability during the reentry flight. However, the vehicle remains unstable in spin in the on-orbit condition. This vehicle configuration is acceptable for missions which do not require spin for artificial gravity. The 90.7 kg of dead weight in the inertia ring is a large penalty to pay. An additional 90.7 kg in the ring (a total mass of 181.4 kg) is required to make the Modification 4 Configura-

tion dynamically stable in spin about its longitudinal axis in the wet, on-orbit condition. The final interior layout of the principal elements is shown in figure 2(a).

There are other configuration alternatives to make the vehicle stable in spin which should be examined in further system design studies. These options include:

(a) the inclusion of deployable masses for stability,
(b) change the exterior configuration to sphere-cone of greater half-angle, say perhaps 30-45°, or
(c) active nutation damping using the ASCS system.

CONCLUSIONS

The mission and system design study reported in this paper has indicated the essential feasibility of a properly designed reusable, reentry satellite vehicle for the conduct of a continuing program (spanning, perhaps, 10 years) of life science research on small animals and plants in Earth orbit. The vehicle is designed to provide the maximum flexibility, within program cost limitations, to the life science researcher and is adaptable to a variety of expendible launchers, orbital characteristics, and mission durations up to 60 days. The vehicle is designed to provide a micro-gravity enviroment of 10^{-5} g or to be spun about its longitudinal axis to provide an artificial gravity up to 1.5 g. The vehicle is capable of carrying up to 240 kg of experimental hardware and supporting those experiments with utility sources of power (up to 45 kW-hr), thermal control, and data transmission. The total launch weight for the vehicle and experiment allowance is about 1270 kg. The vehicle is recovered from orbit completely intact within the continental U.S. at the WSMR. Every effort will be made to make the recovery operations completely safe to the general populace. After recovery, the vehicle is designed to allow rapid access to the Payload Module and the experiment specimens. The vehicle is also designed to be quickly and relatively inexpensively refurbished for a subsequent reflight.

The design of the vehicle and its subsystems is well within the state-of-the-art. Some development and testing will be required to create an operational system, but expensive new technologies need not be developed to enable this project. Most subsystems are either available off-the-shelf or are copies or slight extensions of designs which exist from previous flight programs. A notable exception to this general condition is the terminal descent parafoil. To date, a parafoil has been successfully drop-tested and landed with a suspended weight of about 1000 kg. The extension of that capability to about 1270 kg should be fairly straightforward, but will require more testing. If efforts aimed at increasing the parafoil capability should encounter difficulties, a conventional parachute design could be used. The decision on the type of parachute system to be used should be made as early in the development program as possible and drop tests should be initiated.

Another subsystem which should be examined in the future is the power subsystem. Batteries, and most particularly lithium thionyl chloride batteries, appear to be the best choice for the power source. However, fuel cells or other battery types should be examined in detail with particular attention paid to safety and to the total life cycle costs (i.e., development and refurbishment costs) for power for the 10- year flight program.

For this conceptual design study, a vehicle exterior configuration similar to that of the previously flown Discoverer and Biosatellite programs is assumed. This vehicle configuration has a number of advantages and a considerable amount of flight experience. However, it should be noted that it is very difficult to package the subsystems into this configuration and simultaneously maintain center of gravity position for aerodynamic flight and moments of inertia required for stable, spinning orbital flight. Indeed, only through the use of a rather heavy ballast, or interia ring, could the current design be made stable in spin. Future system design studies should consider alternative vehicle configurations to see if this problem can be eliminated.

APPENDIX A

INTEGER ORBITS, DUAL OVERFLIGHTS, AND DAY/NIGHT CYCLES

Integer Orbits - A class of orbits referred to as "integer" orbits are circular Earth orbits that have a repeating ground track each day. The term "day" refers to the period of time required for the orbit ground track to return to given position on the surface of the Earth. The effects of planetary oblateness on the orbit plane make this time period somewhat different from a sidereal day. Integer orbits are discussed in detail in reference 9.

The altitude of such a circular orbit can be determined by equating the time for N (integer) revolutions of the orbiter in the orbit plane and the time for a given point immediately below the orbiter on the surface of the Earth to return to a position coplanar with the orbit plane and again immediately under the orbiter. Figure A1 illustrates the inertial motion of an inclined orbit plane from the first orbit to the Nth orbit. Oblateness causes the orbit plane to be perturbed inertially such that the ascending node of each orbit is changed by an amount $\Delta\Omega$. This nodal movement is given by (see ref. 25):

$$\Delta\Omega = -3\pi J_2 \left(\frac{R}{a}\right)^2 \cos i \qquad \text{(A1)}$$

where $J_2 = 0.001082$, and R is the radius of the Earth. Here, i, is the orbit inclination and, a, is the radius of the orbit and is given by:

$$a = R+h$$

where, h, is the altitude of the orbit. It can be seen that the motion is regressive for inclinations less than 90°.

Equating the the two times of rotation (i.e., that of the orbiter and that of any point immediately below the orbiter on the surface of the Earth) yields:

$$N\tau = \frac{86164.1}{2\pi}(2\pi+N\Delta\Omega) \qquad \text{(A2)}$$

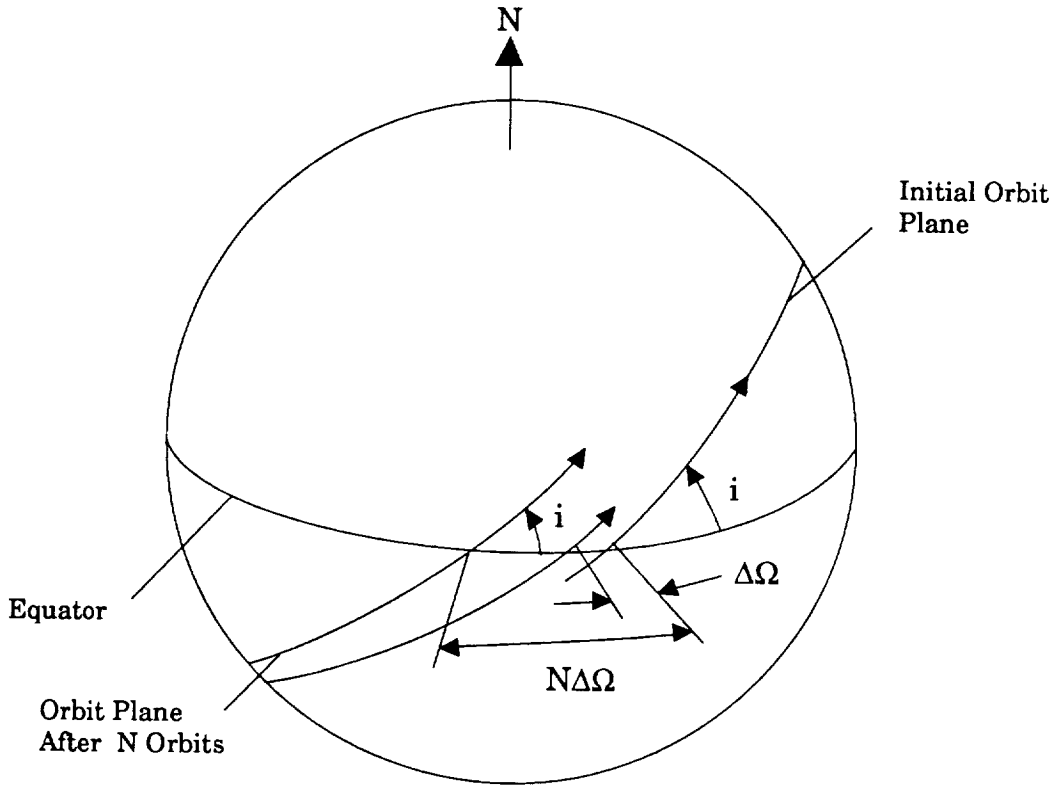

Figure A1. Orbit Plane Geometry

where the period of the orbit, τ, is given by:

$$\tau = \frac{\tau_o}{1 + (3/2)\, J_2\, (R/a)^2\, [\, 1 - (3/2) \sin^2 i\,]} \qquad \text{(A3)}$$

where, τ_o, the unperturbed period of the orbit, is given by:

$$\tau_o = 2\pi \sqrt{a^3/\mu} \qquad \text{(A4)}$$

and μ is the gravitational potential.

Substituting equations (A1), (A3), and (A4) into equation (A2), making an obvious first order approximation to make the equation tractable, and solving for the highest power term of the orbit radius yields:

$$a^{7/2} = \frac{86164.1\sqrt{\mu}}{2\pi N}\left(a^2 - \frac{3}{2}J_2 R^2 N \cos i\right) + \frac{3}{2}J_2 R^2\left(1 - \frac{3}{2}\sin^2 i\right) a^{3/2} \qquad \text{(A5)}$$

Equation (A5) can now be solved in an iterative fashion. Since oblateness effects are small, an excellent starting solution for the orbit radius, a, to be used in the right-hand side of equation (A5) in the first iteration is the zero oblateness solution. That is, from equation (A5) with $J_2 = 0$,

$$a = \left(\frac{86164.1\sqrt{\mu}}{2\pi N}\right)^{2/3}$$

It is found that accuracies in the orbital radius of 0.01 percent are obtained from the iterative procedure in less than 10 iterations. The altitudes of integer circular orbits are shown in figure A2 by the solid, nearly horizontal lines as a function of orbit inclination for several values of the integer, N.

Orbits with characteristics as indicated in figure A2 overfly any point immediately under any orbit once every day. Thus, there is a single landing opportunity for any point on the surface of the Earth overflown by orbiter once a day. Note that not all points on the surface are accessible, but only those points directly under the orbiter on any of the N orbits. The accessible points are determined by the value of the longitude of the ascending node (on the surface of the rotating Earth, not inertially) on any of the N orbits.

Dual Overflights - An interesting subset of these accessible points are points which are accessible twice every day (N orbits). These points on the surface of the Earth see the orbiter immediately overhead twice a day; once on an ascending, southwest to northeast pass and once on a descending, northwest to southeast pass. These orbits depend upon the latitude of the surface site and are further characterized by the second overflight occuring on the Kth orbit following the first pass. This is shown schematically relative to the surface of the Earth in figure A3 for K = 2. The altitude of the orbit which creates this dual overflight condition is determined by equating the time spent by the orbiter in K revolutions plus the time in the partial orbit repre-

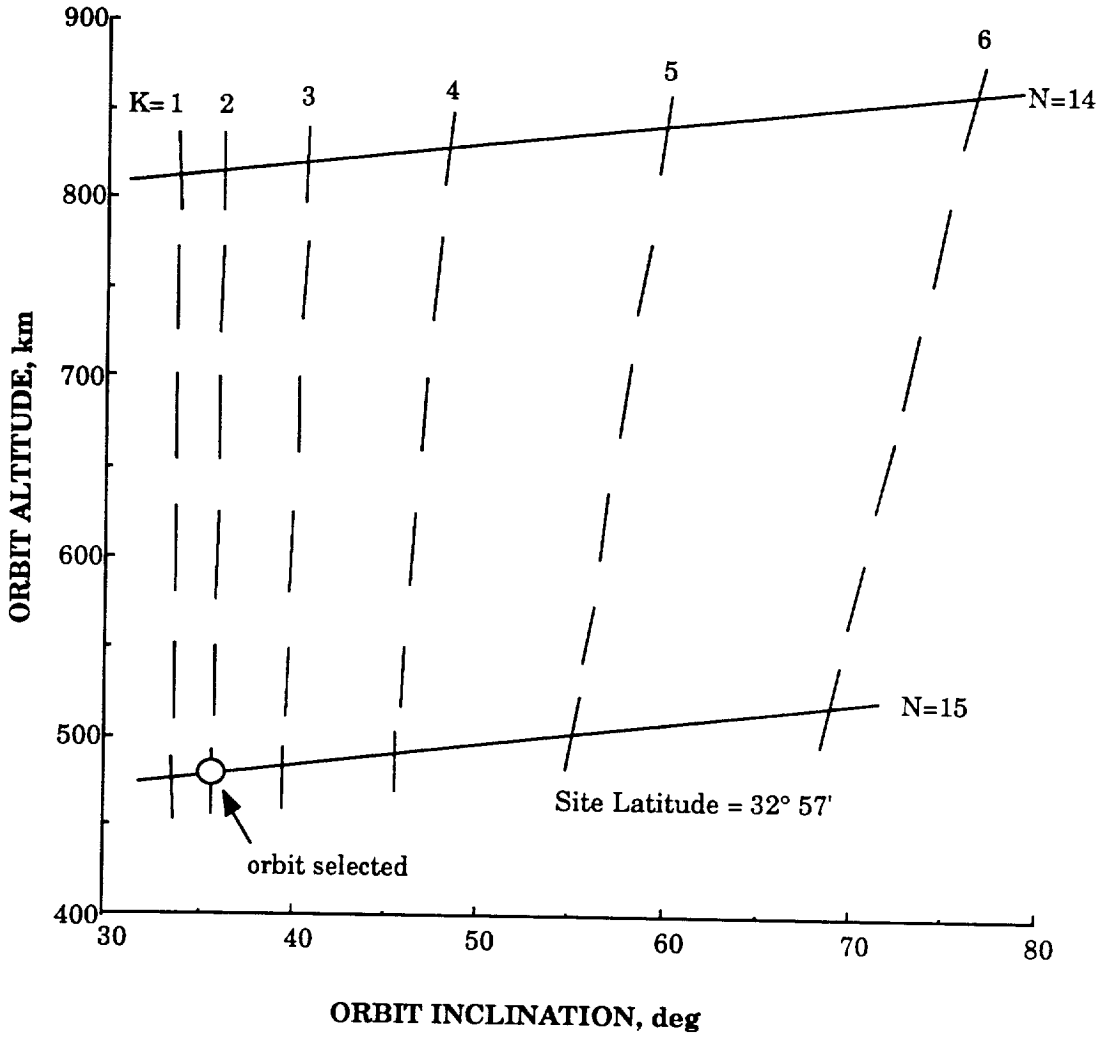

Figure A2. Integer Orbit Characteristics

sented by the angle $\Delta\phi$ (fig. A4) to the time spent at the surface site to rotate about the Earth's axis the angle ΔL in longitude (fig. A4).

$$K\tau + \frac{\Delta\phi}{2\pi}\tau = \frac{\Delta L}{2\pi} 86164.1 \qquad \text{(A6)}$$

Note that the above equation holds for any orbit (not necessarily an integer orbit) for which a second overflight occurs during the Kth orbit following the first pass. The equation does not, however, imply that this dual overflight necessarily occurs again.

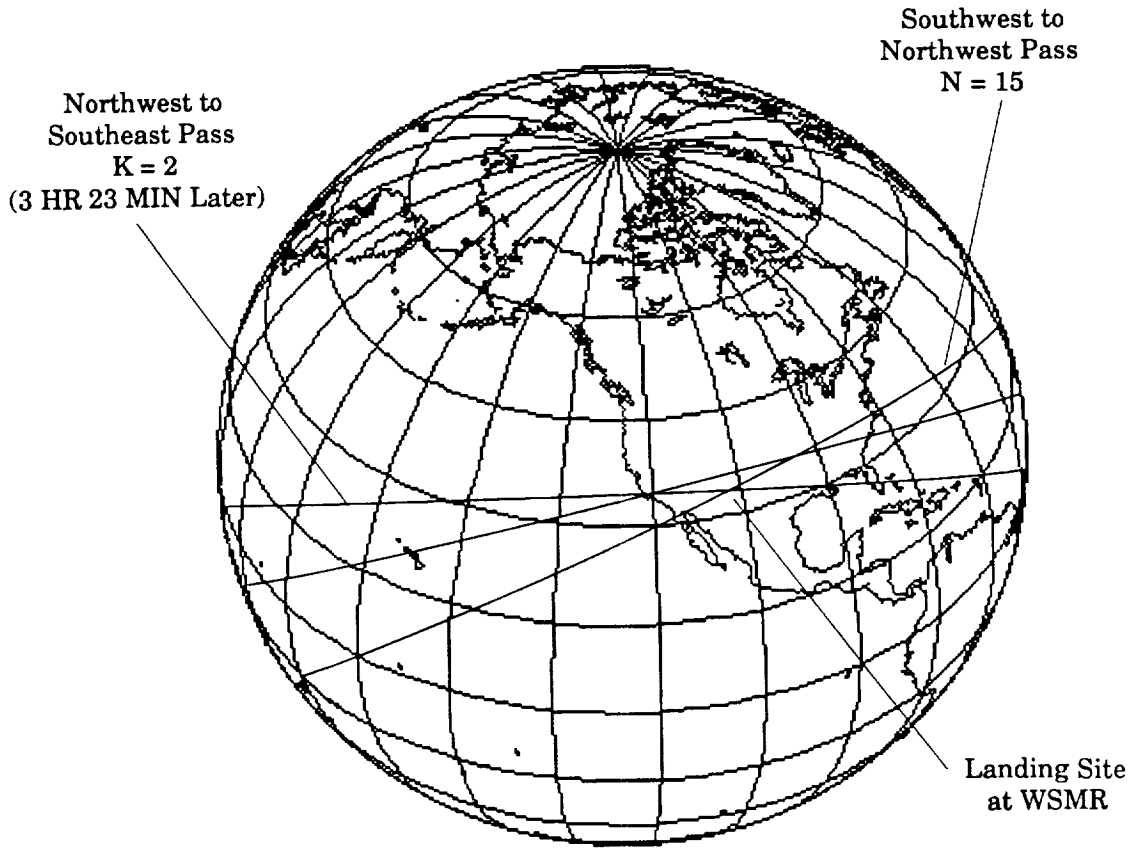

Figure A3. Integer Orbit Geometry

For a given orbit inclination and site latitude (obviously less than the orbit inclination), the angles $\Delta\phi$ and ΔL can be calculated. Substitution of these angles and equations (A1), (A3), and (A4) into equation (A6) and rearranging in a similar manner as with equation (A5) yields equation (A7) which can be iterated to solve for the orbit radius, a.

$$a^{7/2} = \frac{86164.1\sqrt{\mu}}{(2\pi K+\Delta\phi)}\left[\frac{\Delta L}{2\pi}a^2 - \frac{3}{2}KJ_2R^2\cos i\right] + \frac{3}{2}J_2R^2\left(1-\frac{3}{2}\sin^2 i\right)a^{3/2} \quad (A7)$$

The starting value for the iteration on the orbit radius, a, for the right-hand side of the equation is:

$$a = \left(\frac{86164.1(\Delta L/2\pi)\sqrt{\mu}}{2\pi K+\Delta\phi}\right)^{2/3}$$

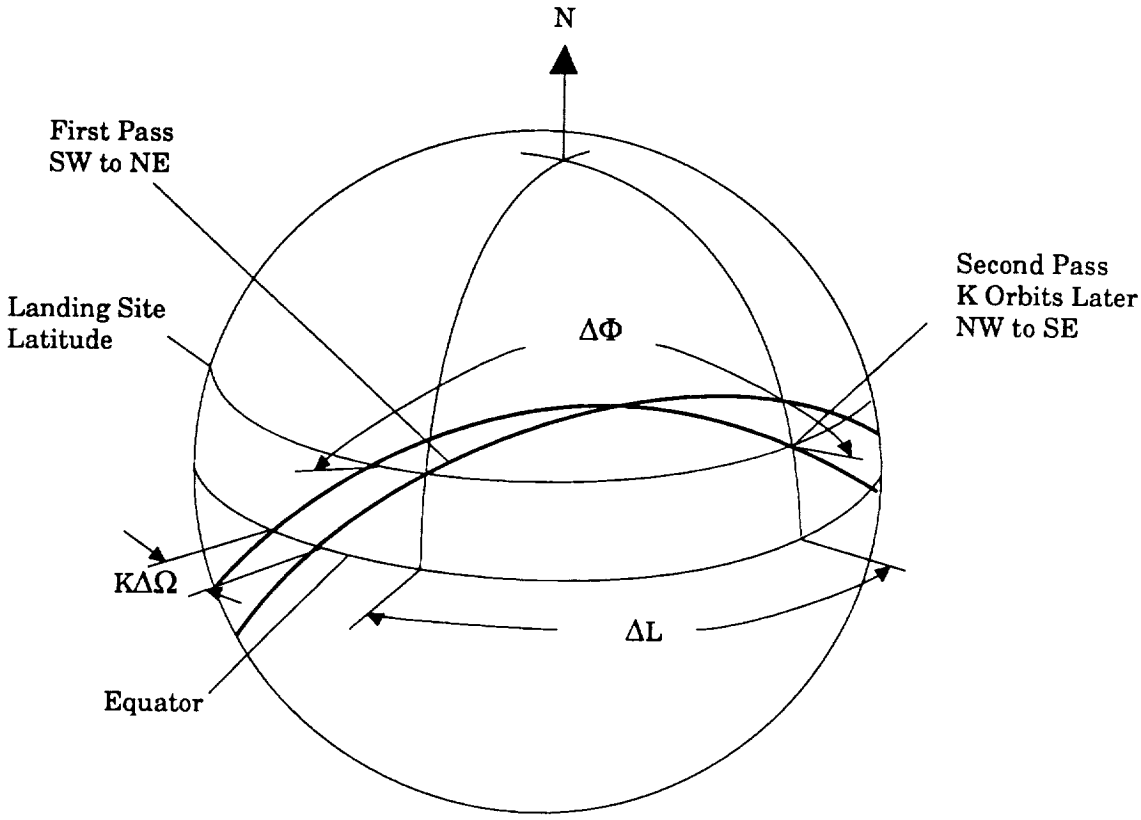

Figure A4. Dual Overflight Geometry

The resultant orbit altitudes as a function of orbit inclination, for a site latitude corresponding to the Northrup Strip in WSMR (32° 57') and for various values of the parameter K are shown by the dashed lines in figure A2.

The intersections of the solid lines (N integer orbits) and the dashed lines (dual overflights separated by K orbits) are the subset of altitudes and orbit inclinations which represent orbits which have repeating dual overflights every day. The characteristics of those orbits are tabulated on the next page.

Integer Orbit Characteristics:

N	K	Orbit Inc, deg	Orbit Alt, km
14	1	33.70	812.7
14	2	36.10	814.5
14	3	40.61	818.1
14	4	48.11	824.9
14	5	59.86	837.7
14	6	76.61	859.3
15	1	33.59	477.4
15	2	35.65	479.1
15	3	39.45	482.5
15	4	45.62	488.7
15	5	55.16	499.8
15	6	69.00	518.8

Day/Night Cycles - The time of an overflight of the orbiter (or of a landing) at a given site on the surface of the Earth cycles through day to night as the orbit plane is perturbed due to planetary oblateness and as the Earth moves through the seasons. This day/night cycle is a function principally of orbit inclination because that parameter drives the orbit plane perturbation. The cycles are also more weakly dependent upon the orbit altitude, the season of the year (i.e., solar declination), and the latitude of the site. Day/night cycles are discussed in detail in reference 9.

To first order, the general characteristics of the day-night cycle can grasped by the consideration of two inertial rates; the orbital node perturbation rate and the rate of rotation of the Earth about the sun. The orbital node perturbation rate is obtained from equation (A1), the orbital perturbation per orbit, modified by dividing by the orbital period to obtain the orbital node perturbation per unit time. The motion of the orbital node is regressive (i.e., the motion is clockwise as viewed down from the north pole) for inclinations less than 90° and varies from about -5.5 to -6.5°/day at a 35° inclination (over the orbit altitude range of interest) to zero for a 90° inclination. The rate of rotation of the Earth about the sun is, of course, about 1°/day and advances (i.e., as seen from the Earth, the sun appears to be moving, relative to a planet centered inertial reference frame, counterclockwise as viewed down from the north pole). Thus, the motion of the orbit plane relative to the sun varies from approximately -6.5 to -7.5°/day at 35° of inclination to about -1°/day for a 90° inclination finally reaching zero for the so-called sun-synchronous orbit at an inclination of about 98°.

For the lowest orbit inclinations consistent with the WSMR site, the apparent motion of the orbit node relative to the sun (i.e., about -7.5°/day) means that the daily

orbit passes occur about 30 min earlier each day. Thus, for example, the daylight cycle for the ascending (southwest to northeast) pass lasts for about 24 days followed by a like period of night passes. Similarly, the daylight cycle for the descending (northwest to southeast) pass is also about 24 days. Depending on the orbit inclination and the latitude of the site, the two cycles overlap. For example, if K = 2, the descending pass occurs about 3 1/2 hr after the ascending pass and the total daylight cycle for the combination of the two passes is increased to about 31 days and the night cycle is decreased to 17 days.

For more highly inclined orbits, the motion of the orbit plane relative to the sun is considerably smaller and the lengths of the cycles are inversely longer. In addition, for high inclination orbits and low-to-moderate site latitudes, the value of K increases toward N/2 and the two cycles for ascending and descending passes overlap to such an extent that the combined night cycle is reduced to just a few days.

The day and night cycles are also a weak function of the Earth season of the mission. This is illustrated in figure 7 where the day/night cycles at the selected site in the WSMR are shown for the N = 15, K = 2 orbit. It can be seen that, starting at the equinox, the combined daylight cycle for the two passes lasts for 33 days followed by a night cycle of 19 days. The last 19 days of the day cycle affords a landing opportunity during the morning hours. It can be seen that the cycles then repeat with slight variation over the year.

APPENDIX B

ORBITAL SYNCRONIZATION WITH THE LANDING SITE FOR DEORBIT

If the RRS is in an integer orbit, the synchronization of the orbital passes with the landing site occurs early in the mission and, except for a possible correction due to atmospheric drag, the orbiter overflys the landing site twice each day. If the RRS is part of a shared launch, the choice of orbit characteristics may not, in general, be such that this continuous synchronization is available. Therefore, at some time prior to the deorbit maneuver, the RRS must adjust, with its attitude control and spin system (ASCS), the projected ground track so as to be coincident with the landing site. This is accomplished by a slight adjustment in the orbit period which gradually changes the longitude of future ground tracks; thereby phasing the ground track to the landing site. The propulsion requirement for that adjustment is, of course, a function of: (a) the required longitude change from some future near pass of the landing site to make it exactly coincident and (b) the number of orbits over which the time phasing is to occur. The maximum required change in longitude, $\Delta\omega$, is less than one-half of the longitude difference between two adjacent orbit ground tracks.

$$\Delta\omega < \frac{1}{2}\frac{2\pi\tau_o}{86164.1} \qquad \text{(B1)}$$

Note that in equation (B1), the effects of planetary oblateness have been neglected as small effects, particularly between two consecutive orbits. It is also obvious that this change in longitude represents a total time phasing with the landing site of less than $\tau_o/2$

The total time phasing is to occur over, say, P orbits. Therefore, the orbit period change per orbit is:

$$\Delta\tau_o = \frac{\tau_o}{2P}$$

To first order, a change in orbital period is related to a change in the semi-major axis of the orbit by:

$$\frac{\Delta\tau_o}{\tau_o} = \frac{3}{2}\left(\frac{\Delta a}{a}\right)$$

In addition, it can be easily demonstrated that, to first order, the minimum impulsive velocity change, ΔV, required to change a circular orbit of radius, a, to a slightly elliptical orbit of semi-major axis, $a+\Delta a$, is given by:

$$\frac{\Delta V}{V_c} = \frac{1}{2}\left(\frac{\Delta a}{a}\right)$$

where, V_c, is circular velocity at an orbital radius of value a. Therefore, the phasing velocity requirement to adjust the orbit ground track, which occurs P orbits in the future through the maximum possible shift in longitude in order to align it with the landing site, is given by:

$$\Delta V = \frac{1}{6P} V_c = \frac{1}{6P}\sqrt{\frac{\mu}{a}}$$

In order to not have an effect on the magnitude of the deorbit maneuver, the orbit state must be returned to a circular state of radius, a, just before the deorbit maneuver. Therefore, the total phasing requirement is actually twice that given by the equation above.

$$\Delta V_{Total} = \frac{1}{3P}\sqrt{\frac{\mu}{a}}$$

The total sizing of this sequence of velocity impulses is conservative in that the second maneuver could be combined with the deorbit trim maneuver thereby reducing the total requirement. The total impulsive velocity allowance for the site phasing maneuvers is shown in figure 6 in the main text.

REFERENCES

1. Dyer, J.W., Ed.: Biosatellite—A Historical Summary Report. NASA Ames Research Center. December 1969.

2. Givens, J. G. and Schaupp, R. S.: RRS—A Multipurpose Reusable Reentry Satellite. in Proceedings on the First Annual Conference on Small Satellites, Utah State University, Logan, Utah, 1987.

3. LifeSat - An International Biological Satellite Program - Science, Uniqueness, and Necessity. Life Science Advisory Committee and the LifeSat ScienceWork ing Group, publication pending.

4. Rodent Module Science Requirements Document. NASA Ames Research Center, July 1988.

5. Plant Module Science Requirements Document. NASA Ames Research Center, July 1988.

6. General Biology Module Science Requirements Document. NASA Ames Research Center, July 1988.

7. Delta II Commercial Spacecraft User's Manual. McDonnell Douglas Astronautic Company, Huntington Beach, CA, 1987.

8. Mascy, A. C., Swenson, B. L., and Keller, R. G.: The Reusable Reentry Satel lite—Keeping it Up and Bringing it Down. Paper presented at the AIAA/AAS Astrodynamics Conference, AIAA-88-4257-CP, Minneapolis, MN, August 15-17, 1988.

9. Swenson, B. L.: Orbit Selection Considerations For Earth Resources Observa tions. NASA TM-X-2156, February, 1971.

10. U. S. Standard Atmosphere, 1962. United States Committee on Extension to the Standard Atmosphere (COESA), (GPO: Washington), December, 1962.

11. Wercinski, P. F.: A Theoretical Prediction of the Attitude Dynamics Due to Aerodynamic Effects of the Reusable Reentry Satellite. Paper at the AIAA/AAS Astrodynamics Conference, AIAA 88-4257-CP, Minneapolis, MN, August, 1988.

12. Hamilton Standard—A Commanding Force. Descriptive brochure of hydrazine propulsion systems developed by United Technologies-Hamilton Standard.

13. Pioneer F/G: Spacecraft Operational Characteristics. NASA Ames Research Center, Doc. No. PC-202, May, 1971

14. Space Rocket Motors. Morton Thiokol, Inc. Aerospace Group, Manufacturer's catalog, June, 1987. Also private discussions with Thiokol representatives.

15. Formulas for Stress and Strain. 5th Ed. — by Roark & Young, McGraw Hill, 1982.

16. Buckling of Thin Walled Circular Cylinders. NASA-SP-8007 (GPO: Washington), Rev. August 1968.

17. Design Handbook for Honeycomb Sandwich Structures. Hexcel Corp. TSB 123. March, 1970.

18. Uy, O. M., and Maurer, R.H.: Quality Assurance Requirements for a Large LI/SOCl2 Battery for Spacecraft Applications. Paper at the 22nd Intersociety Energy Conversion Engineering Conference, IECEC-879062, Philadelphia, PA, August 10-14, 1987.

19. Final Design Review, Galileo Probe Program Power Electronics. Hughes Aircraft Company Document, No. 816433-52, July 31, 1981.

20. Galileo Probe Final Design Review, Data and Command Processor. Hughes Aircraft Company, HS 373-0020-799, February, 1981.

21. Galileo Probe System, Critical Design Review - Book 1. Hughes Aircraft Com pany, 816663-305, November 4, 1981.

22. Vega Precision Laboratories C-Band Radar Tracking Transponder Model 366C-2. Manufacturer's catalog description. Also, private discussion with officials of White Sands Missile Range, NM.

23. Proceedings of the AIAA 8th Aerodynamic Decelerator and Balloon Technology Conference. April 2-4, 1984.

24. Final Study Report for Advanced Recovery Systems Development, Vol. II. Pioneer Systems, Inc., NASA Contract NAS 8-36631, September, 1987.

25. Roy, Archie E.; The Foundations of Astrodynamics. The MacMillan Company, 1965, pp. 217-225.

NASA National Aeronautics and Space Administration

Report Documentation Page

1. Report No.	2. Government Accession No.	3. Recipient's Catalog No.
NASA TM 101043		

4. Title and Subtitle	5. Report Date
A Conceptual Design Study of the Reusable Reentry Satellite	October 1988
	6. Performing Organization Code

7. Author(s)	8. Performing Organization Report No.
Byron L. Swenson, Alfred C. Mascy, Bruce Carter, Alan Cartledge, Robert E. Corridan, Larry E. Edsinger, Robert W. Jackson, Robert Keller, Marcus S. Murbach, Paul F. Wercinski, and Thomas Wong	A 88310
	10. Work Unit No. 805-45-01

9. Performing Organization Name and Address	11. Contract or Grant No.
Ames Research Center Moffett Field, CA 94035	
	13. Type of Report and Period Covered
12. Sponsoring Agency Name and Address	Technical Memorandum
National Aeronautics and Space Administration Washington, DC 20546	14. Sponsoring Agency Code

15. Supplementary Notes

Point of Contact: Paul F. Wercinski, Ames Research Center, M/S 244-14
Moffett Field, CA 94035 (415) 694-3157 or FTS 464-3157

16. Abstract

Experimentation leading to an understanding of life processes under reduced and extremely low gravitaitonal forces will profoundly contribute to the success of future space missions involving humans. In addition to research on gravitational biology, research on the effects of cosmic radiation and the interruption and change of circadian rhythms on life systems is also of prime importance. Research in space, however, is currently viewed by biological scientists as an arena that is essential, yet largely inacessible to them for their experimentation. To fulfill this need, a project and spacecraft system described as the Reusable Reentry Satellite or "Lifesat" has been proposed by NASA.

17. Key Words (Suggested by Author(s))	18. Distribution Statement
Reusable reentry satellite Lifesat Life sciences Spacecraft design	Unclassified-Unlimited Subject Category - 18

19. Security Classif. (of this report)	20. Security Classif. (of this page)	21. No. of pages	22. Price
Unclassified	Unclassified	93	A05